PHASE TRANSITIONS OF MULTIVALENT ADAPTOR PROTEINS

APPROVED BY SUPERVISORY COMMITTEE

_____

Michael K. Rosen, Ph.D., Advisor

_____

Luke M. Rice, Ph.D., Chair

_____

Elliott M. Ross, Ph.D.

_____

Jen Liou, Ph.D.

PHASE TRANSITIONS OF MULTIVALENT ADAPTOR PROTEINS

by

SUDEEP BANJADE

DISSERTATION

Presented to the Faculty of the Graduate School of Biomedical Sciences

The University of Texas Southwestern Medical Center at Dallas

In Partial Fulfillment of the Requirements

For the Degree of

DOCTOR OF PHILOSOPHY

The University of Texas Southwestern Medical Center

Dallas, Texas

August, 2015

Acknowledgments

I would like to acknowledge my mentor Michael Rosen for his support throughout my graduate years. I appreciate the trust he put in me to be a major part of a new direction of the lab. From him, I have also learned a great deal about how to be cautious and thorough in interpreting scientific data.

I would also like to thank my thesis committee members Luke Rice, Elliott Ross and Jen Liou for their inputs during my various committee meetings, and for guiding me through my graduate years.

I thank Pilong Li and Hui-Chun Cheng for the experimental and intellectual guidance they provided in the initial phase of the phase separation project. I would like to thank my other collaborators Baoyu (Stone) Chen for assistance with characterization of multivalent polymers; Soyeon Kim, Jonathon Ditlev and Xu Zhang for discussions regarding 2D clusters; Qiong Wu for help with NMR spectroscopy; William B. Peeples for collecting PolySUMO – PolySIM data during the Nck linker project; Marc Llaguno for help with cryo-electron microscopy; Javoris Hollingsworth for assistance with multi angle dynamic light scattering; Thomas Scheuermann and Chad Brautigam for guidance with isothermal titration calorimetry; and Kate Luby Phelps, Abhijit Bugde and Karen Rothberg for support with imaging.

My thesis work would not have been successful without the input and guidance from all past and current members of the Rosen lab, for which I am deeply thankful.

I have spent an exciting and fun seven years in the Molecular Biophysics (MB) program, and I thank all the colleagues, mentors and friends of the MB program for creating a great atmosphere.

I thank my parents and sisters for instilling the value of hard work and persistence in me. These values have guided me throughout my graduate years and will be a major part of me as I continue my scientific career.

I also thank my partner and friend May Taw for her patience with me through these years of graduate school training. Her support has been instrumental in my scientific progress and personal happiness, and will be for many years to come.

PHASE TRANSITIONS OF MULTIVALENT ADAPTOR PROTEINS

SUDEEP BANJADE, Ph.D.
The University of Texas Southwestern Medical Center at Dallas, 2015

Supervisor: Michael K. Rosen, Ph.D.

Abstract

Eukaryotic cells efficiently organize their activities to achieve their functional capabilities. This organization of biochemical reactions is a direct result of the cells' ability to compartmentalize their molecules. For example, within a eukaryotic cell, compartments like the nucleus, the endoplasmic reticulum and the vacuoles exist, which are relatively well known for their specific functions. These aforementioned compartments are surrounded by membranes. However, for the past hundred years, we have also known about assemblies of biomolecules that are not bound by membranes. After the initial discovery of nuages, other structures such as Cajal bodies, the nucleolus, promyelocytic leukemia (PML) bodies, paraspeckles, etc., were also described as

membraneless organelles. Furthermore, membranes themselves are self-assembled entities of lipids, proteins and carbohydrates. Additionally, within and on surface of membranes, molecules cluster into signaling compartments in many different biological pathways.

Interactions between individual biomolecules have been studied comprehensively in biology. One of our goals as biophysicists is to attempt to propose physical properties that allow these interactions at the subnanometer scale to give rise to formation of cellular structures, the compartments that are listed above. This thesis proposes a hypothesis based on polymerization of multivalent proteins that causes these complexes to phase separate in solution. The behavior of multivalent proteins and their ligands to phase separate may be a general property that allows cells to regulate their activities in certain localized compartments.

To study this larger goal, I used a specific example of proteins involved in creating the slit-diaphragm, which is the filtration barrier of our kidneys. Nephrin, an integral membrane protein at the slit-diaphragm, interacts with its partners Nck and N-WASP in a multivalent fashion. I show here that these interactions create large assemblies that phase separate into liquid droplets, both in solution and on membranes. I also find that the creation of these assemblies affects the downstream biochemical activity of N-WASP toward the Arp2/3 complex and

actin. The widespread existence of multivalent molecules suggests that these findings may have broad corollaries in different biological systems.

TABLE OF CONTENTS

List of Figures

List of Tables

List of Abbreviations

°C	degrees Celsius
µL	microliter
µm	micrometer
µM	micromolar
2D	2 dimensions
3D	3 dimensions
APC	antigen presenting cell
Arp2/3	actin related protein 2/3
CD3	cluster of differentiation 3
CD45	cluster of differentiation 45
CheA	chemotaxis protein A
CheW	chemotaxis protein W
DLS	dynamic light scattering
DNA	deoxyribonucleic acid
DOGS	dioleoyl-glycero-succinyl
DOPC	dioleoyl-phosphocholine
DTT	dithiothreitol
EC	extracellular cadherin regions
EDTA	ethylenediaminetetraacetic acid
EGFR	epidermal growth factor receptor

EM	electron microscopy
Eph	erythropoietin producing hepatocellular
FNIII	Fibronectin type III
FRAP	fluorescence recovery after photobleaching
FUS	fused in sarcoma
GPI	glycophosphatidylinositol
HEK	human embryonic kidney
HSQC	heteronuclear spin quantum correlation
IgG	immunoglobulin G
IPTG	isopropy-β-D-thiogalactopyranoside
ITAM	immunoreceptor tyrosine-based activation motif
ITC	isothermal titration calorimetry
K_D	equilibrium dissociation constant
kDa	kilo Dalton
L	liter
LAT	linker for the activation of T cells
MEF	mouse embryonic fibroblast
MCP	methyl-accepting chemotaxis
MHC	major histocompatibility complex
min	minute
mL	milliliter
mM	millimolar

mol	mole
ms	millisecond
Nck	non-catalytic kinase
Ni-NTA	nickel nitriloacetic acid
nm	nanometer
nM	nanomolar
NMR	nuclear magnetic resonance
Nsp1p	nucleoskeletal-like protein
Nup	nucleoporin
N-WASP	neural Wiskott Aldrich syndrome protein
OG-DHPE	oregon green 1,2-dihexadecanoyl-glycero -phosphoethanolamine
PML	promyelocytic leukemia
p-Nephrin	phosphorylated Nephrin
PRM	proline rich motif
p-TIR	phosphorylated TIR
pTyr	phosphorylated tyrosine
ppm	parts per million
RNA	ribonucleic acid
sec	second
SH2	src homology 2
SH3	src homology 3
Src	sarcoma

TCR	T cell receptor
TIR	translocated intimin receptor
TIRFM	total internal reflection microscopy
TROSY	transverse relaxation-optimized spectroscopy
ZA	zonula adherens

Chapter 1. Introduction: 3D and 2D Phase Separation in Biology

Phase Separation as a Mechanism of Cellular Body Formation

Eukaryotic cells consist of many organelles to properly compartmentalize their biochemical reactions. Many of the known organelles are membrane bound, such as the endoplasmic reticulum, lysosomes, mitochondria, etc. These complex structures demarcate themselves from the cytoplasm through membranes. Other organelles are non-membrane bound bodies such as P-granules, Cajal bodies, promyelocytic leukemia (PML) bodies, etc.

Some of these non-membrane bound bodies were first discovered over a hundred years ago. In 1890, aggregates were discovered in the cytoplasm of insect germ cells that could be stained with RNA dyes (Ritter, 1890). Studies performed in 1975 found such bodies to be present in over 80 species across the animal kingdom (Eddy, 1975), which are now called “nuages” in mammalian cells and P-granules in *C. elegans*. There are several hypotheses for what may be the function of these bodies. Some of these hypotheses invoke germ cell specification and differentiation, mitosis and chromatin organization and regulation of mRNAs (translation and localization) (Voronina et al, 2011). Other cellular bodies called Cajal bodies were first discovered in 1903 as nuclear

bodies in neuronal cells, and function as sites of snRNP biogenesis and modification of spliceosomal snRNAs (Cajal, 1903; Gall, 2000). Processing bodies or P bodies are cytoplasmic foci that are thought to be involved in mRNA processing and degradation (Parker & Sheth, 2007). Paraspeckles are another kind of membrane-less nuclear body that are believed to function in mRNA processing and mRNA retention in the nucleus (Fox & Lamond, 2010). PML bodies are protein rich bodies initially thought to be involved in transcriptional regulation or nuclear protein sequestration, and now also found to function in the cytoplasm (Carracedo et al, 2011; de The et al, 1990).

Despite our knowledge of the existence of such various kinds of bodies for over a century and the acknowledgment that these bodies have physiologically important functions, the understanding of how they form remains incomplete. In recent years, as described below, the findings that P-granules and nucleoli exhibit liquid-like properties guided us to think about such bodies as possible phase separated entities. These findings have opened the possibility of understanding many of these bodies through the concept of phase separation of proteins, RNA and DNA, and therefore the ideas that the molecular properties that govern phase separation of these biomolecules could also explain the nature of these cellular bodies. As described further below in the review of recent literature, phase separation into macroscopic liquid or gel-like states could occur in different biological systems.

P-granules Exhibit Liquid-like Properties

In studies that used *C. elegans* embryos, Brangwynne and colleagues found that P-granules could fuse and relax their shape within the timeframe of a minute (Brangwynne et al, 2009). These bodies were observed to be spherical in shape unless they wet surfaces, and fluorescence recovery after photobleaching (FRAP) suggested a recovery time of ~ 6 seconds, highlighting rapid dynamics within the structures. All of these data were consistent with a model of P-granules behaving as liquid droplets, within which molecules are rearranging rapidly, and from which molecules can exchange in and out easily. When MEX-5, a polarity protein involved in stabilizing P-granules, was depleted through RNAi, dissolution of P-granule was reduced. Another study found that the gradient of MEX-5, which was believed to be important for establishing P-granule polarity and condensation, was regulated by a kinase called PAR-1. These studies therefore suggested a possible mechanism by which the formation of P-granule droplets could be regulated (Griffin et al, 2011). Brangywnne et al. hypothesized that “a collection of weak and sticky” molecules could induce the formation of P-granules and other non-membrane bound bodies in cells (Brangwynne et al, 2009). In another recent study, Seydoux and colleagues suggest that despite the liquid-like behavior of P-granules, these structures are not homogeneous entities and some components of the body surround the droplets and act as boundaries (Wang et al, 2014b). How these two seemingly inconsistent findings relate to each other is a matter of interesting future work. Another interesting finding in the

Seydoux work suggests that the formation of such bodies can be regulated by phosphorylation of serine-rich disordered proteins that are present in the bodies (Wang et al, 2014b).

The Nucleolus as a Phase-Separated Body

In a study that followed the P-granules work, Brangwynne and colleagues also characterized the physical properties of nucleoli and have proposed that they also are phase-separated bodies (Brangwynne et al, 2011). Analyses of *X. laevis* oocyte nucleoli demonstrated that the aspect ratio of the nucleoli shapes was ~ 1.07, nearly equal to 1 that exists for a perfectly spherical shape. Size distribution of the nucleoli exhibited a power law dependence, which could be simulated and described for a process that has a constant influx of molecules and a high degree of coalescence of droplets, where coalescence is suggestive of a liquid-like behavior. Fusing nucleoli were also observed.

These studies of P-granules and nucleoli demonstrated that two naturally existing bodies are formed probably via the process of phase separation. The existence of such liquid-like bodies therefore highlighted a need for the understanding of mechanisms that lead to phase separation of the constituent molecules.

Low Complexity Sequences Induce Formation of Hydrogels

The existence of bodies in cells that could be viewed through the lens of phase separation highlighted the need to understand protein properties that are important for the process of phase separation. Recently, fiber formation through low complexity sequences has been proposed to be a potential mechanism of formation of such bodies found in cells. Low complexity sequences are defined as polypeptide sequences that have low diversity in their amino acid composition. These sequences are present in a variety of RNA and DNA binding proteins, and are unstructured. Using a region of low complexity sequence of the fused in sarcoma (FUS) RNA binding protein, Kato et al. discovered that such a low complexity sequence forms a hydrogel-like component in a concentration dependent fashion (Kato et al, 2012). Different RNA binding proteins are retained in the hydrogel in a biochemical experiment, and mutations of tyrosine to serine in the low complexity sequences inhibit hydrogel formation and also association of FUS protein to stress granules in cells. Electron microscopic analyses suggested that the hydrogels contained amyloid-like fibers, and X-ray diffraction studies suggested the presence of cross-β strands. Strong evidence for the involvement of low-complexity sequences in RNA granule formation was presented with deep sequencing of mRNAs precipitated with hydrogels containing low-complexity sequences and comparing them to mRNAs reported in the literature to be present in RNA granules (Han et al, 2012). These studies have provided evidence for the involvement of low-complexity sequences in the

formation of phase separated non-membrane bound bodies in cells. It will be interesting to study how the self-association of low-complexity sequences interact with other partners in the cellular context to provide dynamic structures at the seconds timescale.

Hydrogel Formation of Nuclear Pore Components

Hydrogel formation similar to those observed in Kato et al. and Han et al. had been previously observed in the case of nuclear pore component Nsp1p. Nsp1p also contains low complexity sequences, although these contain FG repeats compared to [G/S]Y[G/S] repeats that are present in FUS. Solid-state NMR experiments suggested cross-β strands as the core structure of the hydrogels. As in the case of FUS hydrogels that formed at millimolar concentrations, the concentrations required for hydrogel formation was > 100 mg/mL (Frey & Gorlich, 2007; Frey et al, 2006). However, in a recent study, Schmidt and Gorlich found that nucleoporins with FG repeats (Nup100) spontaneously phase separated into nearly-spherical particles at nanomolar concentrations upon changing from a buffer containing 2 M Gdn-HCl to nearly negligible GdnHCl concentration and physiological pH (tris saline buffer) (Schmidt & Gorlich, 2015). As a control, a highly charged part an FG domain from *S. cerevisiae* protein Nsp1p did not phase separate, suggesting that the hydrophobic nature of the FG repeat is responsible for inducing phase separation. Interestingly, the authors also observed that certain phase-separated particles (made from a nucleoporin called

MacNup98A FG from *Tetrahymena*) did not retain thioflavin T in the particles. Since thioflavin T recruitment is a property of cross-β strands, these data led the authors to suggest that cross-β strand formation may not be a strict requirement for phase separation of these low complexity sequences. However, it is possible that different structures possess different kinetics of thiofalvin T recognition and recruitment. Also, more thorough structural analyses of the phase-separated particles from diverse species (through solid-state NMR or X-ray diffraction methods) would be interesting to ascertain the presence or absence of cross-β strands in different phase-separated structures. Nevertheless, these studies highlight the ideas that we can identify differences in structural properties of phase-separated structures that arise due to differences in the amino acid composition of low complexity sequences.

Remarkably Schmidt and Gorlich observed phase separation using nucleoporin FG repeats from species as diverse as humans, *D. melanogaster* and *Tetrahymena* among more than 10 species that they experimented with. These data strongly suggest that self-assembly and phase transitions into liquid-like and phase-separated structures are conserved phenomena in biological systems.

Ddx4 Proteins Are Components of Nuages That Phase Separate through Electrostatic Interactions

Ddx4 proteins are constituents of cellular bodies called nuages in mammals (called P-granules in worms) (Nott et al, 2015). These bodies localize molecules present in the RNAi pathway and are believed to be important for mRNA localization and processing (Voronina et al, 2011). Ddx4 consists of a DEAD-box RNA helicase domain, and N and C termini that are predicted to be disordered. Nott et al. observed that the N-terminal region of Ddx4 spontaneously phase separates *in vitro* and in cells. NMR experiments also provided evidence that the N terminus of Ddx4 is disordered, as the $^{1}H/^{15}N$ HSQC experiments showed a narrow range of amide-proton chemical shift (Nott et al, 2015).

TEM experiments suggested that the droplets of Ddx4 were devoid of any fibrillar structures inside them, suggesting a dynamic nature of the droplets. A drop in temperature favored droplet formation *in vitro* and in cells. *In vitro*, droplet formation was also favored by a decrease in salt concentration. These data suggested that electrostatic interactions stabilize these droplets. Interestingly, the authors found that the N-terminus consists of blocks of charges, where positive and negative charges are distributed in blocks. A mutant construct that preserves the overall sequence feature but scrambles the charges did not phase separate, suggesting that the specific interactions of the charges, not just the non-specific interactions of those particular amino acids, is important for phase separation of Ddx4 (Nott et al, 2015).

The authors also found that Ddx4 contained blocks of FG and RG repeats. When the phenylalanines (F) were mutated to alanines (A), phase separation was inhibited both in cells and *in vitro*. These data have led the authors to propose that cation-pi interactions between the phenyalanlines and arginines allow the protein to self-assemble, causing them to phase separate. While these studies highlight the importance of blocks of phenylalanines and arginines in phase separation, further analyses will be necessary for us to identify the involvement of cation-pi interactions in phase separation of these proteins. Whether the cation-pi interactions can be substituted by other self-assembling repeated motifs would be an interesting question to consider in the future.

Phase Separation of Multivalent Molecules as a Principle of Cell Organization

The aforementioned studies suggest that phase separation of biological molecules seems to be a general concept in the organization of cells into different compartments. It is interesting that many of the purported phase-separated bodies in cells contain a large number of multivalent proteins, as detailed in Chapter 2. In addition, RNA and DNA are effectively multivalent.

Interestingly, mechanisms of phase transitions have been explained in polymer chemistry with the formation of infinitely large polymers through interactions of multivalent molecules with their multivalent ligands (Benedek, 1982; Flory, 1953;

Tanaka, 2011). In the seminal papers of the 1940s, Paul J. Flory described the process of gelation (at a critical concentration) led by a process of polymerization through the interactions of multivalent small molecules (Flory, 1941; Flory, 1953). He described two kinds of polymers. The first kind of polymer does not form gels (and therefore remains soluble) regardless of the degree to which polymerization takes place. These kinds of polymers are linear chains of polymers. The other kinds of polymers form a gel-like state at a certain critical concentration, as long as the polymerization process takes place to the extent required.

In those studies, small molecules such as tricarballylic acid, succinic acid and diethylene glycol were allowed to polymerize (Flory, 1941). The viscosities of the solution were measured at different times after allowing enough time for polymerization to take place. These experiments found that the solution viscosities changed sharply as a function of the concentration of the polymerized components, which corresponded to the formation of insoluble “gelatinous precipitates suspended in solution.” Importantly, the critical point obtained by experiments correlated well to the calculated critical point obtained by assuming formation of infinite networks of polymers through multivalent interactions. Even though the theory neglected the formation of intramolecular associations, measurements from calculation and theory differed from one another by less than 6%. These experiments provided contrary results to the previous ideas

suggesting that gelation could not occur due to formation of infinite networks of polymers (Flory, 1941).

This phenomenon, named sol-gel transitions, suggested formation of a gel-like meshwork. As suggested by Flory, the experimental observation of the formation of a “gel” was suspended particles in solution, which lead to change in viscosity of the solution. The experimental observation of Flory suggests that the gels do not have to occupy the whole solution. In other words, precipitates suspended in solution, which are the experimental observation of “gels,” also can be explained through a process of a sol-gel transition. Other works have suggested that upon changes in environmental conditions, such gels may occupy the whole solution, or may only occupy a small volume fraction (Tanaka, 1980; Tanaka, 1978).

These theories described the critical extent of reaction of multivalent polymerization as the point at which the system changes from forming small aggregates in the sol phase (polymers of small sizes – dimers, tetramers oligomers) to forming a few very large aggregates (the so called infinitely large polymers). As early as the 1950s, reactions of bivalent antibodies with an f-valent antigen were thought to form precipitates through the same mechanism, forming at a critical extent of reaction (Goldberg, 1952). Theories of interactions between bivalent immunoglobulin E (Ig-E) antibodies with trivalent Fc receptors predicted sol-gel transitions to occur with these multivalent interactions

(Goldstein & Perelson, 1984). Sol-gel transition required polymerization between a ligand of at least two valency interacting with a receptor of at least three valencies (or vice versa). Additionally, as in theories of polymer chemistry, sol-gel transition would not occur for linear polymers or linear aggregates. Despite these theoretical studies, the nature of the gels formed via multivalent protein-protein interactions had not been studied experimentally with biological proteins.

This phenomenon of polymerization of multivalent molecules suggested that biological molecules containing multivalent interactions may also lead to phase transitions into large polymers, and this phenomenon may be the mechanism of nucleation of non-membrane bound bodies in cells, since many of the proteins, DNA and RNA found in such bodies are multivalent. Additionally, this same mechanism may also be involved in organizing the plasma membrane into different compartments, should there be membrane-bound proteins that are also multivalent.

Phase Separation as a Concept of Membrane Organization

As with the compartmentalization of cells into different “cellular bodies,” compartmentalization of the membrane has been observed for decades. This thesis studies multivalent proteins that assemble specifically at the plasma membrane, and therefore the idea of multivalency induced phase separation could also be a way to compartmentalize the membrane. Before explaining in

detail the exact biological system that this thesis studies, it is important to review the research studying the organization of the plasma membrane.

Structure of the Biological Membrane

The fluid mosaic model of 1972 proposed by Singer and Nicholson is a well-known and powerful hypothesis of the organization of lipids, proteins and carbohydrates as the membrane bilayer (Jacobson et al, 1995; Singer & Nicolson, 1972). The model describes biological membranes as two-dimensional fluids in which proteins, carbohydrates and lipids can diffuse freely. This model was an improvement upon the previous 1930s model of Davson and Danelli, which regarded the membrane as a bilayer sandwiched between layers of globular proteins (Davson, 1935). Singer-Nicholson model is now prevalent, and is the first description of a biological membrane in any cell biology textbook. However, with studies from many different labs and in many different biological pathways, we have now begun to understand that molecules on the membrane are not distributed homogeneously and do not diffuse randomly. The following paragraphs will describe the studies that have led up to the conclusion that biological membranes, especially the plasma membrane, is highly organized into compartments made up of clusters of biological molecules.

The Concept of Lipid Rafts Could Explain How Membrane Clusters Form

The concept of lipid rafts originated during studies of epithelial cells, which can be distinguished into apical and basolateral parts. In 1987, Kai Simons and colleagues observed a difference in the lipid composition in these two domains of epithelial cells (Simons & van Meer, 1988). They observed that a fluorescently labeled glycosylceramide sorted to the apical part of the cell to a larger degree than the basolateral part. Based upon these data, they hypothesized that the ability of sphingolipids and glycoproteins to cross-link with each other allowed them to sort differentially, making compartments enriched in these molecules (Simons & Ikonen, 1997; Simons & van Meer, 1988).

These studies were followed by other works, which showed that glycosphingoinositol (GPI) anchoring of proteins was sufficient to sort such anchored proteins to the apical surface in epithelial cells, because replacing the GPI anchor with a transmembrane domain shifted the expression of a normally GPI-anchored protein placental alkaline phosphatase to the basolateral part (Brown et al, 1989). In subsequent studies, such GPI-anchored proteins were found to be insoluble in the detergent Triton-X 100 (Brown & Rose, 1992; Low, 1989). The insoluble Triton-X 100 fractions were found to contain membranes, and the lipid composition analysis by thin layer chromatography suggested that the insoluble fractions contained cholesterol:sphingolpids:glycerophospholipids in a 1:1:1 ratio (Brown & Rose, 1992), similar to the previously reported ratio of

membrane composition in apical surfaces of intestinal epithelial cells (Simons & van Meer, 1988). These data led to the hypothesis that the ability of cholesterol, sphingolipids and glycerolipids to assemble together into domains caused the asymmetry in the distribution of associating proteins between apical and basolateral surfaces of epithelial cells.

These data were supported by *in-vitro* experiments, where vesicles composed of cholesterol, sphingolipids and phospholipids at certain ratios formed macroscopic phase separated domains (Veatch & Keller, 2002; Veatch & Keller, 2003). These studies have formulated the idea of lipid rafts as assemblies of cholesterol, sphingolipids and phospholipids that form distinct domains on the surface of the membrane (Harder & Simons, 1997). Additionally, glycosphingolipids were observed to be involved in forming caveloae (Tran et al, 1987), structures that are involved in endocytosis (Mayor et al, 2014), which also required cholesterol to function (Rothberg et al, 1990). Therefore, lipid rafts were thought to be involved in the formation of caveolae, and therefore a function of lipid rafts in endocytosis was proposed (Simons & Ikonen, 1997).

According to the lipid raft model, any protein that associates with lipids that phase separate could be localized differentially at the membrane, thereby localizing the protein's activity. It is a powerful general model applicable to different systems described below. However, the lipid raft hypothesis remains

controversial and may not completely explain the mechanisms of compartmentalization of the membrane (Weimbs et al, 1997). Triton X 100 treatment and insolubility experiments are crude biochemical methods that are unlikely to maintain cellular and physiological states of the membrane and proteins associated with them, and cholesterol depletion studies performed to reflect importance of cholesterol in forming rafts could also inhibit several other cellular functions (Edidin, 2003). Furthermore, confusion remains on the exact definition of rafts in cells (Rao & Mayor, 2005), as some ideas are consistent with rafts to be large and > 50 nm in size (Simons & Ikonen, 1997) while others suggest structures < 50 nm in size (Pralle et al, 2000). Other ideas proposed lipid rafts to be "lipid shells" encased with cholesterol and sphingolipids (Anderson & Jacobson, 2002). By conventional fluorescence microscopy, rafts, or clusters of molecules on the cell surface, were not observed in the 1990s when these experiments were first performed with GPI-anchored proteins, which were predicted to be raft associated from the aforementioned biochemical experiments (Mayor & Maxfield, 1995). These experiments suggested the idea that perhaps these raft like assemblies that consisted of GPI-anchored proteins could not be micron scaled and large as observed with *in vitro* experiments in model membranes. The possibility that the rafts could be diffraction-limited remained plausible.

GPI Anchored Protein Clusters are Nanometer-Scale Clusters that are Organized by the Underlying Cytoskeleton

Microscopy experiments were inconsistent with the hypothesis that GPI-anchored proteins could be micrometer scale clusters as demonstrated with phase separated lipids in biochemical experiments. However, it was found that these proteins could form nanometer-sized clusters. It is first important to review the experiments that led to this conclusion that GPI anchored proteins did form clusters in cells, since these analyses of clustering experiments performed in cells is one of the few such quantitative experiments that exist in the literature.

Using fluorescence resonance energy transfer (FRET) and loss of polarization due to FRET, Varma and Mayor observed that anisotropy at different values of the fluorescence intensity (density) of a GPI-anchored protein (GPI anchored folate receptor, FR-GPI) remained constant over the entire range of the density (Varma & Mayor, 1998). In these experiments, the FR-GPI was labeled exogenously by binding a monovalent fluorescent folic acid analogue (N^{α}-pteroyl-N^{ε}-(4'-fluorescein-thiocarbamoyl)-L-lysine). These data suggested that perhaps the GPI-anchored proteins were distributed at such low density that the there was no energy transfer between flourophores, and therefore no change in anisotropy. However, when the fluorescent GPI anchored proteins were "diluted" by photobleaching a fraction of molecules on the surface, the anisotropy values increased with an increase in photobleaching time. These data suggested that

the presence of constant values of anisotropy with density could not occur due to a possible lack of energy transfer between these molecules, because photobleaching (dilution) led to an increase in the anisotropy values (or a decrease in energy transfer). The simplest explanation for these data was that the GPI-anchored proteins were maintained on the cell surface in small patches with a constant number of molecules. At several densities of the protein the patches were maintained with a specific number of molecules in them without dissociation. The authors also found that depletion of cholesterol increased the anisotropy values, suggesting that cholesterol plays a role in maintaining these patches of GPI-anchored proteins.

Inconsistent with a thermodynamically equilibrated process predicted by the raft hypthesis, the GPI-anchored proteins also do not exhibit a Gaussian spatial distribution (Goswami et al, 2008). In an interesting finding, the authors observed that the ratio of association rate constant of cluster formation to the dissociation rate constant changes sharply at 24°C. This effect resembled a similar activity of actomyosin complex previously seen in the literature (Sheetz et al, 1984). To understand whether the actomyosin complex also plays a role in stabilizing the clusters, the authors inhibited actin and myosin, and found that the inhibition of either abrogates the dynamics of interconversion between monomers and clusters. Based on these data, the authors have suggested a hypothesis behind the formation of GPI clusters on the cell surface, where they suggest that the

active nature of actomyosin assembly stabilizes the clusters, and maintains the cluster to monomer ratio.

This model based on active assembly due to the actomyosin complex is an additional model that could be a way the cell membrane could organize its reactions, through coupling to the cytoskeleton. This model is independent of the lipid raft concept, although the authors do find that cholesterol plays a role in the actomyosin-based assembly of the membrane-anchored receptors.

Other examples of membrane-clusters exist in the literature. Some of them include the T Cell Receptor (TCR) Clusters, Ephrin Clusters, Chemotaxis Receptor Clusters and Cadherins-mediated junctions. Many of these examples cite the possible roles of lipid rafts or actomyosin based assemblies, as these are two models that could be general in different systems. While going through this review of the literature, it is clear to me that the existence of macroscopic clusters at the cell membrane is a prevalent phenomenon that is important in signaling through the membrane, but also therefore that a general mechanism to describe the formation of such structures would be a major step in understanding the structure of the cell membrane and the biochemistry of signal transduction through the membrane.

T Cell Receptor Clusters Form During the Activation of a T Cell

Upon ligand binding by the T cell receptor (TCR), biochemical changes occur in the cytoplasmic regions of the TCR that are important for the activation of a T cell. The TCR is composed of a multi-subunit receptor complex. The CD3 complex is a unit of the TCR, which gets phosphorylated upon binding of the TCR to an antigen-presenting cell (APC) (van der Merwe & Dushek, 2011). MHC protein on the surface APCs interacts with the TCR on T lymphocytes to initiate communication between the two cells. How binding of a ligand on the cell surface of a cell induces intracellular changes remains an unsolved question in this field. The three proposed models include aggregation (clustering) of the TCR, conformational changes in the TCR and segregation of the TCR complexes (van der Merwe & Dushek, 2011). It remains to be determined if these seemingly disparate models act cooperatively with each other.

Clustering of TCR has been proposed to be important for signal transduction through the APC to the TCR (Lillemeier et al, 2010). Clustering of the TCR by antibodies or multimeric peptide-MHC complexes can activate a T cell (Cooper & Qian, 2008). Numerous studies that observed TCR clusters suggested the possibility that these clusters could be lipid-rafts (Kabouridis et al, 1997; Xavier et al, 1998). In other works, upon stimulating TCR by TCR-specific antibodies on a coverslip, dynamic micron-sized clusters were observed that included TCR and the cytoplasmic proteins Zap 70, LAT, Grb2, Gads and SLP-76, and excluded a

lipid-raft marker YFP-GPI (Bunnell et al, 2002). An interesting feature of these clusters was that despite the stability of clusters over minutes, Zap 70 was dynamic within seconds as studied through fluorescence recovery after photobleaching (FRAP) (Bunnell et al, 2002). Similar rapid dynamics of the kinase Lck and the adaptor protein LAT was observed via single-molecule studies in clusters of TCR, which also highlighted the role of protein-protein interactions giving rise to formation of TCR clusters, that did not involve lipid-rafts or the actin cytoskeleton (Douglass & Vale, 2005). Similarly, other studies have observed formation of micron-sized TCR clusters upon stimulation with its ligands (Douglass & Vale, 2005; Lillemeier et al, 2010; Varma et al, 2006; Yokosuka et al, 2005). Therefore, several groups have observed clustering of TCR, but a clear understanding of how these clusters are formed is lacking.

Interestingly, only a single MHC peptide has also been found to be sufficient to induce activation of a T-cell (Sykulev et al, 1996). On similar lines, a feature of the T cell signaling system is that only a few molecules of the antigen is necessary for the full activation of the cell. If clustering of the intracellular components is a necessary feature for activation of the T cell, it will be interesting to study how a single or only a few molecules of the ligand can communicate to the intracellular region to cluster the intracellular molecules and thus fully activate the T cell.

In a recent study, signaling molecules involved in the activation process of a T cell were reconstituted in non-immune cells (HEK cells corresponding to a T cell and Raji cells corresponding to an APC) (James & Vale, 2012). This study suggested a novel model for the clustering of membrane receptors. In this study, exclusion of CD45 from TCR clusters was found to be sufficient for the recruitment of the kinase Zap 70, whose recruitment at the contact zone is believed to initiate signaling in this system, as Zap 70 binds to phosphorylated TCR conserved motifs (ITAMs). The authors found that binding interactions between the TCR and pMHC was sufficient to induce the exclusion of the phosphatase from the contact zone. Furthermore, replacing the extracellular domains of TCR and pMHC with FKBP and FRB respectively, the authors were able to reconstitute the exclusion of the phosphatase.

These experiments led the authors to propose a model of clustering of membrane proteins due to the bulkiness of these membrane proteins, steric clashes and bending of the membrane induced by these bulky proteins. Importantly, these effects would be unique to a two-dimensional system, and therefore is an interesting concept to consider while studying membrane-based clusters. It is possible that additional factors such as repulsive charges could also exclude proteins from these contact zones in addition to the bulkiness of membrane proteins suggested by this study.

Other studies have suggested a role of the actin cytoskeleton in the ability of the TCR to cluster (Comrie et al, 2015; Smoligovets et al, 2012; Yu et al, 2013). James and Vale found that depolymerization of actin filaments in HEK cells before mixing with APCs significantly decreased the number of (TCR-APC) conjugates in the reconstituted system (James & Vale, 2012). But cells that did interact still showed ZAP 70 recruitment, suggesting that the cytoskeleton facilitates initial cell-cell interactions but may not be essential for TCR triggering in this reconstituted system. More quantitative analyses of the correlation between depolymerization of actin and failure to form TCR-APC conjugates will be interesting to study the effects of the cytoskeleton on TCR clustering.

Chemotaxis Receptor Clusters Guide Bacteria

Although several features about the organization of the bacterial cell have been only realized in the past few years, clustering of the signaling machinery of bacteria at the membrane was proposed two decades ago (Alley et al, 1992; Maddock & Shapiro, 1993). The bacterial chemotaxis signaling machinery has been thoroughly investigated and laid the foundation to understand signaling mechanisms in eukaryotic cells. Despite this thorough investigation, the mechanism for clustering of the receptors is still not clearly understood.

In this system, the methyl-accepting chemotaxis protein (MCP), which is a membrane bound receptor, interacts with the intracellular proteins CheW and CheA in the process of enabling the bacteria to sense their environments accordingly. Using immuno-electron microscopy and immuno-fluorescent microscopy, Maddock and Shapiro observed that the chemoreceptor and the intracellular proteins were localized preferentially at the cell poles in clusters, compared to the overall distribution of the receptor elsewhere in the cell (Maddock & Shapiro, 1993). In bacterial strains deleted of the chemotaxis receptors, the intracellular proteins were cytoplasmic and unclustered, but in the presence of an induced receptor, the localization was polar and clustered, suggesting an aggregation mechanism of these proteins in the presence of the membrane bound receptor.

In vitro analysis through negative stain electron microscopy showed filamentous structures of the complexes of the MCP receptor Tar (aspartate receptor), CheA and CheW (Liu et al, 1997). A structural analysis of the intracellular region of another MCP, the serine chemoreceptor Tsr, demonstrated the presence of a dimer consisting of a four helical bundle, and crystallographic packing suggested that these dimers could possibly form a trimer (Kim et al, 1999). This supposed trimer of dimers was then proposed to be an important component of the clusters observed *in vivo* and of the filaments observed *in vitro*.

At present, the trimer of dimers of the chemotaxis receptors is thought to be the basic unit of their clusters that are observed *in vivo*. However, the precise mechanism behind how these small oligomers coalesce to form large clusters is a yet unclear and a primary question in the field.

Promiscuous Ligand-Receptor Interactions Drive Ephrin Clustering

Eph receptors (Ephs, which stands for erythropoietin producing hepatocellular receptors) belong to a large class of receptor tyrosine kinases that bind to their ligands called ephrin on an opposite cell (O'Leary & Wilkinson, 1999; Pasquale, 2010).

Upon ligand binding, Ephrin receptors are known to form clusters on the cell surface. For example, when cells expressing the receptor EphB2 are treated with its ligand ephrin, the receptor gets phosphorylated. Upon phosphorylation, the receptors concomitantly assemble into punctate spots hundreds of nanometers in size that are absent in ligand-untreated cells. Membrane bound ligands presented to Ephs or antibodies against Ephs are known to activate the receptors, presumably because these interactions cause large-scale aggregation (Davis et al, 1994).

When ephrin is included as a ligand on supported lipid bilayers and cells expressing Ephs are allowed to interact with these ligands, phosphorylation and clustering of Ephs have been observed, which can also be affected by physical barriers created on the supported bilayers (Salaita et al, 2010). Eph clusters on the cell surface are found to be of variable sizes, including monomers, dimers and higher order oligomers (Schaupp et al, 2014). This broad size distribution speaks against the possibility of the Eph clusters having a stoichiometrically defined complex.

Concepts from the lipid raft field have been proposed to understand the clustering of Eph receptors (Marquardt et al, 2005). In other studies, structures of Ephs bound to Ephrins show formation of dimers and oligomers, and also demonstrate the existence of multiple binding sites of the ligands on the same Eph receptor (Nikolov et al, 2014; Seiradake et al, 2013). However, yet again in this system, a clear concept of how cluster formation of ephrins could be explained through the molecular interactions remains missing.

Cadherin Clusters Promote Adherence of Cells

Clustering of proteins is also observed in between apposed cells, structures that are known as adherens junctions. Adherens junctions are zones in between apposed cells or between cells and their extracellular matrix. These junctions

exist in the forms of focal adhesions, desmosomes, hemidesmosomes and zonula adherens (ZA) junctions (Baum & Georgiou, 2011; Yap et al, 1997). Among these, the ZA junctions utilize the function of cadherin proteins to form the junctions (Brasch et al, 2012).

Cadherins are single pass transmembrane proteins with large extracellular regions denoted as EC. The extracellular regions of cadherins possess homophilic interactions (Chappuis-Flament et al, 2001). Although only one (most N-terminal) EC region is purported to be important for homophilic interaction, absence of the other four EC regions among the five reduces binding and adhesive property of cadherins (Chappuis-Flament et al, 2001; Laur et al, 2002; Renaud-Young & Gallin, 2002). The intracellular regions consist of a catenin-binding site that recruits actin to the cell surface, and these interactions seem to play an important role in the formation of the junctions (Hong et al, 2013; Yamada et al, 2005). Deleting the cytoplasmic catenin-binding site reduces the aggregation of cultured cells (Nagafuchi & Takeichi, 1988; Ozawa & Kobayashi, 2014; Simcha et al, 2001), and expression of the cytoplasmic region alone reduces cell-cell adhesion (Brasch et al, 2012; Fujimori & Takeichi, 1993). Catenins interact with the actin cytoskeleton and inhibition of actin polymerization by cytochalasin has been shown to reduce cell-cell adhesion (Angres et al, 1996; Hong et al, 2013; Jaffe et al, 1990; Yonemura, 2011). Considering these data and the fact that catenin bundles actin filaments *in vitro* (Hansen et al, 2013;

Rimm et al, 1995), actin dynamics seem to contribute to the formation and function of cadherin-mediated adherens junctions.

Nevertheless, biochemically purified extracellular regions of cadherins attached to beads can cause aggregation of those beads, indicating homophilic interactions of the cadherin molecules could drive clustering (Brieher et al, 1996). Cadherins also dimerize, and the monomeric form of the extracellular region in the bead aggregation assay has a considerably lower effect on aggregation. Therefore, the functional form of the cadherin's extracellular region is a dimer that possesses homophilic interaction potential and these interactions could also contribute to the stabilization of the adherens junction.

Based on evidence of the extracellular region (EC1) crystallographic packing, models of cadherin interactions at adherens junctions have been proposed to reflect clustering of these proteins (Brasch et al, 2012; Harrison et al, 2011; Jin et al, 2012; Shapiro et al, 1995). Among the clustering models reflect a model consisting of a linear chain of polymeric interaction, or discrete oligomers of variable sizes (Brasch et al, 2012; Shapiro et al, 1995; Yap et al, 1997). Another study found that the cadherin cis binding affinity is too weak to measure (an upper limit of 1 mM) (Harrison et al, 2011). However, interesting theoretical studies have been proposed suggesting that the trans dimerization of cadherins can effectively increase the affinity of the cis-dimerization (Vendome et al, 2014;

Wu et al, 2013; Wu et al, 2011). These studies suggest that a high affinity trans association can increase the oligomerization property of cadherins at cell-cell junctions, creating high-density surfaces at the membrane due to clustering of these proteins.

Slit-Diaphragm: Nephrin, Nck and N-WASP

Adhesion proteins form structural sites in many cases between apposed membranes, without inducing fusion in between these membranes, as described in the previous example of cadherins. The slit-diaphragm, the blood filtration barrier present in the epithelial cells of the kidney, is another example (**Figure 1.1**). In this thesis, proteins in this system have been used as a model experimental system to study the phenomenon of multivalent interactions that lead to phase separation and clustering of these proteins.

The filtering unit of our kidneys is a structure called glomerulus, which is a knot of capillaries (Welsh & Saleem, 2010). Through these capillaries, about 180 L of water passes through each day, while retaining blood plasma and other molecules within the kidney. The epithelial cells called podocytes surround the capillaries of our kidney. Although the podocytes are known to be involved in the filtration of blood, how this filtration is achieved is not yet clearly understood (Pavenstadt et al, 2003).

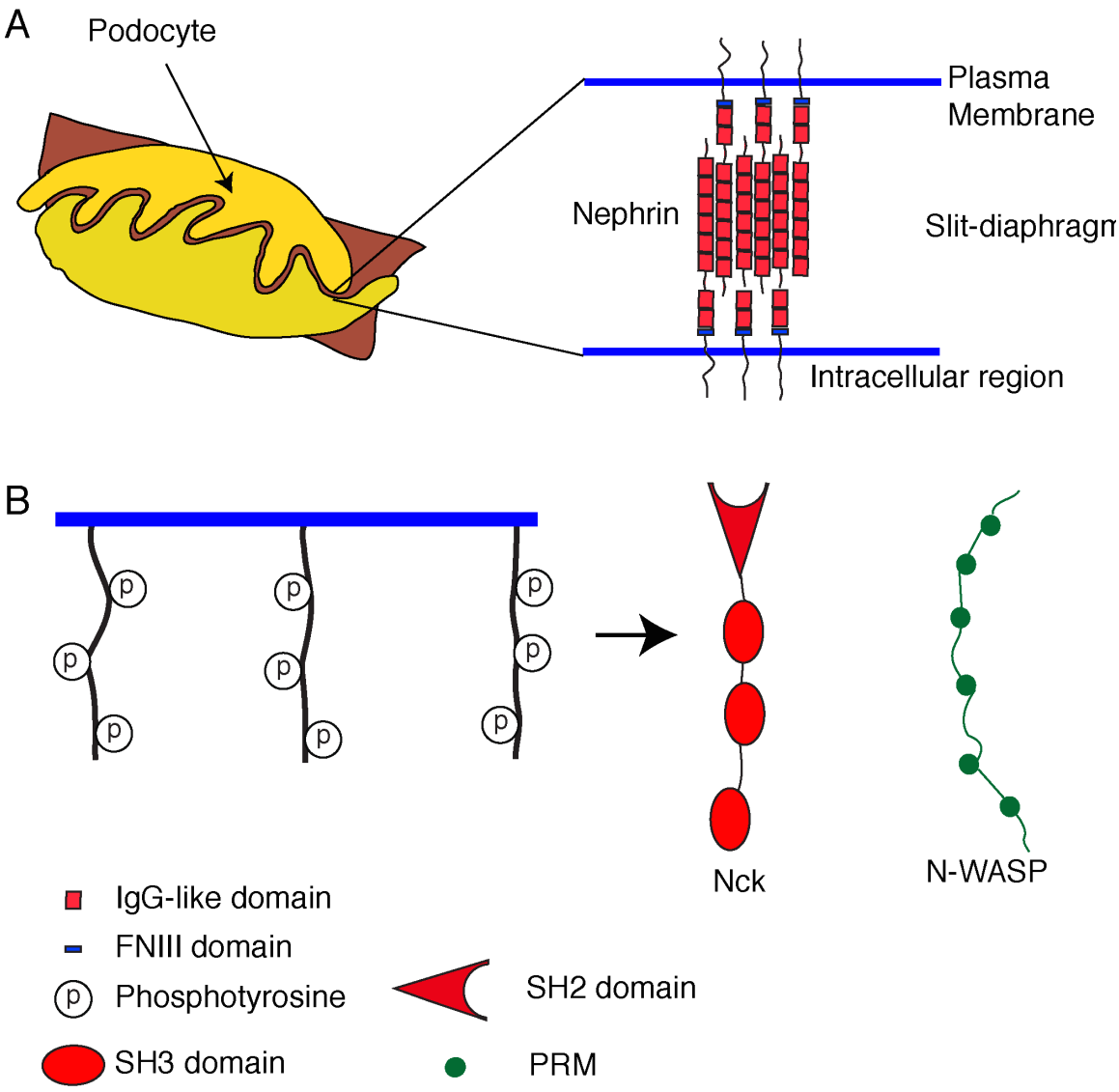

Figure 1.1. Nephrin is an integral membrane protein of the slit diaphragm. **A)** The inter-membrane junction of podocytes is composed of a filter-pore called the slit-diaphragm. **B)** The intracellular portion of Nephrin consists of three phosophotyrosine sites that recruit Nck and N-WASP to the membrane.

The cells attach to the capillaries by structures named foot processes ((Pavenstadt et al, 2003), **Figure 1.1**). These foot processes inter-digitate with one another, and the slit-diaphragm is present at the intercellular junction of the

foot processes. The slit diaphragm is made up of the interactions of the extracellular regions of the membrane receptors of the podocytes, among which Nephrin is a critical member.

Nephrin is a 180 KDa integral membrane protein, with a large extracellular region containing six IgG domains and three FNIII domains, and a shorter cytoplasmic tail of 165 residues (Welsh & Saleem, 2010). The cytoplasmic tail of Nephrin is phosphorylated by the Src family kinase Fyn (Li et al, 2004; Verma et al, 2006). Phosphorylation of Nephrin is important for the normal physiology of the slit diaphragm because mice deficient in the Src family kinases Fyn and Yes (or only Fyn) develop proteinuria, which is a disease caused by an injury to the slit diaphragm that causes abnormal loss of protein to urine (Verma et al, 2006; Yu et al, 2001). There are three phosphorylation sites of Nephrin that are binding motifs for SH2 domains. These sites bind the SH2 domain of Nck, deletion of which also causes proteinuria (Jones et al, 2006; Jones et al, 2009). Experiments with glomerular lysates demonstrated that Nephrin is phosphorylated at these tyrosines (Jones et al, 2009; New et al, 2013). In a series of immunoprecipitation experiments performed with mutations in Nephrin that contained single, double or triple to mutations, it was found that a single mutation did not largely affect binding to Nck, double mutation had a larger effect, and no binding was detected with a triply mutated Nephrin (Jones et al, 2006).

Therefore, these three tyrosine motifs are the Nck binding sites of Nephrin, and in another study, the binding affinities were determined to be in the ~1 μM range (Blasutig et al, 2008). Specifically, in human Nephrin, the three tyrosines are Y1176, Y1193 and Y1217, with K_D's reported to be 1.30, 1.66 and 1.05 μM respectively. Furthermore, Nck also binds to Fyn, the kinase that phosphorylates these tyrosines. Loss of Nck results in decreased phosphorylation of Nephrin in podocytes (New et al, 2013). Therefore Nck forms a multi-protein complex with Nephrin and Fyn to directly regulate phosphorylation and further recruitment of Nck (and most likely N-WASP) to the membrane.

In an engineered study where antibodies were used to cluster Nephrin on mouse embryonic fibroblasts (MEFs), Nck was recruited to these clustered structures at the cell surface, where actin also localized (Blasutig et al, 2008). In the same study, tyrosine mutants of Nephrin and SH3 mutants of Nck were made to study the role of specific tyrosines or SH3 domains on the assembly of the clustered structures and the localization of Nck and actin at those structures. Single, double or triple SH2-binding tyrosine (Y) to phenylalanine (F) mutations were made on Nephrin. Also, tryptophan (W) to lysine (K) mutations were made on Nck on the PRM binding sites of the SH3 domains. The tryptophans on the binding sites of the SH3 domains have previously been reported to be crucial to the association with PRMs, although no quantitative measurements have been performed (Tanaka et al, 1995). In the Blasutig study, in experiments quantifying

the percentage of cells with actin localization, in the background of the wild type Nephrin, mutations in all three SH3 domains (triple mutants in the three SH3's) or mutation in the two C-terminal SH3 domains (double mutant SH3-2-3) reduced the percentage of cells containing actin polymers at clusters (from 70% WT to about or less than 15% in mutants). Double mutations in the first and third SH3 domain (SH3-1-3) had no effect, double mutation in the first and the second domain (SH3-1-2) had subtle effects of reduction of the percent of cells to 50%, and the single mutant SH3-2 also had a small effect, with clustering reduced to 60% of that of the WT. In a similar analysis with the mutants of Nephrin, triple mutant of Nephrin had a substantial effect (10% of cells had actin in clusters), whereas the double mutants had no or subtle effects. In the background of double mutants of Nephrin, all the double mutants of the SH3 domains had substantial effects (~10 % of cells contained clusters compared to 70% for WT). These data led to the interpretation that even though single mutations had some effect in assembling structures that led to actin polymerization, a cooperative interaction between the multiple motifs of Nephrin and the Nck SH3 domains was important for the system to function, and furthermore, a network of cross-linked proteins could be present at these junctions.

These studies were important in formulating the question of what kind of structures could be made upon the interaction of multivalent Nephrin, Nck and N-WASP. As there are three tyrosines that bind to the three SH3's of Nck and

multiple PRM's of N-WASP, this system is highly multivalent. As described in the earlier sections, this multivalent system therefore has the potential to undergo sol-gel transitions, and make higher order oligomers of N-WASP. According to the prediction, at lower concentrations of these proteins the solution should remain clear. As the critical concentration is approached the solution should change sharply into a precipitous or gel-like form. As described below, higher order oligomers of N-WASP are potent activators of the Arp2/3 complex, and therefore the multivalent interactions that drive sol-gel transitions could also promote the oligomerization and activation of N-WASP.

WASP Family Members Are Activated by Higher Order Oligomerization

WASP family members are central proteins that control the assembly of actin in cells. Genetic studies have demonstrated that mutations in WASP family members lead to immune deficiency and thrombocytopenia in humans (Derry et al, 1994). In mice, mutations in WASP cause T cell deficiency (Snapper et al, 1998), mutations in N-WASP causes embryonic lethality (Snapper et al, 2001). In yeast, loss of Las 7 (WASP) causes inhibition of endocytosis and loss of actin patches (Madania et al, 1999). Important cellular structures such as podosomes, filopodia and lamellipodia are created with the assembly of actin at the cell surface, where the actin assembly is mediated by the activation of the Arp2/3 complex by WASP family members.

In addition to the elucidation of the importance of WASP family members through genetic and cell biological mechanisms, a large amount of biochemical studies have focused on the activation of the Arp2/3 complex by WASP family members. Structural and biochemical studies show that the activation of WASP occurs through a hierarchical process. The first is an allosteric process where GTPases release the autoinhibition of WASP created by the interaction of the N-terminal GBD region with the C-terminal VCA (activating region) (Abdul-Manan et al, 1999; Kim et al, 2000). The second is an oligomerization mechanism where VCA dimers created by various ligands (such as those containing SH3 domains) activate WASP to a greater degree (Padrick et al, 2008). Dimers of WASP created by glutathlone-S transferase (GST) are about 100 fold higher activators of the Arp2/3 complex. These data could be explained by the ~100 fold higher affinity of a dimer of WASP to the Arp2/3 complex than that of a monomer (Padrick et al, 2008). A dimer is able to bind to the Arp2/3 complex at two sites (Padrick et al, 2011). Subsequently, an oligomer of WASP would have a higher probability of engaging the Arp2/3 complexes to a dimer (Padrick et al, 2008). These data therefore suggested that higher order oligomers/polymers of WASP would have higher activity than monomers.

These analyses of the literature where multivalent proteins are found in cellular bodies, presence of clusters at membranes in different biological systems, the

potential of presence of higher order structures in the Nephrin/Nck/N-WASP system led to the studies described in subsequent chapters, where I discovered that these complexes phase separate due to multivalent interactions that increases the biochemical activity of N-WASP.

Chapter 2. Phase Transitions of Multivalent Adaptor Proteins

Note: The following chapter contains data that have been published in Li*, Banjade*, Cheng*, et al., *Nature*, 2012. The text here contains my own analyses and description of the published work. Multi-angle DLS experiments were performed in collaboration with Javoris Hollingsworth and Paul Russo (Louisiana State University) and the cryo-electron microscopy was performed in collaboration with Marc Llaguno and Qiu-Xing Jiang (UT Southwestern Medical Center). Other data presented here are my own experimental work.

Nephrin, Nck and N-WASP Phase Separate in Solution

To study the effect of valency on the assembly process of naturally occurring molecules, we chose the adhesion protein Nephrin and its cytoplasmic partners Nck and N-WASP. The cytoplasmic tail of Nephrin gets phosphorylated by Src family kinases (Jones et al, 2006; Jones et al, 2009). For our experiments, we chose a region of the tail (human, residues 1174-1223, with the mutations Y1183F and Y1210F). On Nephrin, three tyrosines: Y1176, Y1193 and Y1217 are phosphorylated. SH2 domain of Nck binds to these sites with ~ 1 μM affinities (Blasutig et al, 2008).

We first started studying only Nck and N-WASP, excluding Nephrin. Nck has three SH3 domains (30% identical to each other) and N-WASP has six to nine proline-rich motifs (PRMs). At lower concentrations (5 to 10 μM), the solution remains clear. At higher concentrations (40 μM Nck and 40 μM N-WASP), the solution becomes turbid. Upon observing the turbid solution under a bright-field microscope, droplets of variable sizes appear (Figure 2.1). The droplets are spherical in shape, since the surface tension of the liquid droplet ensures that a spherical shape is the most energetically stable shape. Droplets also fuse with each other, suggesting liquid like behavior.

In Figure 2.2, a phase diagram is shown, where the appearance or absence of droplets were looked for upon mixing various concentrations of Nck and N-WASP. At concentrations 15 μM N-WASP and 40 μM Nck, droplets appear, and are indicated by the red dots in the figure. As N-WASP is titrated up at a fixed concentration of Nck (40 μM), droplets no longer appear, indicated by blue dots in the figure. The absence of phase separation upon titrating to higher concentrations of one of the proteins indicates that the stoichiometry of interactions between the SH3 domains and PRMs is important for these proteins to assemble and phase separate.

Phase Separation Is Dependent upon Valency of Phosphotyrosine Sites

Upon the inclusion of a doubly phosphorylated Nephrin peptide, the concentrations required for phase separation decreases to 7 μM N-WASP and 15 μM Nck (Figure 2.2). Upon adding the triply phosphorylated Nephrin at 3 μM (the same pY concentration in both cases of doubly and triply phosphorylated versions, phase separation occurs at much lower concentrations of 1 μM N-WASP and 5 μM Nck. These data suggest that there is a strong correlation between the number of phosphorylation sites and the phase separation behavior of these molecules. This phenomenon is similar to phase separation observed with multivalent interactions between SH3 domains and PRMs with engineered proteins, as shown previously in the Rosen lab by Hui-Chun Cheng and Pilong Li (Li et al, 2012).

The dependency of phase separation on the degree of phosphorylation also suggests that kinases and phosphatases could play an important role in regulating this phenomenon. Activity of a kinase would directly affect the degree of phosphorylation, which would in turn affect association of these multivalent molecules. In addition, the activity of the kinase could in turn be affected by the phase separation behavior of the proteins (increase in viscosity, higher degree of recruitment of the proteins into droplets, etc.), creating feedback. These interesting possibilities could be aspects of future considerations.

Upon addition of a phosphatase VHR (a dual specificity phosphatase), the droplets dissolved. 10 μM VHR was added to droplets consisting of 3 μM p-Nephrin, 2 μM N-WASP and 10 μM Nck. Over the time course of 4 hours, droplets shrink and finally disappear (data not shown). These dissolution data suggest that formation and deformation of the phase-separated assemblies could be regulated by phosphorylation and dephosphorylation.

Monovalent Peptide Competes Droplets

Our data regarding valency dependence suggest that multivalent interactions drive the formation of large polymers, which phase separate in solution, as at the same module concentration, higher-valent molecules phase-separated at lower concentrations. Subsequently, a monovalent component in the mixture should also be able to inhibit the formation of the droplet phase. To test this hypothesis, I used droplets made from proteins consisting of multiple SH3s and PRMs, and tested for the presence or absence of droplets with the inclusion of a monovalent component. In the presence of a pentavalent SH3 construct (SH3-5R, see Table 2 for sequence) and an octavalent PRM (PRM-8R, Table 2), phase separation was observed at 100 μM of each protein (Figure 2.3). In the presence of 1 mM PRM(H), a monovalent peptide with a K_d of 10 μM towards the SH3 domain (Li et al, 2012), phase separation did not occur up to a concentration of 300 μM of

each protein. Inclusion of another peptide at 1 mM (PRM) that has a K_d of 350 μM towards the SH3 domain does not have any effect on the concentration required for phase separation, inducing droplets at 100 μM each of SH3 and PRM proteins. Therefore, the monovalent peptide specifically inhibits the SH3 – PRM interaction and causes an inhibition of phase separation, strongly suggesting that specific interactions of SH3 and PRMs (and not the non-specific assembly between the two proteins), drive the molecular assembly that is important for phase separation of the complexes.

Multivalent Interactions Induce Formation of Large Species

Our data suggest that specific interactions between the SH3 domains and PRMs drive formation of large polymeric species. We used light scattering methods for the determination of the sizes of the polymeric species formed by these interactions. Dynamic light scattering (DLS) uses a monochromatic light source (a laser) to irradiate a sample. The scattered light fluctuates over time because of the random diffusion of the molecules. The fluctuation in scattered intensity then allows us to plot an autocorrelation function between the scattered intensities over time. The autocorrelation function of the intensity is used to measure diffusion coefficients. At short times, the autocorrelation is high as the diffusion is over short distance, and at long times the autocorrelation function decays

exponentially. The decay time is used to obtain the diffusion constant by fitting the decay plot to exponential functions (Berne, 1976).

Consistent with an infinitely large cross-linked polymer, DLS of the droplet phase consists of a very slowly decaying phase (initial observation made by Hui-Chun Cheng). Here, we cannot conclusively define the correct size of the molecular species because we have to assume a globular shape of the species formed. However, it is clear from the data (**Figure 2.4**) that the droplet phase consists of components with complex decay rates that can be divided into a faster phase and a slower phase. The faster phase shows a decay time constant of 0.2 ms, whereas the slower phase shows decay rates up to 20 ms. The multiphasic property of the decay time constants suggests that the multivalent proteins form sizes with complex distributions.

To measure the sizes of the particles formed by the multivalent interactions of the SH3 domains and PRMs, I used SH3-5R, and different valencies of the PRMs (PRM-4R, PRM-2R, and PRM-1R). The hydrodynamic radii of the complexes were obtained from the diffusion coefficients by assuming that the species are globular in shape. At a fixed concentration of SH3-5R, (850 μM module and 170 μM total protein concentration, different concentrations of PRMs were added. As shown in **Figure 2.5**, addition of PRM-4R to SH3-5R demonstrates a steady increase in the hydrodynamic radii of the species formed until the critical

concentration for phase separation is reached (orange, filled circles). After the critical concentration (orange, open circles), the hydrodynamic radii of the solution (with the droplet phase removed after centrifugation), decreases. If the same experiment is performed with the divalent protein PRM-2R, a similar increase in the hydrodynamic radii is observed (**Figure 2.5**), blue. However, at each concentration, the hydrodynamic species formed with PRM-4R are larger than the species formed with PRM-2R. These data suggest that the higher-valent molecules form larger species than lower-valent molecules. The increase in hydrodynamic radii observed does not result from an increase in the concentration of the molecules (which could cause an increase in viscosity and therefore a decrease in diffusion coefficients), because addition of monovalent peptides PRM-1R and PRM (H)-1R to SH3-5R at the same total concentrations results in lower increases in the hydrodynamic radii compared to the divalent or tetravalent PRMs (**Figure 2.5**, green and red).

In the DLS experiment shown in **Figure 2.5**, after phase separation occurs, the sizes of the species in the solution (with the droplets removed after centrifugation) decreases. This result was observed for experiments with either PRM-4R or PRM-2R, suggesting that after phase separation has occurred, the higher-valent species formed in solution (and therefore the larger species) have a higher propensity to associate with the droplet phase. This observation is similar to that predicted in the theory of polymeric sol-gel transitions (Flory, 1953).

Therefore, it is possible that the droplets also consist of species formed by a sol-gel transition and the approach to phase separation could be thermodynamically coupled to a sol-gel transition.

We further analyzed the droplet phase using a multi-angle DLS apparatus. The frequency of the faster phase shows a linear dependence upon q^2, where q represents the wave-vector (and corresponds to the scattering angle), whereas the intermediate and slower phases show a non-linear behavior with q^2 (**Figure 2.6**). The frequency of the supernatant phase (after removing the droplet phase) also shows a linear dependence upon q^2. If the solution contained only discrete species, the decay times of the autocorrelation function of the scattered intensity would result only due to the translational diffusion of the discrete species. Therefore, in this case the frequency of a particular decay time would be linear to the square of the wave-vector (dependent upon q^2). However, if the solution contained species that were entangled or interacting with each other, the decay times of the scattered intensities would also depend upon the dynamics of entanglement of the species in solution. In this latter case, q^2 is independent of the frequency, and such a solution would be unlikely to consist of discrete species (Li, 2010). These data are consistent with the faster phase and the supernatant consisting of discrete species that have a single relaxation mode and the droplets representing species that have multiple relaxation modes and therefore could be cross-linked species.

Characterization of Droplets Using Cryo-Electron Microscopy

We attempted to observe the probable cross-linked species inside the droplets using cryo-electron microscopy. Droplets were captured immediately after mixing SH3-5R and PRM-4R, and frozen on an EM grid. Droplets were too dense to structurally analyze the internal contents. However, edges of the droplets were highly irregular at the ~10 nm scale **(**Figure 2.7**,** Figure 2.8**).**

The irregularity at such scale suggests presence of large molecules inside the droplets. However, we could not conclusively determine with EM whether the droplets do consist of cross-linked species. An attempt at tomography (taking cryoEM images) of the droplets also suggested presence of a dense assembly, but we were unable to conclusively determine the molecular structure because of a high density of proteins.

Multivalent Interactions are Widely Observed in Biology

Data in the Rosen lab suggest that multivalent molecules of many different biological systems could undergo phase separation. To determine whether modular domains have been observed in the literature to form large punctate bodies in cells, I took different modular domains from (Pawson & Nash, 2003; Schultz et al, 1998; Seet et al, 2006) and analyzed them through the SMART database (Schultz et al, 1998) to determine if they exist in multivalent forms.

Then, the modular domains that exist in multivalent forms were searched on Pubmed to associate with the terms “punctate," “cellular bodies,” etc.

The search was also extended further to specially include observations made in the literature of different RNA bodies found in the nucleus (Spector, 2006). The analysis suggested that many different multivalent proteins exist that form some sort of punctate bodies in cells **(Table 1)**. The analysis further suggested that multivalent interactions could generally produce large assemblies in cells, and that the phenomenon of phase separation due to multivalent interactions could possibly be the mechanism behind formation of several such bodies observed in the literature.

Phase Separation through Multivalent Interactions Induce Switch-like Activation of the Arp2/3 Complex

These analyses of multivalent proteins in biology suggest a possible way to regulate biochemical activity of several of these proteins through clustering of those molecules in the droplet phase, if in fact some of these clusters are formed via phase separation of multivalent interactions. Several observed features of phase separation could affect their biochemical functions. For example, the clusters probably contain higher order oligomers, which in many cases could induce higher degree of activation. If this were true, the sharpness with which

these entities form would enable a switch-like activation of these proteins. Higher viscosity of the clusters and therefore lower mobility would also slow dynamics of these molecules in the clusters, increasing the localization times of N-WASP and Arp2/3 in the clustered areas, and thereby locally affecting their activities.

To test a possible biochemical regulation of N-WASP through its phase separation with Nck and Nephrin, I used a pyrene-actin kinetic assay. Actin labeled with the fluorophore pyrene shows an increase in fluorescence of pyrene upon assembling into filaments (Cooper et al, 1983; Kouyama & Mihashi, 1981). To test the effect of phase separation on the activation of N-WASP, I made two different versions of N-WASP. The first one was GBD-P-VCA, which includes the regulatory region GBD, the proline-rich region, and the activity bearing VCA region. The second molecule is the inactive N-WASPΔ, which consists of the GBD and P motifs, but lacks the VCA region. Therefore, the N-WASPΔ molecule is able to incorporate into the higher order assemblies through the proline-rich motifs, but does not activate the Arp2/3 complex.

In the assays, I used fixed concentrations of 4 μM actin with 10% pyrene labeled, 10 nM Arp2/3 complex,10 μM Nck, 3 μM Nephrin and 50 nM GBD-P-VCA. In the presence of only actin (4 μM with % pyrene labeled), or actin with 10 nM Arp2/3 complex, the fluorescence increases slowly within 30 minutes, not reaching a steady state (**Figure 2.9**, **Figure 2.10**). With Nck, Nephrin and GBD-P-VCA

added, the activity towards the Arp2/3 complex increases modestly, reaching steady state around 1700 s. I then used several concentrations of the N-WASPΔ protein. With 200 nM, 500 nM and 700 nM concentrations of N-WASPΔ, activity remains the same as without the N-WASPΔ protein. However, above 700 nM N-WASPΔ, the activity increases sharply, reaching steady state at around 900 s. In a separate experiment, I found that the phase separation of Nck, Nephrin and N-WASP occurred at and above 700 nM of the N-WASPΔ molecule. Therefore, phase separation coincides with a sharp increase in activity of N-WASP. This occurs presumably because of oligomerization or polymerization of N-WASP in the droplet phase.

I performed similar experiments replacing the GBD-P-VCA construct with GBD-VCA, lacking the multivalent proline-rich region (**Figure 2.9**). In these experiments, adding the N-WASPΔ construct did not have any effect on the increase in activity of the GBD-VCA molecule. These data suggest that the proline-rich region is important for the higher degree of activation of N-WASP in the presence of Nephrin and Nck, most likely because of its incorporation into polymers of Nephrin, Nck and N-WASP.

I also observed that actin filaments specifically localize to the droplets. Using a fraction of actin labeled with rhodamine (at 10 %) and also using phalloidin-Alexa488, I observed that phalloidin-Alexa488 specifically localizes to regions of

actin-rhodamine, as imaged by fluorescence microscopy (**Figure 2.10**). The filaments of actin were only observed inside the droplets, suggesting that the droplets were sites of higher actin assembly. Together with the kinetic data from **Figure 2.9**, these localization data suggest that droplets are preferential sites of actin assembly, and upon formation of droplets there is a large degree of enhancement in the rate of actin assembly.

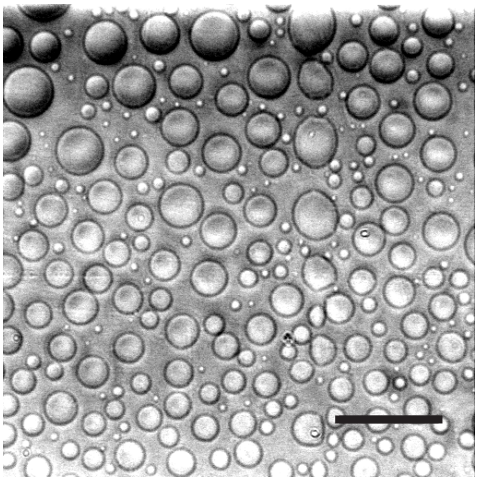

Figure 2.1. Wide range of droplet sizes are observed with phase separation. Droplets observed under a bright field microscope, using Nck, N-WASP and p-Nephrin. Scale bar is 100 μm wide.

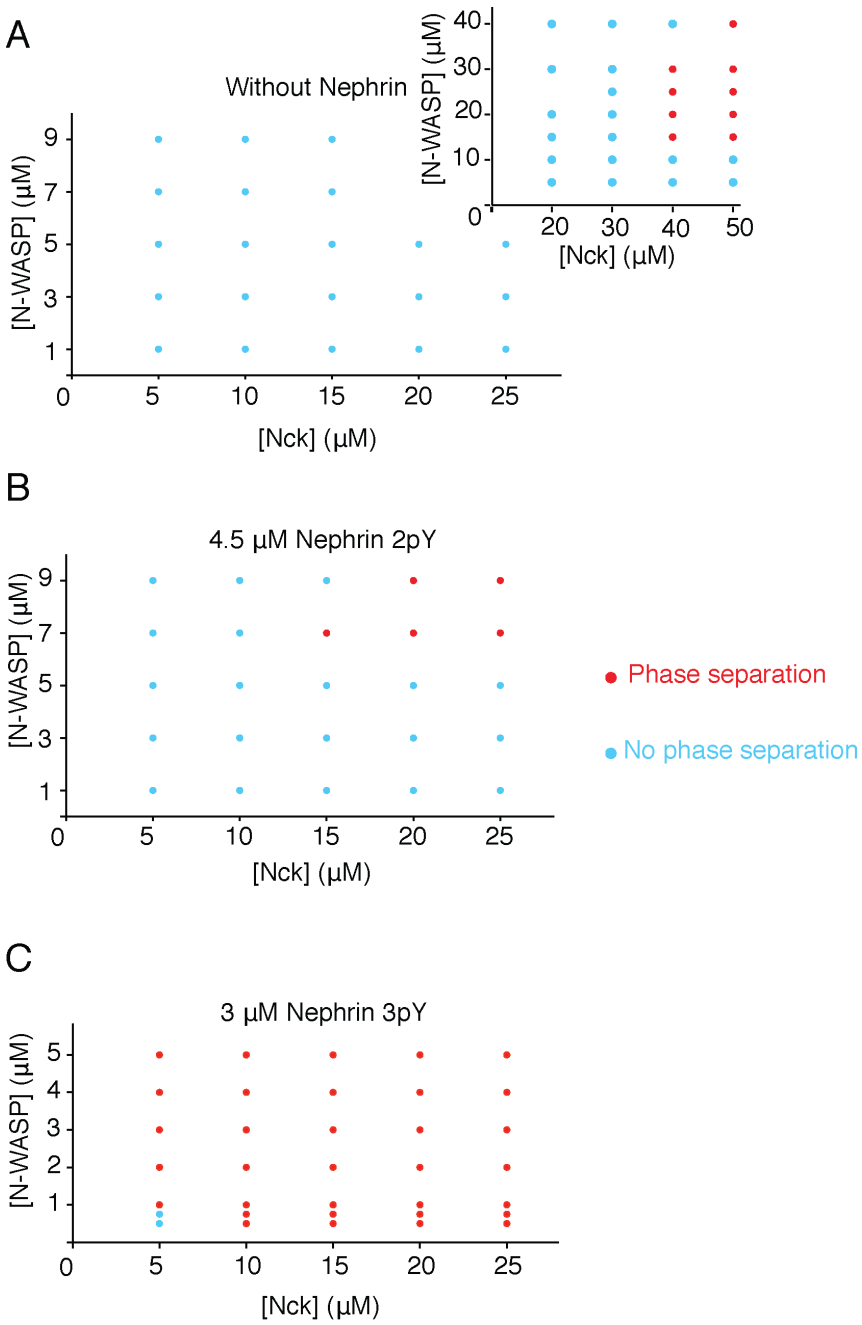

Figure 2.2. Number of phosphotyrosines in Nephrin controls degree of phase separation of Nephrin, Nck and N-WASP polymers. A) Phase diagram showing phase separation (red dots) or absence of phase separation of Nck and N-WASP. Inset shows higher concentrations of Nck and N-WASP. B-C) Phase diagrams of Nephrin, Nck and N-WASP in the presence of di-phosphorylated and tri-phosphorylated Nephrin, respectively.

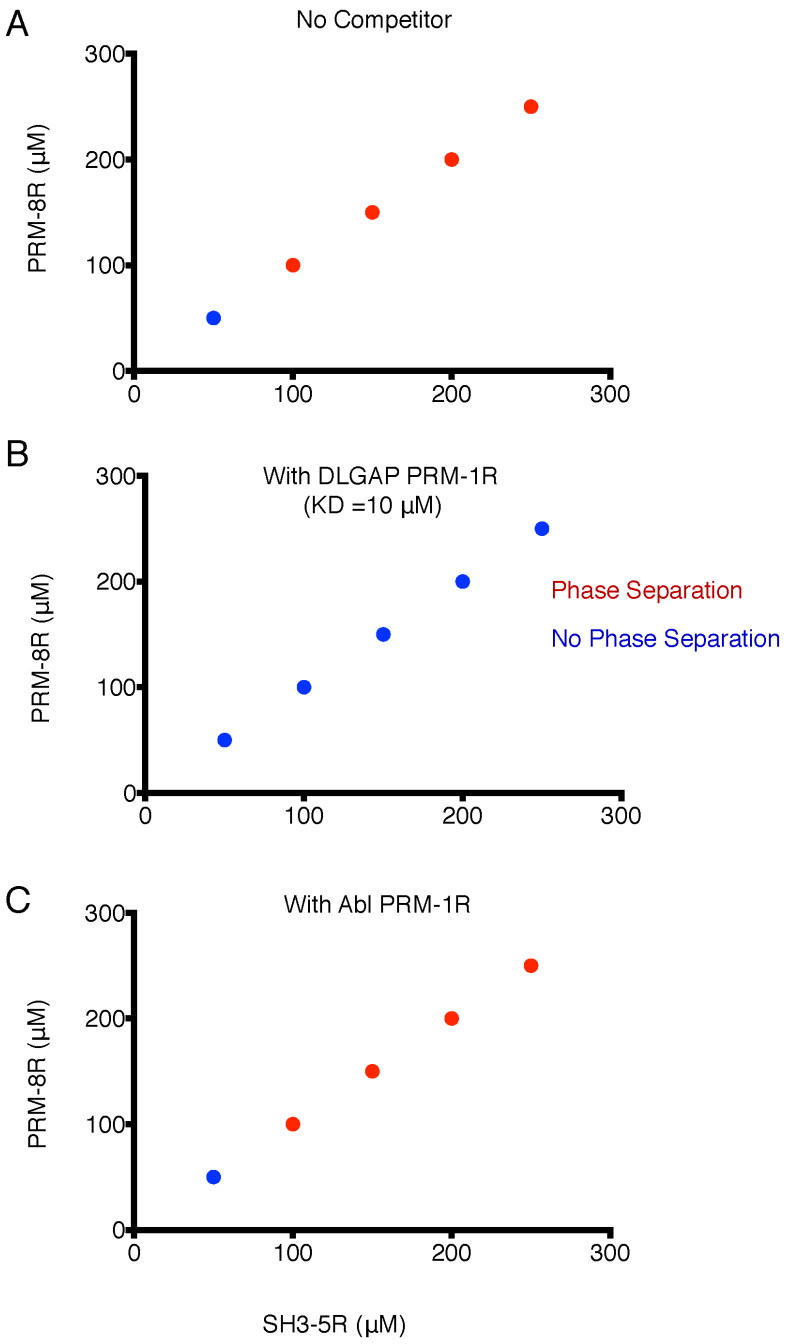

Figure 2.3. Monovalent peptide inhibits phase separation. Phase diagrams showing presence (red dots) or absence (blue dots) of liquid droplets. X-axes correspond to SH3-5R concentrations and y-axes correspond to PRM-8R concentrations. Experiments were performed in the absence of another peptide (A), or in the presence of monovalent DLGAP PRM-1R (B) or Abl PRM-1R (C).

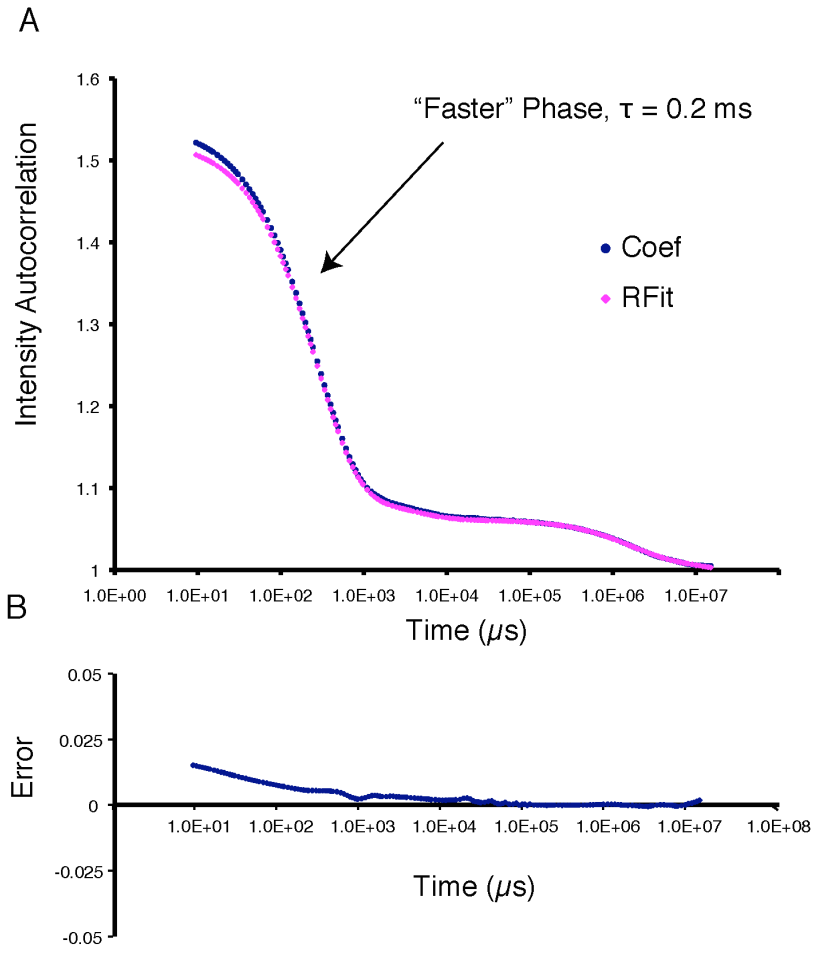

Figure 2.4. Droplets consist of slowly diffusing large polymers. A) Dynamic light scattering experiment performed with droplets made using SH3-5R with PRM-8R. Blue dots represent obtained measurements of intensity autocorrelation and the pink dots represent fits. The faster phase among the multiple decay rates corresponds to 0.2 ms. **B)** Error in fitting the data obtained in **(A)**.

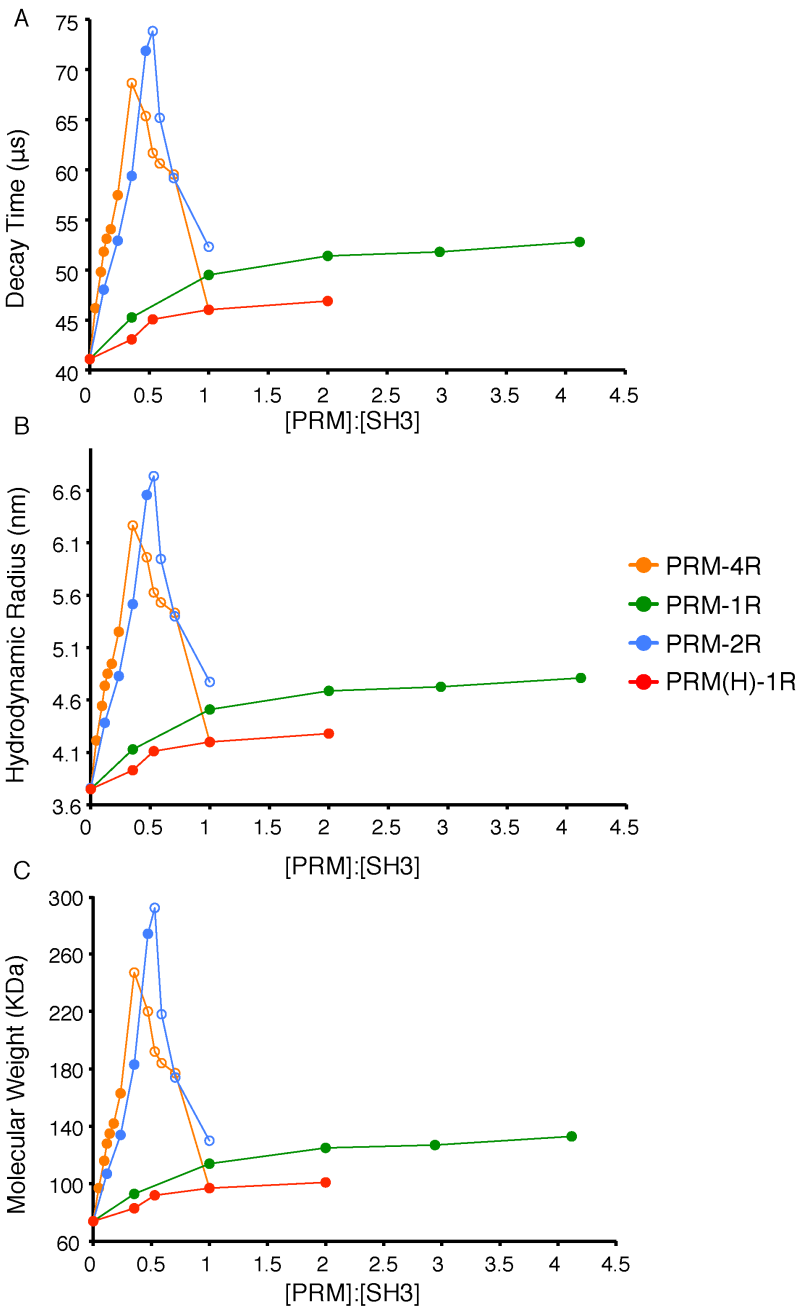

Figure 2.5. Dynamic light scattering experiments suggest formation of large species through multivalent interactions. A) – C) Decay time constants, hydrodynamic radii and molecular weights of species formed using SH3-5R and PRM-1R (green), PRM(H)-1R (red), PRM-2R (blue) and PRM-4R (orange). Data were collected at a fixed concentration of SH3-5R at 170 µM and varied PRM concentrations.

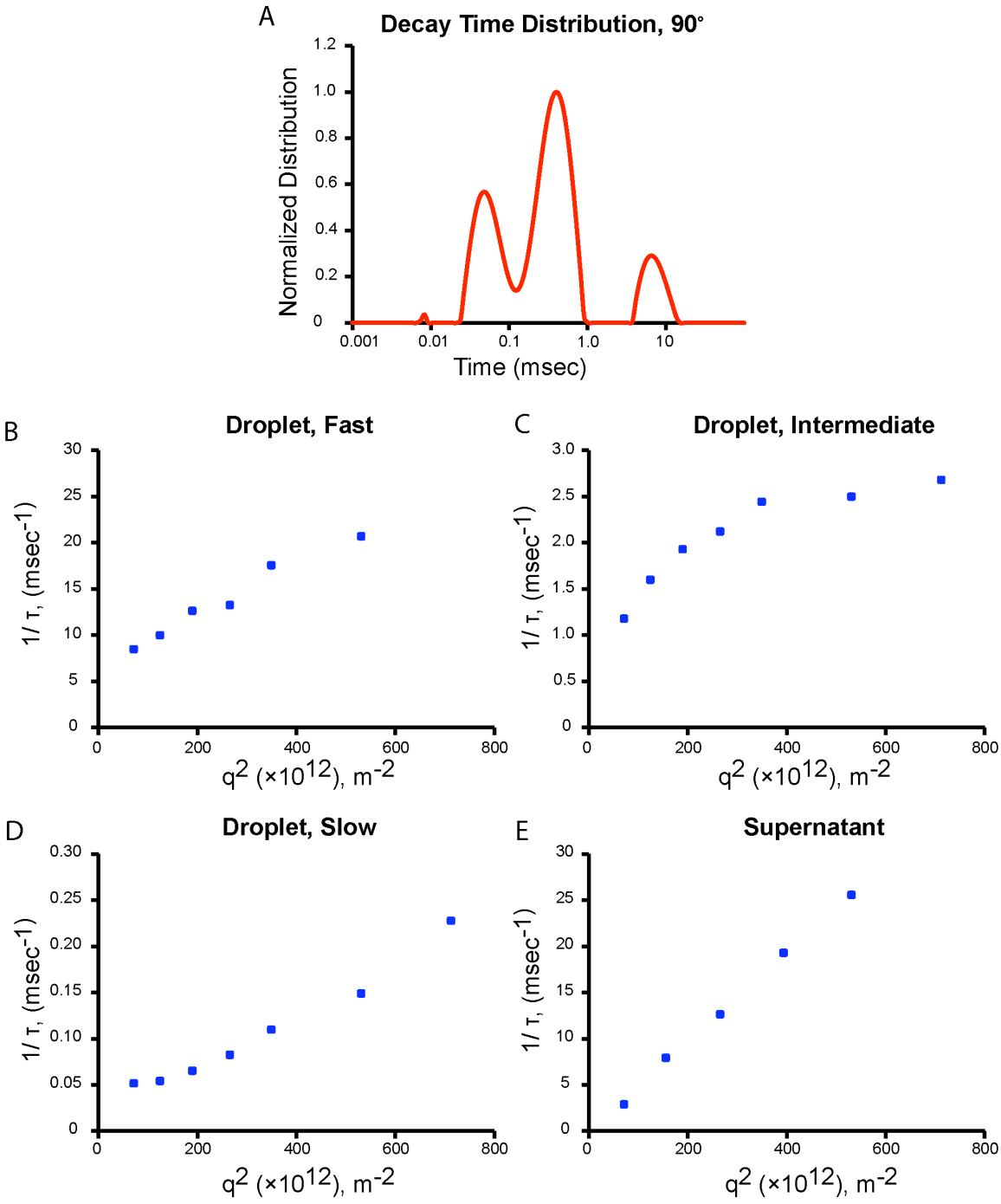

Figure 2.6. Multi-angle dynamic light scattering (MA-DLS) experiments suggest presence of complex mixtures of particles in the droplets, inconsistent with a discrete specimen. A) Decay time distribution obtained with droplets of SH3-5R + PRM-5R. **B) – D)** Variation in $1/\tau$ with q^2 for the fast, intermediate and slow phases. **E)** Similar analysis for the supernatant removing droplets shows a linear change in $1/\tau$ with q^2, similar to the data for the fast phase within the droplets.

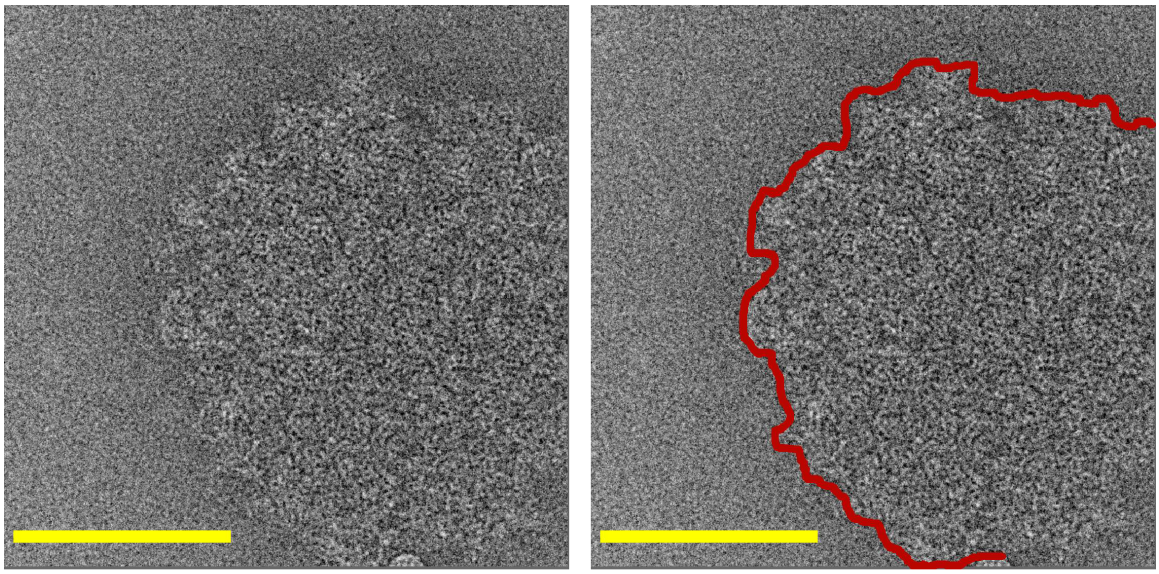

Figure 2.7. Cryo-electron microscopy images of droplets. Images show droplets having disordered edges. The disordered edge in the droplet is highlighted by the red curves on the right image. Scale bar is 100 nm wide.

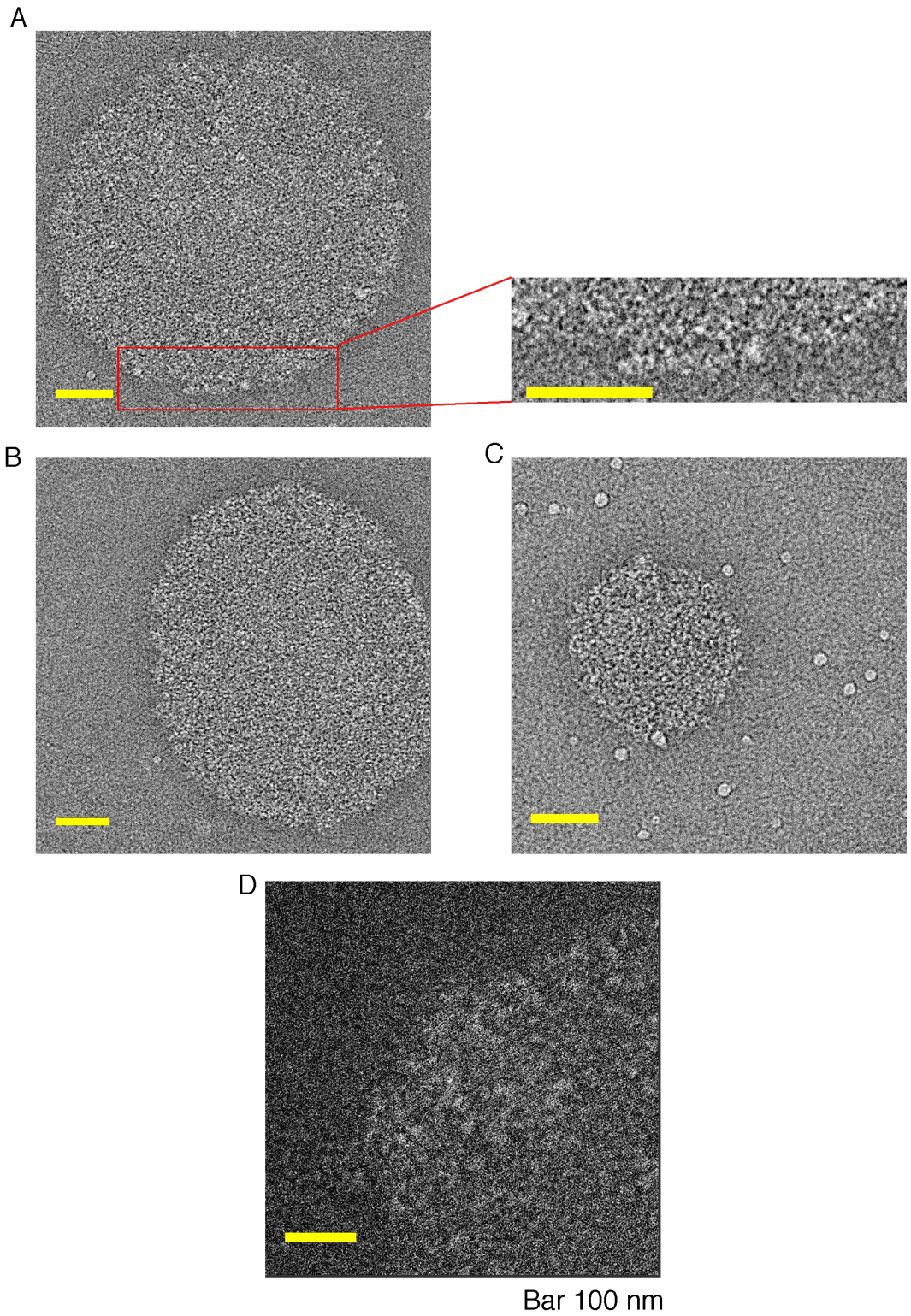

Figure 2.8. **Cryo-electron microscopy images of droplets.** Additional cryo-electron images of droplets.

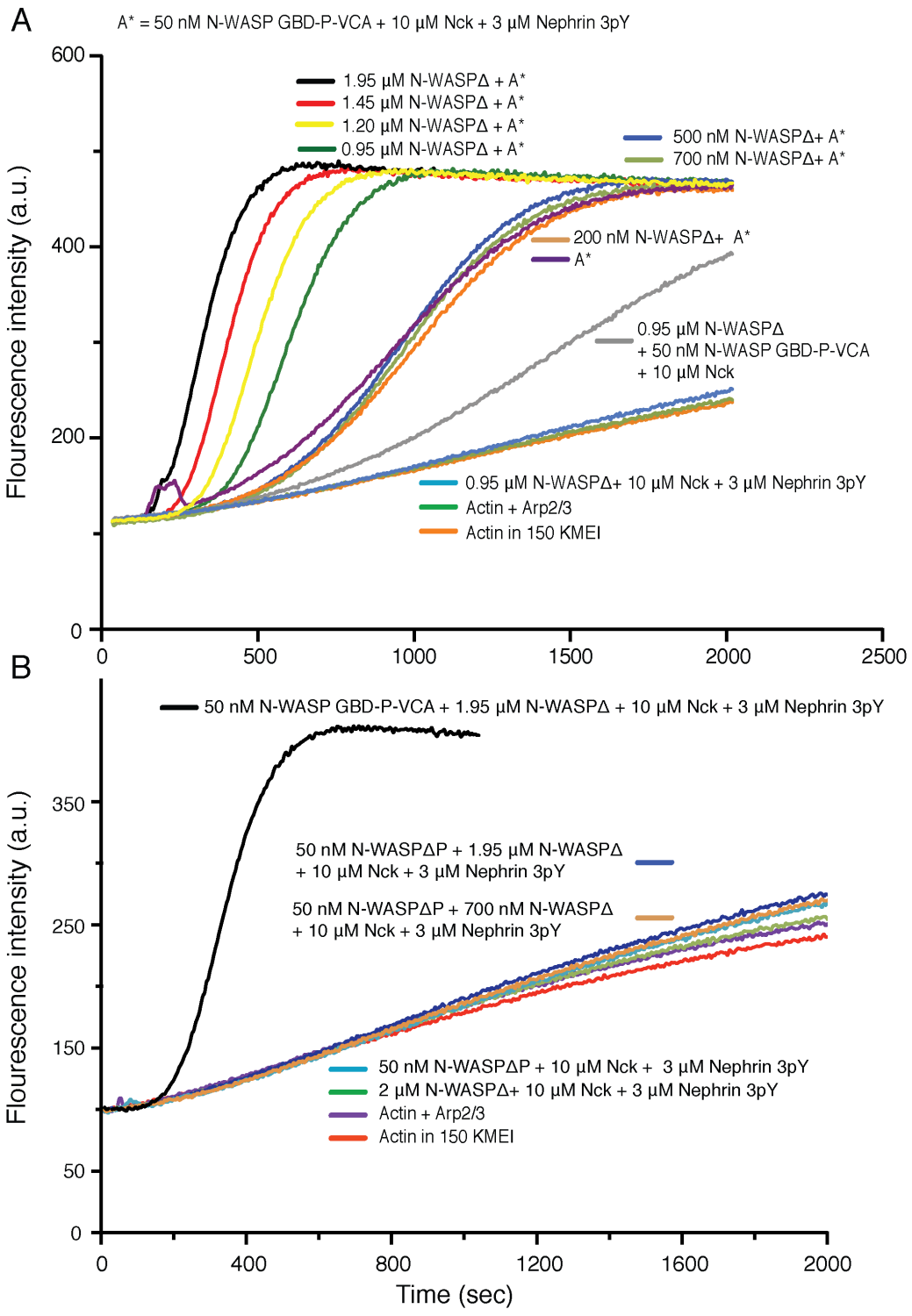

Figure 2.9. Phase separation enhances actin assembly. A) Fluorescence increase of pyrene-actin upon assembling into actin filaments. Experiments were performed at fixed concentrations of the Arp2/3 complex (10 nM), actin (4 µM), p-Nephrin (3 µM), Nck (10 µM) and N-WASP B-GBD-P-VCA (50 nM), and varied

concentrations of N-WASPΔ, as indicated in the figure. At 700 nM N-WASPΔ (green curve), the rate of actin assembly changes sharply as compared to lower concentrations. B) The sharp change is not observed when the N-WASP B-GBD-P-VCA construct is replaced by a B-GBD-VCA construct lacking the proline-rich (P) region.

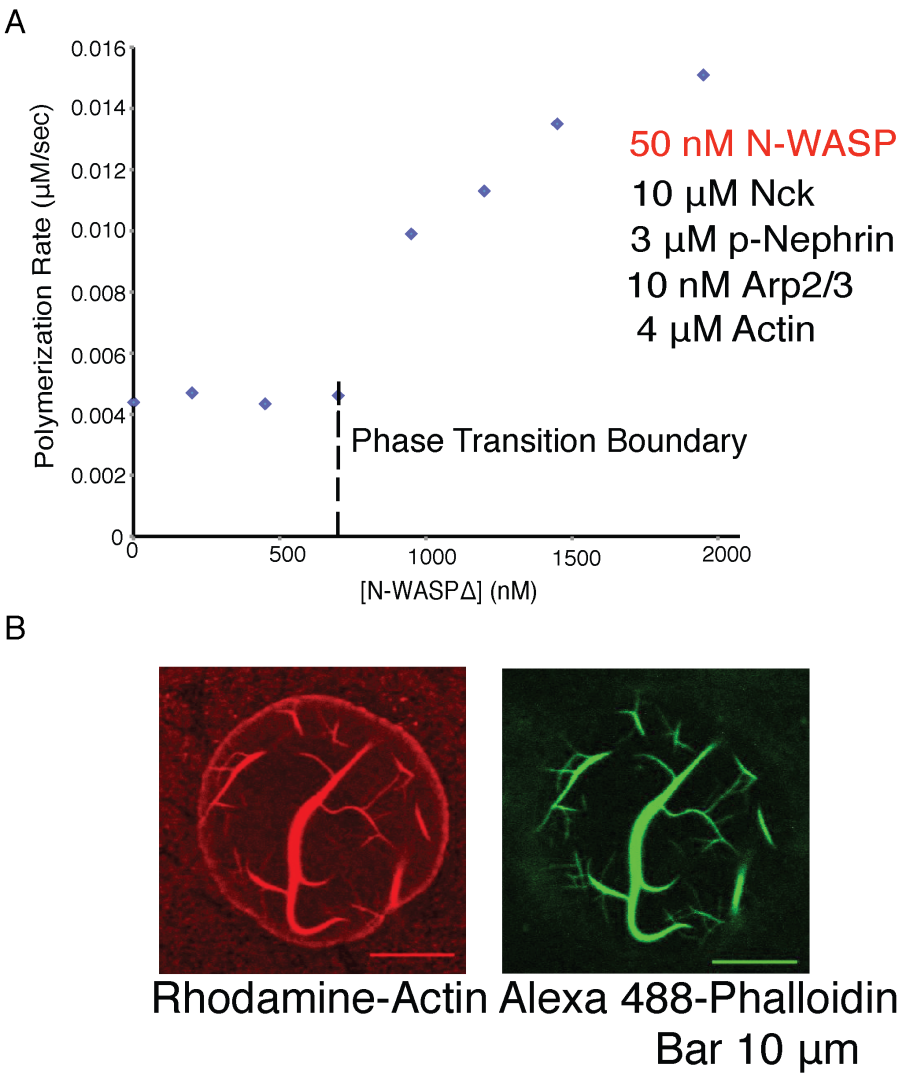

Figure 2.10. Phase separation enhances actin assembly. A) Polymerization rates plotted as a function of N-WASPΔ concentration. Rates were obtained from the raw data shown in Figure 2.8 (A). B) Actin filaments specifically localize inside the droplets (left), as shown in confocal images taken with droplets made using 10 μM Nck, 3 μM p-Nephrin and 2 μM N-WASP (B-P-VCA, including 10 nM Arp2/3 complex, 4 μM actin (with 10 % rhodamine-labeled) and 300 nM Alexa-488 phalloidin. Left image depicts rhodamine-actin while the right image shows Alexa-488 phallodin staining. Scale bars are 10 μm wide.

Table 1. List of multivalent proteins found in various cellular bodies.					
Protein	**Domain**	**Valency**	**Localization**	**Genome**	**Reference**
Tud	Tudor	10	Polar Granules	*D. melanogaster*	[1]
Pasilla	KH	3	Nuclear Puncta	*D. melanogaster*	[2]
Staufen	DSRM	4	P-bodies	*D. melanogaster*	[3]
Vgl1	KH	13	Stress Granules	*S. pombe*	[4]
SCP160	KH	7	Stress Granules	*S. cerevisiae*	[4]
Pab1	RRM	4	Stress Granules	*S. cerevisiae*	[5]
Hek2p	KH	3	Uncharacterized Cytoplasmic Puncta	*S. cerevisiae*	[6]
EDE1	EH	3	Uncharacterized Cytoplasmic Puncta	*S. cerevisiae*	[7]
FRQ1	EfH	3	Uncharacterized Cytoplasmic Puncta	*S. cerevisiae*	[7]
PAN1	EfH	4	Uncharacterized Cytoplasmic Puncta	*S. cerevisiae*	[7]
Puf-5	Pumilio	7	P-body like mRNP granules	*C. elegans*	[8]
UNC-75	RRM	3	Nuclear Speckles	*C. elegans*	[9]
UNC-97	LIM	5	Focal Adhesion	*C. elegans*	[10]
Microcephalin	BRCT	3	DNA-damage Foci	*H. sapiens*	[11]
TopBP1	BRCT	7	DNA-damage Foci	*H. sapiens*	[12]
PABP	RRM	4	Stress Granules	*H. sapiens*	[13]
IMP1	KH	3	RNP Granules	*H. sapiens*	[14]
TIA1	RRM	3	Stress Granules	*H. sapiens*	[15]
PABP-1	RRM	4	Stress Granules	*H. sapiens*	[16]
c-Myb	SANT	3	Nuclear Speckles	*H. sapiens*	[17]
PTB-associated splicing factor	Poly-proline	>6	Nuclear Speckles	*H. sapiens*	[18]
Splicing Factor 3b	Poly-proline	>7	Nuclear Speckles	*H. sapiens*	[19]
SNP70	Poly-proline	>7	Nuclear Speckles	*H. sapiens*	[20]
Mucin	Poly-proline	>10	Mucin Granules	*H. sapiens*	[21]
WIP	Poly-proline	>6	Lytic Granules	*H. sapiens*	[22]
IQGAP1	IQ	4	hStaufen-containing Granules	*H. sapiens*	[23]
Leupaxin	LIM	4	Focal Adhesion	*H. sapiens*	[24]
Zyxin	LIM	3	Focal Adhesion	*H. sapiens*	[25]
HuR	RRM	3	Stress Granules	*H. sapiens*	[26]
PTB1	RRM	4	Perinucleolar Compartment	*H. sapiens*	[27]
CUG-BP	RRM	3	Perinucleolar Compartment	*H. sapiens*	[28]
KSRP	KH	4	Perinucleolar Compartment	*H. sapiens*	[29]
Sp1	ZnF	3	PML Bodies	*H. sapiens*	[30]
PLZF	ZnF	9	PML Bodies	*H. sapiens*	[30]
RNF17	Tudor	4	Nuages	*H. sapiens*	[31]
hnRNP Q	RRM	3	P-Bodies	*H. sapiens*	[32]
HuD	RRM	3	P-Bodies	*H. sapiens*	[32]
PCBP2	KH	3	P-Bodies	*H. sapiens*	[32]

hnRNP E1	KH	3	Interchromatin Granules	*M. musculus*	[33]
hnRNP E2	KH	3	Interchromatin Granules	*M. musculus*	[33]
hnRNP K	KH	3	Interchromatin Granules	*M. musculus*	[33]
KH type splicing regulatory factor	KH	4	Interchromatin Granules	*M. musculus*	[33]
APOBEC-1	RRM	3	Interchromatin Granules	*M. musculus*	[33]
Rod1	RRM	4	Interchromatin Granules	*M. musculus*	[33]
HnRNPL	RRM	3	Interchromatin Granules	*M. musculus*	[33]
hnRNP F/H	RRM	3	Interchromatin Granules	*M. musculus*	[33]
hnRNP H'	RRM	3	Interchromatin Granules	*M. musculus*	[33]
hnRNP I	RRM	4	Interchromatin Granules	*M. musculus*	[33]
hnRNP L	RRM	3	Interchromatin Granules	*M. musculus*	[33]
hnRNP M	RRM	3	Interchromatin Granules	*M. musculus*	[33]
Siah binding protein	RRM	3	Interchromatin Granules	*M. musculus*	[33]
Splicing factor HCC1	RRM	3	Interchromatin Granules	*M. musculus*	[33]
U2AF65	RRM	3	Interchromatin Granules	*M. musculus*	[33]
Elav-like 1	RRM	3	Interchromatin Granules	*M. musculus*	[33]
RNA binding protein HuR	RRM	3	Interchromatin Granules	*M. musculus*	[33]
Rnpc2	RRM	3	Interchromatin Granules	*M. musculus*	[33]
Zinc finger RNA bindingprotein, ZFR (KIAA1086)	ZnF	3	Interchromatin Granules	*M. musculus*	[33]
POZ domain protein FBI-1	ZnF_C2H2	4	Interchromatin Granules	*M. musculus*	[33]
POZ/zinc finger transcription factor, ODA-8	ZnF_C2H2	5	Interchromatin Granules	*M. musculus*	[33]
CPSF 30 kDa subunit	ZnF_C3H1	5	Interchromatin Granules	*M. musculus*	[33]
KIAA0663 protein	ZnF_C3H1	3	Interchromatin Granules	*M. musculus*	[33]
TDRD6	Tudor	7	Nuages	*M. musculus*	[34]
TDRD7	Tudor	3	Nuages	*M. musculus*	[34]
HSF1	HSF	Oligomer	Stress Granule	*M. musculus*	[35]

1. Arkov, A.L., et al., *The role of Tudor domains in germline development and polar granule architecture.* Development, 2006. **133**(20): p. 4053-62.
2. Seshaiah, P., et al., *pasilla, the Drosophila homologue of the human Nova-1 and Nova-2 proteins, is required for normal secretion in the salivary gland.* Dev Biol, 2001. **239**(2): p. 309-22.
3. Barbee, S.A., et al., *Staufen- and FMRP-containing neuronal RNPs are structurally and functionally related to somatic P bodies.* Neuron, 2006. **52**(6): p. 997-1009.
4. Wen, W.L., et al., *Vgl1, a multi-KH domain protein, is a novel component of the fission yeast stress granules required for cell survival under thermal stress.* Nucleic Acids Res, 2010.
5. Hoyle, N.P., et al., *Stress-dependent relocalization of translationally primed mRNPs to cytoplasmic granules that are kinetically and spatially distinct from P-bodies.* J Cell Biol, 2007. **179**(1): p. 65-74.
6. Noree, C., et al., *Identification of novel filament-forming proteins in Saccharomyces cerevisiae and Drosophila melanogaster.* J Cell Biol, 2010. **190**(4): p. 541-51.
7. Huh, W.K., et al., *Global analysis of protein localization in budding yeast.* Nature, 2003. **425**(6959): p. 686-91.
8. Noble, S.L., et al., *Maternal mRNAs are regulated by diverse P body-related mRNP granules during early Caenorhabditis elegans development.* J Cell Biol, 2008. **182**(3): p. 559-72.
9. Loria, P.M., et al., *Two neuronal, nuclear-localized RNA binding proteins involved in synaptic transmission.* Curr Biol, 2003. **13**(15): p. 1317-23.
10. Norman, K.R., et al., *UNC-97/PINCH is involved in the assembly of integrin cell adhesion complexes in Caenorhabditis elegans body wall muscle.* Dev Biol, 2007. **309**(1): p. 45-55.
11. Wood, J.L., et al., *MCPH1 functions in an H2AX-dependent but MDC1-independent pathway in response to DNA damage.* J Biol Chem, 2007. **282**(48): p. 35416-23.
12. Zhang, F., J. Wu, and X. Yu, *Integrator3, a partner of single-stranded DNA-binding protein 1, participates in the DNA damage response.* J Biol Chem, 2009. **284**(44): p. 30408-15.
13. Ralser, M., et al., *An integrative approach to gain insights into the cellular function of human ataxin-2.* J Mol Biol, 2005. **346**(1): p. 203-14.
14. Nielsen, F.C., et al., *Cytoplasmic trafficking of IGF-II mRNA-binding protein by conserved KH domains.* J Cell Sci, 2002. **115**(Pt 10): p. 2087-97.
15. Delestienne, N., et al., *The splicing factor ASF/SF2 is associated with TIA-1-related/TIA-1-containing ribonucleoproteic complexes and contributes to post-transcriptional repression of gene expression.* FEBS J, 2010. **277**(11): p. 2496-514.
16. Kedersha, N., et al., *Stress granules and processing bodies are dynamically linked sites of mRNP remodeling.* J Cell Biol, 2005. **169**(6): p. 871-84.

17. Alm-Kristiansen, A.H., et al., *FLASH acts as a co-activator of the transcription factor c-Myb and localizes to active RNA polymerase II foci.* Oncogene, 2008. **27**(34): p. 4644-56.
18. Shav-Tal, Y., et al., *Nuclear relocalization of the pre-mRNA splicing factor PSF during apoptosis involves hyperphosphorylation, masking of antigenic epitopes, and changes in protein interactions.* Mol Biol Cell, 2001. **12**(8): p. 2328-40.
19. Terada, Y. and Y. Yasuda, *Human immunodeficiency virus type 1 Vpr induces G2 checkpoint activation by interacting with the splicing factor SAP145.* Mol Cell Biol, 2006. **26**(21): p. 8149-58.
20. Craggs, G., et al., *A nuclear SH3 domain-binding protein that colocalizes with mRNA splicing factors and intermediate filament-containing perinuclear networks.* J Biol Chem, 2001. **276**(32): p. 30552-60.
21. Verdugo, P., *Mucin exocytosis.* Am Rev Respir Dis, 1991. **144**(3 Pt 2): p. S33-7.
22. Krzewski, K., X. Chen, and J.L. Strominger, *WIP is essential for lytic granule polarization and NK cell cytotoxicity.* Proc Natl Acad Sci U S A, 2008. **105**(7): p. 2568-73.
23. Villace, P., R.M. Marion, and J. Ortin, *The composition of Staufen-containing RNA granules from human cells indicates their role in the regulated transport and translation of messenger RNAs.* Nucleic Acids Res, 2004. **32**(8): p. 2411-20.
24. Tanaka, T., et al., *LIM domain-containing adaptor, leupaxin, localizes in focal adhesion and suppresses the integrin-induced tyrosine phosphorylation of paxillin.* Cancer Sci, 2010. **101**(2): p. 363-8.
25. Krylyshkina, O., et al., *Nanometer targeting of microtubules to focal adhesions.* J Cell Biol, 2003. **161**(5): p. 853-9.
26. Gallouzi, I.E., et al., *HuR binding to cytoplasmic mRNA is perturbed by heat shock.* Proc Natl Acad Sci U S A, 2000. **97**(7): p. 3073-8.
27. Huang, S., et al., *The dynamic organization of the perinucleolar compartment in the cell nucleus.* J Cell Biol, 1997. **137**(5): p. 965-74.
28. Timchenko, L.T., et al., *Identification of a (CUG)n triplet repeat RNA-binding protein and its expression in myotonic dystrophy.* Nucleic Acids Res, 1996. **24**(22): p. 4407-14.
29. Markovtsov, V., et al., *Cooperative assembly of an hnRNP complex induced by a tissue-specific homolog of polypyrimidine tract binding protein.* Mol Cell Biol, 2000. **20**(20): p. 7463-79.
30. Vallian, S., K.V. Chin, and K.S. Chang, *The promyelocytic leukemia protein interacts with Sp1 and inhibits its transactivation of the epidermal growth factor receptor promoter.* Mol Cell Biol, 1998. **18**(12): p. 7147-56.
31. Pan, J., et al., *RNF17, a component of the mammalian germ cell nuage, is essential for spermiogenesis.* Development, 2005. **132**(18): p. 4029-39.
32. Kulkarni, M., S. Ozgur, and G. Stoecklin, *On track with P-bodies.* Biochem Soc Trans, 2010. **38**(Pt 1): p. 242-51.
33. Saitoh, N., et al., *Proteomic analysis of interchromatin granule clusters.* Mol Biol Cell, 2004. **15**(8): p. 3876-90.

34. Hosokawa, M., et al., *Tudor-related proteins TDRD1/MTR-1, TDRD6 and TDRD7/TRAP: domain composition, intracellular localization, and function in male germ cells in mice.* Dev Biol, 2007. **301**(1): p. 38-52.
35. Sarge, K.D., S.P. Murphy, and R.I. Morimoto, *Activation of heat shock gene transcription by heat shock factor 1 involves oligomerization, acquisition of DNA-binding activity, and nuclear localization and can occur in the absence of stress.* Mol Cell Biol, 1993. **13**(3): p. 1392-407.

Chapter 3. Phase Transitions of Multivalent Proteins Can Promote Membrane Receptor Clustering

Note: The following chapter is an earlier draft of the publication Banjade and Rosen, *eLife*, 2014. All the experiments presented here are my own.

Abstract

Heterogeneity of the plasma membrane in the form of clustering of proteins and lipids is well documented in many signaling pathways. However, the general mechanisms behind the organization of the membrane remain unclear. Here, we report the *in vitro* reconstitution of membrane protein clusters, using Nephrin and its cytoplasmic partners Nck and N-WASP. We demonstrate that multivalent cytoplasmic protein Nck and N-WASP organize the membrane receptor Nephrin, producing micron sized dynamic clusters on lipid bilayers. The clustering can be understood as two dimensional phase separation, induced by polymerization of the proteins through multivalent interactions. The clusters are sites of actin assembly, supporting the hypothesis that clustering of nucleation promoting factors could be a general way to localize and enhance actin assembly processes on the plasma membrane. Our studies demonstrate that protein-protein interactions are sufficient to produce clusters on the plasma membrane, and that cytoplasmic adaptor proteins can act as ligands to organize membrane receptors into signaling zones.

Introduction

The plasma membrane is a self-assembled bilayer of lipids that demarcates and protects the cell from the environment. Numerous studies have now reported the existence of compartments within the plasma membrane, both on the outer and inner leaflets. For example, signaling clusters at the membrane are found in the EGFR system, the bacterial chemotaxis system, the immunological synapse, in the endocytotic events of GPI anchored proteins, and in the assembly of the vesicular fusion machinery (Ariotti et al, 2010; Goswami et al, 2008; Sourjik & Berg, 2004; van den Bogaart et al, 2013; Varma et al, 2006). The existence and the importance of these compartments have been widely accepted. However, the description of the mechanisms of their formation is still immature.

One of the prevailing models for the formation of many of these clusters is the longstanding idea of lipid rafts. Lipid rafts are phase separated assemblies of cholesterol, sphingomyelin and phosphocholine, which are observed as large domains (microns) in biochemical experiments (Lingwood & Simons, 2010), and purported to be small (nm scale) and short lived in cells (Hancock, 2006). The other existing reported mechanism for the formation of the clusters proposes that the self-assembly of the actin-myosin complex organizes membrane receptors (Gowrishankar et al, 2012). Whether the concept of lipid rafts alone explains the existence of all of these different kinds of clusters is debatable. Whether the actin-myosin complex forms de novo clusters or whether it plays a feedback role

of organization after the formation of smaller clusters remain to be fully elucidated. There are reports of protein-protein interactions inducing clustering, but the specific nature of these interactions and the properties of these clusters remain unclear (Sieber et al, 2007). The absence of biochemical reconstitution of such protein assemblies in a two dimensional context has hindered a complete understanding of these mechanisms.

Many of these clusters at the membrane are found to colocalize with actin filaments. Actin based processes are involved in numerous fundamental biological processes such as division and motility. In the past two decades, more than a hundred proteins have been discovered which play a role in actin filament nucleation, elongation, severing, capping, etc. In spite of the discovery of numerous proteins and their individual molecular mechanisms in regulating actin assembly, how these proteins work together to provide a functional output remains mysterious. Because actin nucleation promoting factors (in the family of N-WASP) are reported to form 500 nm to micron sized clusters at the plasma membrane, it is possible that clustering of proteins is a general mechanism to localize signaling proteins to a specific area to localize actin assembly.

Many membrane associated signaling proteins contain multiple repeats of a single domain. For example, ephrin receptor contains two phosphotyrosine motifs in its intracellular region, LAT (linker for the activation of Tcells) contains four

phosphotyrosine motifs, and Nephrin in the podocytes of the kidney contains three phosphotyrosine motifs. All of these receptors recruit SH2-domain containing adaptor proteins to the cell surface. These adaptor proteins often consist of multiple SH3 domains as well. As explained in the introduction of the thesis, these receptors have been observed to form clusters in cells.

In this study, we show that Nephrin interacts with its cytoplasmic partners Nck and N-WASP through multivalent interactions to form dynamic micron sized clusters on supported lipid bilayers. Our biochemical approach allows us to control the clustering process and define the rules necessary for their formation. Our study demonstrates that specific protein-protein interactions result in the formation of macroscopic clusters, without the necessity of lipid segregation or actin-myosin assembly, and the clustering can be defined as phase separation of proteins on the surface of a membrane. This process of assembling proteins at the plasma membrane should be an additional way to structure the plasma membrane.

Results

Nephrin, Nck and N-WASP Phase Separate on Supported Lipid Bilayers

We started with the cytoplasmic region of Nephrin containing the three phosphotyrosines that bind to Nck (amino acids 1174-1223, Nck binding sites at phosphorylated Y1176, Y1193 and Y1217). To anchor the protein to the lipid bilayer, we designed a Nephrin construct with a His8 (eight tandem histidines) tag at the N-terminus, followed by a (GlyGlySer, linker that includes a cysteine, labeled with an Alexa488 fluorophore (see Table 2 for sequence). This triply phosphorylated Nephrin construct is named p-Nephrin hereafter.

The phosphorylated protein was anchored to supported lipid bilayers composed of nickel chelating lipids (Ni-NTADOGS, at 1%) included in the membrane composition (Figure 3.1). His-tag association to the bilayer and the surface density can be controlled and quantified as reported in the literature (Galush et al, 2008; Nye & Groves, 2008; Salaita et al, 2010).

To ascertain the fluidity of the anchored p-Nephrin, we performed fluorescence recovery after photobleaching (FRAP) experiments. A 1 μm bleached region recovers fully in a matter of seconds (τ = 1.3 s, Figure 3.2). Upon addition of either 1 μM Nck or 1 μM N-WASP separately, the membrane remains homogeneous (Figure 3.2). However, upon addition of 1 μM Nck and 1 μM N-WASP micron sized clusters appear on the membrane (Figure 3.1). Clusters do not form with unphosphorylated Nephrin or in the absence of Ni-NTA phospholipids (not shown). When labeled Nck (Nck-Alexa 568) and N-WASP

(Alexa 647) are used in the experiment, all three proteins colocalize at the clusters (Figure 3.2). The requirement of Ni-chelating lipids for cluster formation suggests that the clustering is a two-dimensional phenomenon. The requirement of the phosphorylated motif of Nephrin and of N-WASP suggests that Nck binding to the membrane-associated Nephrin is necessary for cluster formation, upon recruitment of N-WASP. Quantitative analysis suggests that the clustered regions contain upto 4-fold higher density than the unclustered regions (Figure 3.1).

To understand the dependence of clustering upon concentrations of the molecules, we fixed the concentration of N-WASP at 500 nM and the density of p-Nephrin at 2700 molecules/μm^2 (Figure 3.3). Density of p-Nephrin was calculated as described in the literature (Galush et al, 2008; Salaita et al, 2010) and as shown in Figure 3.4. Density of His-tagged proteins can also be controlled as described in the literature and as demonstrated in Figure 3.4.

To this fixed density of p-Nephrin, we added increasing concentrations of Nck. We calculated the fractional intensity in clusters after thresholding the images by the triangle method in ImageJ. Calculation of fractional intensity of p-Nephrin in the clusters reveals that the fractional intensity increases sharply as a function of Nck concentration (Figure 3.3 A). We define the concentration at which fractional intensity starts increasing as the clustering concentration. From 0 to 100 nM, the fractional intensity remains the same. However, at and above 100 nM Nck, the

fractional intensity starts to increase sharply. At each concentration, we also calculated the variance of intensity across an image. The variance also increases sharply above 100 nM (Figure 3.3 A). Using an independent method of thresholding (the Maximum Entropy method on ImageJ), we found that the increase in fractional intensity occurs at the same concentration (not shown). Therefore, the calculation of the clustering concentration is independent of our method of image analysis. The density of p-Nephrin remains similar at every point in the titration (Figure 3.6). The highly cooperative nature of the cluster formation is reminiscent of the sharp phase transition previously observed in 3D (Li et al, 2012).

One consequence of the phase separation process dictating cluster formation is that the clusters should form randomly and independently of one another. Consequently, in a given space, the clusters should be randomly distributed. The spatial distribution of such processes fits to a Gaussian. We observed that if we analyze the frequency of cluster formation over a given area, this distribution fits well to a Gaussian distribution (Figure 3.3 B). In contrast, a non-random formation of GPI anchored protein clusters suggested that in that system, the formation of clusters could not have been a random process such as that induced by phase separation (Goswami et al, 2008).

Another consequence of phase separation is a broad size distribution of the clusters. In contrast, a system where the size distribution is actively maintained to be constant would not be considered as a phase separation process. The example of an actively maintained cluster includes a constant ratio of clusters to monomers of the GPI anchored proteins (Sharma et al, 2004). In our system, an analysis of the size distribution of the clusters of p-Nephrin, Nck and N-WASP showed a broad size distribution that could be fit to an exponential function (Figure 3.3 C). Exponential distribution of cluster sizes has been observed for chemotaxis receptor clusters, which emphasized the formation of the clusters through a stochastic process, and not through an actively maintained process (Greenfield et al, 2009).

Additionally, the evolution of clusters for phase-separated entities over time has been reported in the material science literature to proceed through two distinct mechanisms - nucleation and spinodal decomposition (Zinke-Allmang et al, 1992). The morphologies of clusters in these two regimes are distinct and allow us to differentiate between the two processes. When the clusters were formed with p-Nephrin, Nck and N-WASP at lower and higher densities of p-Nephrin (a ~ 5 fold difference in initial density), we were able to observe sparsely distributed clusters at lower densities that corresponded to the nucleation regime, whereas an interconnected morphology that spans the whole surface area of the membrane that corresponds to a spinodal decomposition regime (Figure 3.3 D).

The sharp induction of clustering, the random spatial and size distribution of clusters, and the presence of spinodal and nucleation regimes of cluster formation together strongly suggest that the clusters are two dimensional phase separated assemblies.

Clusters Are Dynamic

Over time, all the clusters demonstrate fluctuations over minutes. We also observe coalescence and occasional fission events, which suggest that these clusters are fluid like.

Over time, clusters coalesce and become larger (Figure 3.7 A). When we photobleach the molecular components, all the components recover rapidly (Figure 3.7 B). The recovery curves fit well to a double exponential function, but do not fit to a single exponential (Figure 3.7 B, Table 4). The two phases represent kinetic processes demonstrating lateral diffusion, binding and unbinding of proteins from the membrane, binding and unbinding of proteins within the clusters, etc. Presently we cannot deconvolute all these kinetic processes using the resolution afforded by FRAP. Most likely the faster phase (τ-fast) demonstrates recovery due to diffusion and the slower phase (τ-slow) demonstrates recovery due to binding interactions. We find that N-WASP shows recovery time constants of τ-fast = 2.6 s (37 %), τ-slow = 43 s (63%); Nck shows

τ-fast = 1.6 s (49%) and τ-slow = 72 s (51 %) and p-Nephrin of τ-fast = 86 s (76 %) and τ-slow = 526 s (24 %). p-Nephrin demonstrates slower recovery than Nck and N-WASP because it exhibits 2D diffusion and binding to the Nck/N-WASP complexes. Nck and N-WASP are both in solution, and therefore have faster recovery rates. In the unclustered regions, p-Nephrin recovers similarly to the faster phase of the clustered regions, with the data able to be fit to a single exponential (τ = 31 s). Interestingly, even if the individual components recover rapidly in the timescale of seconds to minutes, the clusters themselves remain stable. This phenomenon is reminiscent of macroscopic clusters found in cells such as the spindle assembly where it has been observed that even if the spindle is a stable structure, molecules forming the spindle are rapidly exchanging with the surrounding (Hyman & Brangwynne, 2011).

At lower densities (2500 molecules/μm^2) over time, the size distribution of the clusters remains exponential (Figure 3.8 A). However, due to coalescence, the number of smaller clusters decreases and the number of larger clusters increases (Figure 3.7 A, Figure 3.8). At higher densities, the size distribution could not be fit to an exponential distribution but fits better to a power law distribution (Figure 3.9). Currently we don't have a comprehensive model that allows us to identify the differences in these two regimes of size distributions. However, it is likely that at lower densities, the predominant mechanism of cluster evolution is deposition of particles on the surface that has equal k-on and k-off,

which in the past has been suggested to provide exponential distributions of cluster sizes (Rosen, 1984). At higher densities, because the rate of coalescence of clusters is higher, the size distribution would change to reflect a higher rate of coalescence, possibly providing a power law behavior. Cluster sizes also depend upon the density of the molecules at the membrane (Figure 3.10), as at higher density the average size of the clusters also remain higher, presumably because the rate of coalescence increases with higher density of molecules at the surface (Zinke-Allmang et al, 1992).

These dynamics data suggest that the structures we have formed are fluid like entities. These data are consistent with a phase-separated assembly where molecules exchange within the clusters and also exchange to and from the surrounding.

Clusters Are Polymers of Nck, N-WASP and p-Nephrin

Our previous data in 3D suggested that phase separation depends upon the valency of the interacting species. To identify the parameters necessary to form the 2D clusters and to define the mechanism of clustering, we created three versions of p-Nephrin: triphosphorylated (p-Nephrin), di-phosphorylated (Nephrin2pY) and mono phosphorylated (Nephrin1pY). At a density of 1000 molecules/μm^2 and 500 nM N-WASP, we varied Nck concentration. At 1000

molecules/μm^2, p-Nephrin shows a clustering concentration of 200 nM Nck, whereas Nephrin2pY and Nephrin1pY do not cluster even at concentrations greater than 10 μM (Figure 3.11 A) and at a density of 3000 molecules/μm^2. If we raise the concentration of N-WASP to 2 μM N-WASP, Nephrin 2pY produces clusters (Figure 3.12 A). However, Nephrin1pY does not cluster, even at 5 μM N-WASP and 10 μM Nck.

We also created multivalent versions of the SH3 domains, taking the second SH3 domain of Nck, separated by the natural linker in between the first two SH3 domains of Nck. We made three, two or a single repeat of the SH3 domain $(SH3)_3$, $(SH3)_2$, and $(SH3)_1$, respectively, in the presence of the SH2 domain. In these constructs, the SH3 domains are separated by the natural linker between the first and second SH3 domains of Nck. At 500 nM of N-WASP and 1000 molecules/μm^2 of p-Nephrin, $(SH3)_3$ starts clustering at the concentration of 200 nM, whereas $(SH3)_2$ and $(SH3)_1$ molecules do not (Figure 3.11 A). $(SH3)_2$ clusters at higher concentrations of N-WASP (5 μM), but $(SH3)_1$ does not cluster even at concentrations above 5 μM of the SH3 module concentration, 5 μM of N-WASP (Figure 3.12 B) and up to a p-Nephrin density of 3000 molecules/μm^2 (Figure 3.11 B).

To determine the effect of individual affinities on the clustering concentrations, we replaced the phosphotyrosine motifs of Nephrin with that of the bacterial protein

TIR (pTIR). Previous experiments have suggested that all the three pY motifs on p-Nephrin have similar affinities to the SH2 domain of Nck and that p-TIR has a 10 fold higher affinity to the SH2 domain (Blasutig et al, 2008). In our clustering experiments, in the presence of pTIR at a density of 2000 molecules/μm^2, the clustering concentration of $(SH3)_3$ is 100 nM. At the same density, the clustering concentration is 200 nM when p-Nephrin is used (Figure 3.13 A). The higher affinity interaction also slows the recovery of Nck, as FRAP data demonstrate (Figure 3.13 B). Fitting to a double exponential, Nck shows recovery rates of τ-fast = 6.5 s and τ-slow = 89.5 s when clusters of pTIR/Nck/N-WASP are bleached. However, Nck shows recovery rates of 1.6s (τ-fast) and 73.2s (τ-slow) when clusters of p-Nephrin/Nck/N-WASP are bleached. These data show that both the clustering concentrations and the dynamics of the clusters can be affected by molecular affinities.

We also measured the binding affinity of the p-Nephrin motif to the SH2 domain of Nck, using the triply phosphorylated Nephrin (p-Nephrin, assuming that all sites have equivalent affinities to the SH2 domain). This affinity is 370 nM, as determined by isothermal titration calorimetry (Figure 3.14). Similarly, pTIR binds to the Nck SH2 domain with an affinity of 40 nM.

Additionally when a higher affinity monovalent peptide is added to the clusters, the clusters dissipate. In the presence of clusters made from 1 μM $(SH3)_3$ and

500 nM N-WASP and p-Nephrin, we added singly phosphorylated TIR peptide at 10 μM (Figure 3.15 A). The clusters disappear within minutes after the addition of the monovalent peptide. The competition of the clusters occurs sharply, as the fractional intensity decreases sharply within the time frame of two minutes (Figure 3.15 A, 8 to 10 minutes). If we titrate TIR from 100 nM to 100 μM, the fractional intensity of the cluster also decreases sharply above 10 μM (Figure 3.15 B). These data suggest that the deformation of the clusters (similar to the formation) is also cooperative.

The favorability of higher valency and higher affinity on clustering, and the disruption of the clusters by a monovalent molecule suggests that the clusters are polymers of p-Nephrin, Nck and N-WASP, as opposed to structures formed by their non-specific assembly. At a certain critical concentration at which infinite polymers are formed, a phase transition occurs, causing formation of macroscopic clusters on the membrane.

Clusters Promote Actin Assembly

Previously, we showed that phase transition of Nck, Nephrin and N-WASP in 3D corresponds to a sharp change in activity towards the Arp2/3 complex. To test whether clustering of N-WASP promotes localized actin assembly on the membrane, we added 1 μM monomeric actin in the presence of 10% rhodamine

labeled actin and 10 nM Arp2/3 complex to p-Nephrin/Nck/N-WASP clusters. Over a timeframe of 100 minutes, we observed recruitment and assembly of actin to the clusters (Figure 3.16 A). Initially, at earlier times (3 – 6 minutes) the clusters become occupied with actin, as depicted by the fluorescence of rhodamine in every cluster (Figure 3.16 A, Figure 3.17 A, 3 minutes). These data suggest that actin that gets recruited to the clusters at earlier times is monomeric in form, and that the assembly of actin observed at those clusters is not the filamentous form.

In the next few frames (after 6 minutes, Figure 3.16 A), only a subset of clusters light up because of enhanced actin assembly and recruitment. This enhancement of actin assembly occurs independently of the cluster size or p-Nephrin density (Figure 3.16 B, C). At the same time, with identical conditions (105 minutes after initial actin addition, we also found that presence of the Arp2/3 complex recruits a lower degree of actin to the membrane and the clusters (Figure 3.17 B). Furthermore, the stochastic recruitment of actin in a subset of cluster also does not occur in the absence of the Arp2/3 complex (not shown).

Upon actin assembly, the morphology of the clusters also changes according to the morphology of actin, and thus the clusters get reorganized according to the actin assembly (Figure 3.18). In between times 42 and 45 minutes, for reasons we do not yet understand, there is a sharp recruitment of actin to the overall

surface of the membrane. The sharp recruitment of actin also significantly changes the morphology of the clusters, shattering the clusters. It is possible that mechanical force of actin assembly is responsible for breaking up of the clusters in such a manner. Altogether, our data suggest that clusters are zone of localized and enhanced actin assembly, providing a possible reason for the requirement for the clustering of proteins in the actin assembly pathway.

Discussion

In this study, we have reconstituted assemblies of Nephrin, Nck and N-WASP on model membranes of supported lipid bilayers. At a particular concentration of the proteins, in a sharp fashion, micron sized clusters of proteins appear on the membrane. Evidence for a phase separation mechanism exists due to the high cooperativity of cluster formation and dissipation, and the Gaussian spatial distribution of the clusters. Consistent with a dynamic nature of the clusters, all the molecules exchange rapidly with the surrounding. Cluster formation is strongly dependent upon the valency of the interacting motifs and is dependent upon the affinities of the interacting motifs, suggesting that the clusters are driven by the polymerization of the multivalent proteins. All of these data suggest a general way of organizing molecules through multivalent self association, as demonstrated earlier in the case of 3D phase separation.

Nephrin is constitutively phosphorylated at the slit diaphragm, and during podocyte injury, phosphorylation of Nephrin is compromised (Jones et al, 2009). Furthermore, mutation of the SH3 domains of Nck also reduces the phosphorylation levels of Nephrin, suggesting that Nck and its downstream partners also play a role in phosphorylating Nephrin(New et al, 2013). These data suggest that Nephrin (and its kinase), form a complex with Nck and its downstream partner (N-WASP).

The complex of phosphorylated Nephrin, in association with Nck and N-WASP could form a polymeric network that is important for the stabilization of the slit diaphragm. Nephrin's extracellular domains include multiple IgG domains and FNIII domains, which are also predicted to self-associate (Gerke et al, 2003). Association of the extracellular region localizes Nephrin to the slit-diaphragm and should also increase its density in a localized area. When phosphorylated, it is well documented that at these sites Nephrin recruits Nck and N-WASP (Blasutig et al, 2008). These sites of high density are most probably phase-separated polymers of Nephrin/Nck/N-WASP, as our *in vitro* data suggest. The intracellular polymers and the extracellular association of Nephrin could work cooperatively to stabilize the structures at the sites of slit diaphragm. Consistent with a polymeric model, single mutants of different SH3 domains of Nck or the phosphorylation motifs of Nephrin do not have significant effects on antibody mediated cross-linked cluster formation in cells, but creating double mutations and further

lowering valency reduces fraction of cells producing such clusters (Blasutig et al, 2008).

Higher order oligomerization of N-WASP has been reported to activate the Arp2/3 complex more potently than monomers(Padrick et al, 2008). Also, colocalizing N-WASP to the membrane and a relatively small increase in its density has been reported to increase its activity (Wiesner et al, 2003). Clustering of N-WASP by Nephrin and Nck makes higher order polymers of N-WASP and increases its density by 4-fold, which decreases the distances between individual N-WASP molecules. This phenomenon should promote activation of the Arp2/3 complex.

Localizing N-WASP at specific zones of clustering prevents spurious actin assembly at non-specific locations at the membrane. Therefore, clustering of N-WASP would also help to reduce noise (Grecco et al, 2011). We notice that actin assembles stochastically in the clusters. This is probably because individual clusters do not contain N-WASP molecules in the same orientation. Almost certainly N-WASP is organized inside the clusters with different distances in between the individual N-WASP molecules. Whichever N-WASP oligomers and polymers are closest to each other to activate the Arp2/3 complex could first assemble actin in those clusters. Additionally, as the filaments grow at the clusters, there is higher Arp2/3 initiated branching and feedback, which further increases the filament density in the clusters that nucleate the first actin filaments.

The phenomenon of clustering through multivalent interactions should be more robust in 2D in comparison to 3D. If there were weak dimeric or oligomeric interactions between proteins, for example Nck in our system, localizing two Nck molecules close to each other after recruitment by Nephrin would enhance these weak associations by increasing the on rate and therefore the apparent affinity (Groves & Kuriyan, 2010). Importantly, although we have reported the phenomenon for a membrane receptor containing multiple phosphotyrosine motifs, at high densities of a receptor containing a single motif, the same clustering phenomenon through multivalent interactions could occur, if the cytoplasmic proteins possess multivalency. For example, multivalent PDZ-domain containing proteins interact with voltage gated Kv1.3 channels, which are found in clusters at the cell surface (Panyi et al, 2004).

Furthermore, membrane receptors are themselves usually oligomeric in nature. For example, EGF receptors have been reported to form preformed oligomers in the absence of ligand (Clayton et al, 2008), which would increase the valency of the receptor. EGF receptors are activated by dimerization and purported to have enhanced kinase activity upon aggregation (Engel et al, 2013). Higher ordered assembly of receptors and enhanced activity (example the kinase activity in the case of the EGFR) would provide a feedback mechanism to regulate signaling. Such properties of self-assembling receptors should also generate different

structural arrays, which could make ordered polymers (Wu, 2013), or disordered ones, as our system probably creates.

The phenomenon of protein polymerization and clustering should also be thermodynamically coupled to phase separation of lipids. If the transmembrane region of the protein interacts favorably with cholesterol or the fatty acyl chains of sphingomyelin, protein clustering could be driven towards lipid phases. However, if these interactions are unfavorable, the protein and lipid phases may be separate, creating distinct signaling zones.

In summary, we have biochemically reconstituted a novel protein-protein mediated membrane cluster, which nucleates actin filaments. Formation of such dynamic polymers of multivalent signaling proteins could be a general way to localize and enhance biochemical activity at the plasma membrane.

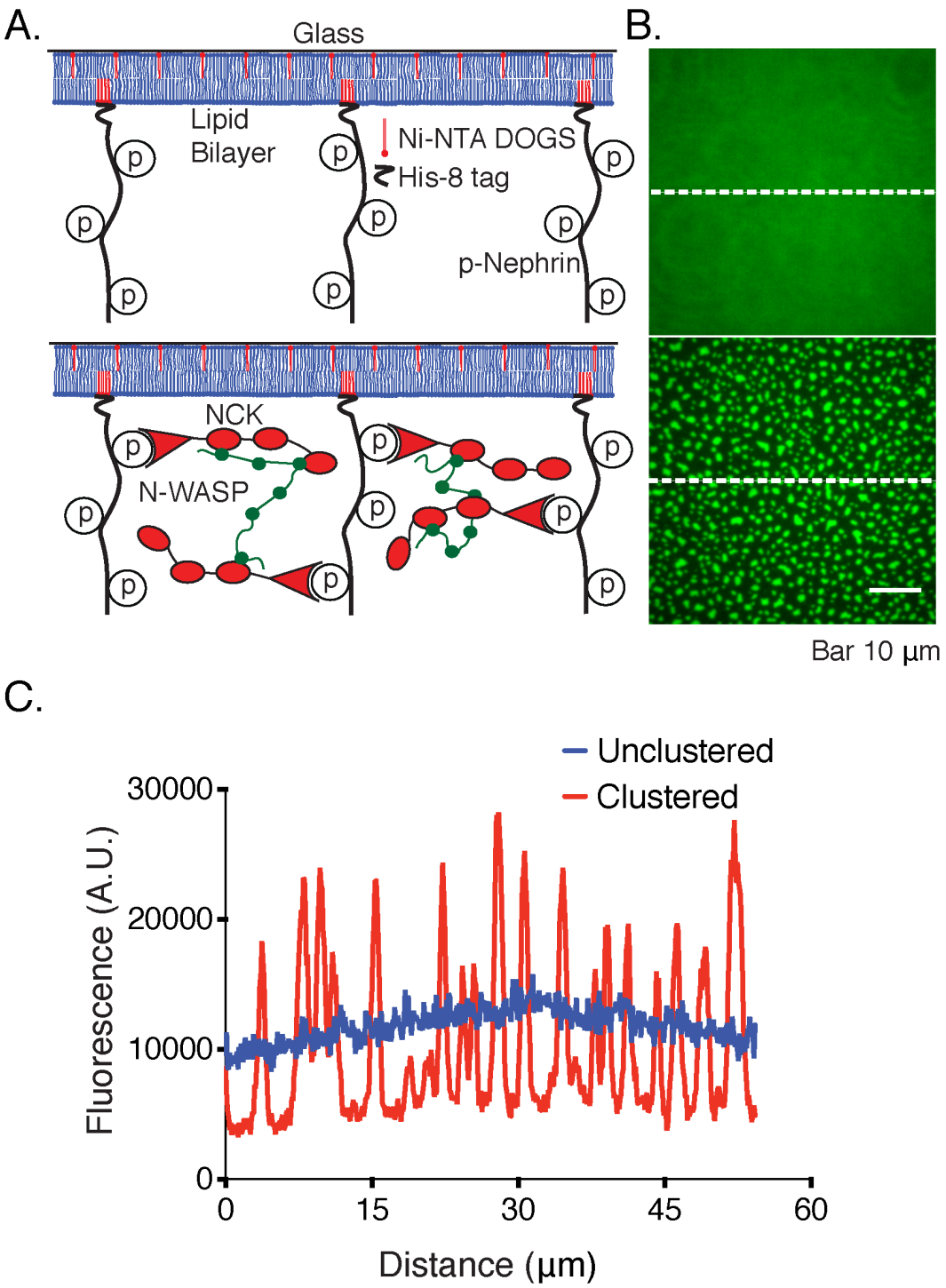

Figure 3.1. Reconstitution of p-Nephrin clusters on supported lipid bilayers. A) Cartoon illustrating the interaction of triply-phosphorylated His_8-tagged Nephrin (p-Nephrin) with its partners Nck and N-WASP. Top panel illustrates p-Nephrin attached to bilayers. Bottom panel illustrates the model for clustered p-Nephrin, upon Nck and N-WASP interactions. B) Top panel is the

experimental observation of a homogeneous membrane with Alexa488 labeled p-Nephrin anchored (corresponding to Figure 1a, top panel). Supported lipid bilayers were made using DOPC doped with 1 % nickel-chelating lipid (Ni^{2+}-NTA DOGS), to which His8-tagged p-Nephrin binds. Bottom figure is the experimental demonstration of the clustered p-Nephrin upon addition of 1 μM Nck and 1 μM N-WASP (corresponding to Figure 1a – bottom panel). C) Line-scan of the unclustered and clustered p-Nephrin from the images shown in B, at the line-scan positions depicted by the white dotted lines.

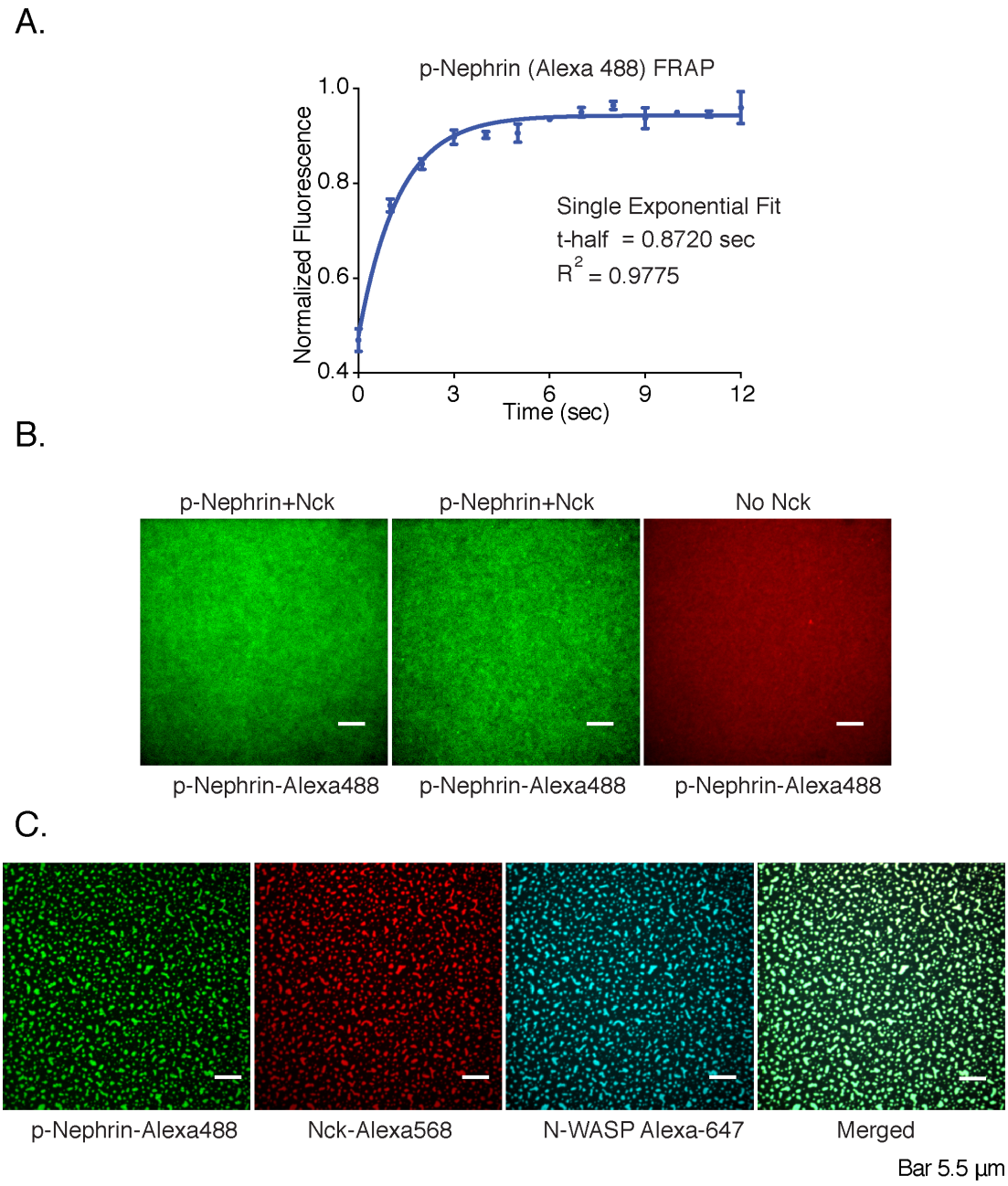

Figure 3.2. Nephrin, Nck and N-WASP colocalize to dynamic puncta on supported bilayers. A) Fluorescence recovery after photobleaching (FRAP) on a supported bilayer with p-Nephrin shows full recovery with exponential recovery time constant τ = 1.3 sec. Line shows fit to a single exponential. B) Clusters do not form with only p-Nephrin on the membrane (left-panel, p-Nephrin Alexa488), or with p-Nephrin (Alexa488) + 1 µM Nck (Alexa568) (middle and right panels). The legend below each panel indicates the fluorophore imaged. C) Three-color imaging shows that p-Nephrin Alexa488, Nck Alexa568 and N-WASP Alexa647 co-localize at the clusters.

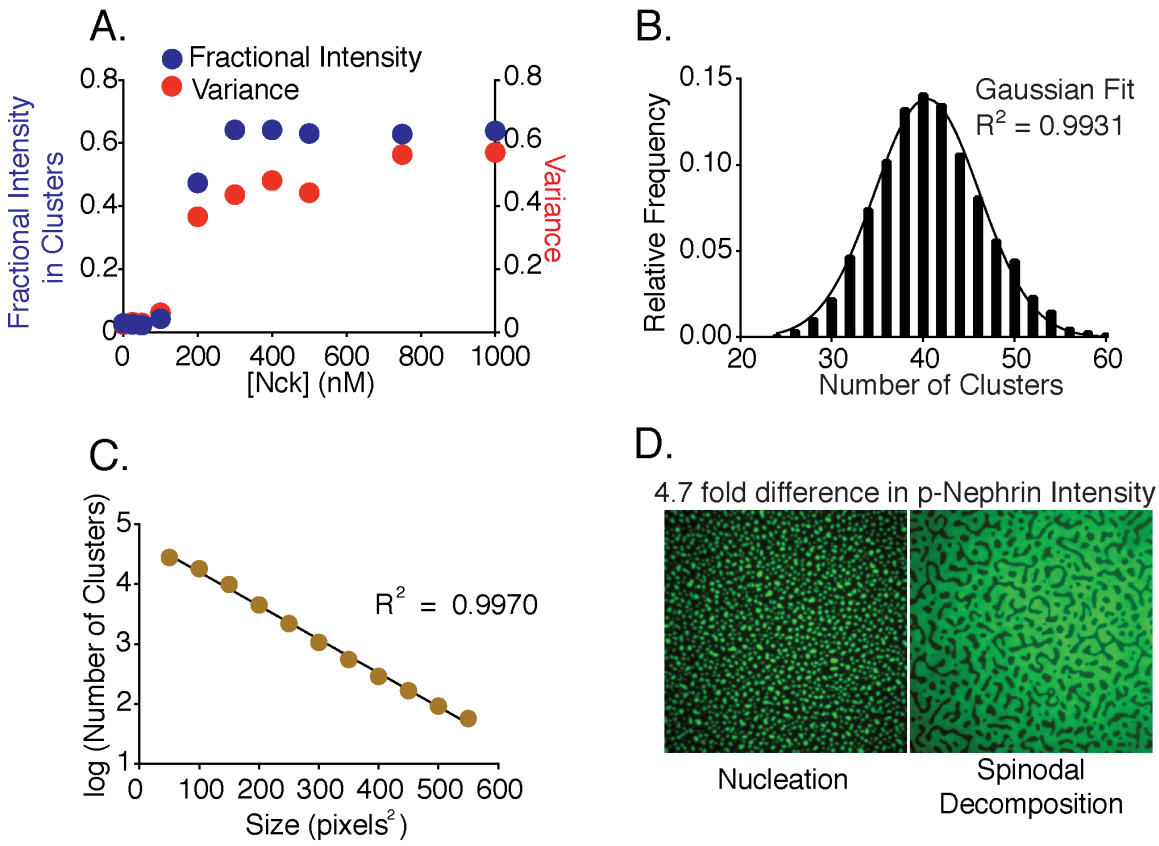

Figure 3.3. Nephrin clusters are created via a two-dimensional phase-transition. A) Fractional intensity in clusters (blue symbols, left ordinate) and signal variance (red symbols, right ordinate) of p-Nephrin fluorescence as a function of Nck concentration for 500 nM N-WASP and total p-Nephrin density of ~2700 molecules/μm^2. B) Plot shows the relative frequency with which a given number of clusters are found within 93 randomly selected 56 x 56 μm regions of a bilayer formed using 1 μM Nck and 1 μM N-WASP. C) Size distribution of clusters formed using 1 μM Nck and 1 μM N-WASP. D) Puncta formed using 1 μM Nck, 1 μM N-WASP and low (left) or 4.7-fold higher (right) density of p-Nephrin. Images were autocontrasted for clarity.

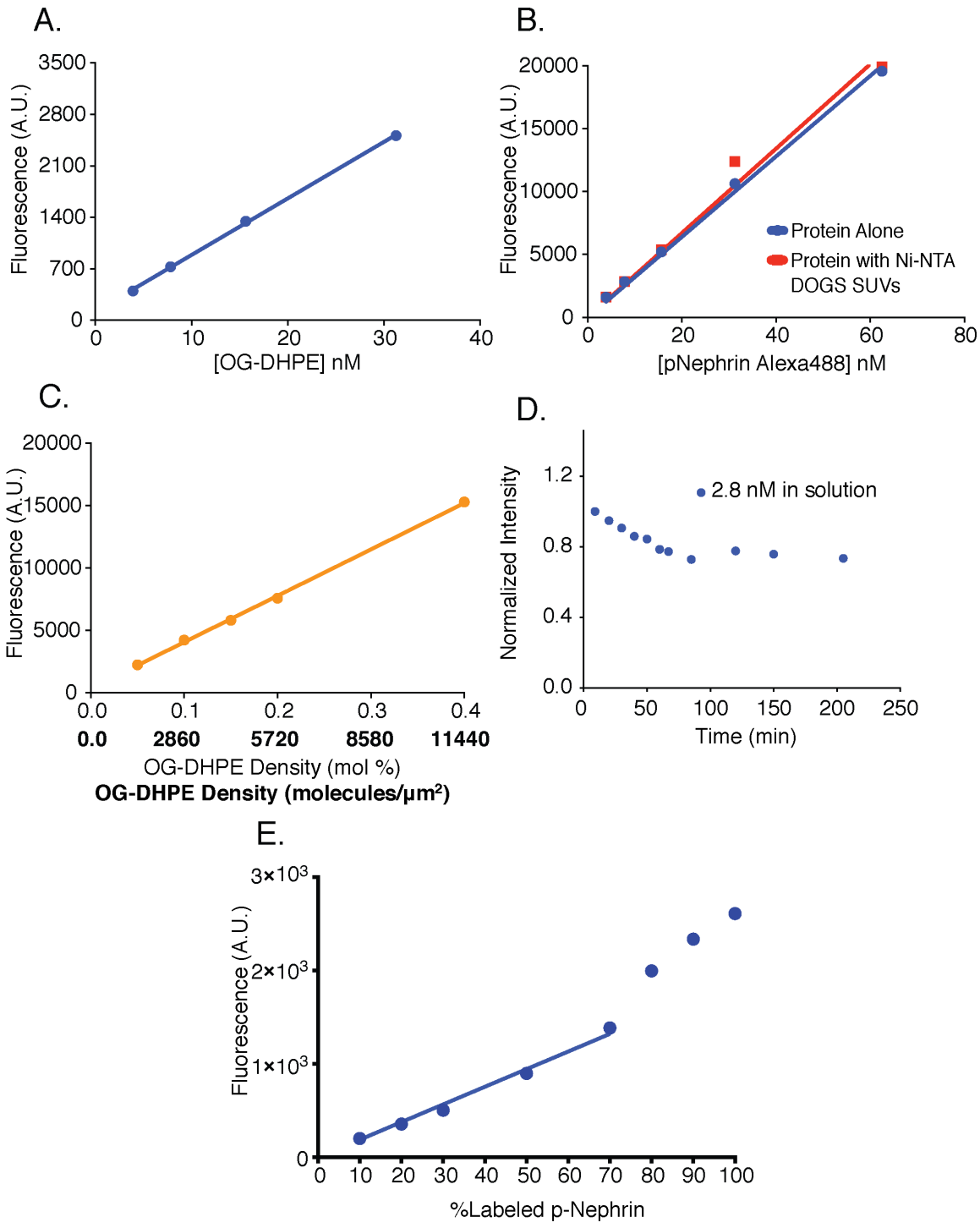

Figure 3.4. Quantitative analysis of the measurement and control of His_8-p-Nephrin density on supported lipid bilayers. A) Fluorescence intensity as a function of fluorescent lipid (OG-DHPE) concentration for a solution of small unilamellar vesicles. B) Fluorescence intensity as a function of p-Nephrin Alexa488 concentrations. Blue points represent data for protein alone, red points represent data for p-Nephrin in the presence of 9.5 μM of Ni^{2+}-NTA DOGS. C)

Fluorescence intensity as a function of OG-DHPE density on supported lipid bilayers. Upper and lower x-axis labels list density as percent total lipid and molecules/μm^2, respectively. Lines in A) to C) represent a linear fits. D) Time course of His_8-tagged p-Nephrin Alexa488 dissociation from supported lipid bilayers, monitored by TIRFM, following washes that left 2.8 nM protein in solution above the bilayer. E) Fluorescence intensity of bilayers containing different percentages of p-Nephrin Alexa488 (with total p-Nephrin density ~2000 molecules/μm^2). The data suggest linearity up to ~60 % labeling.

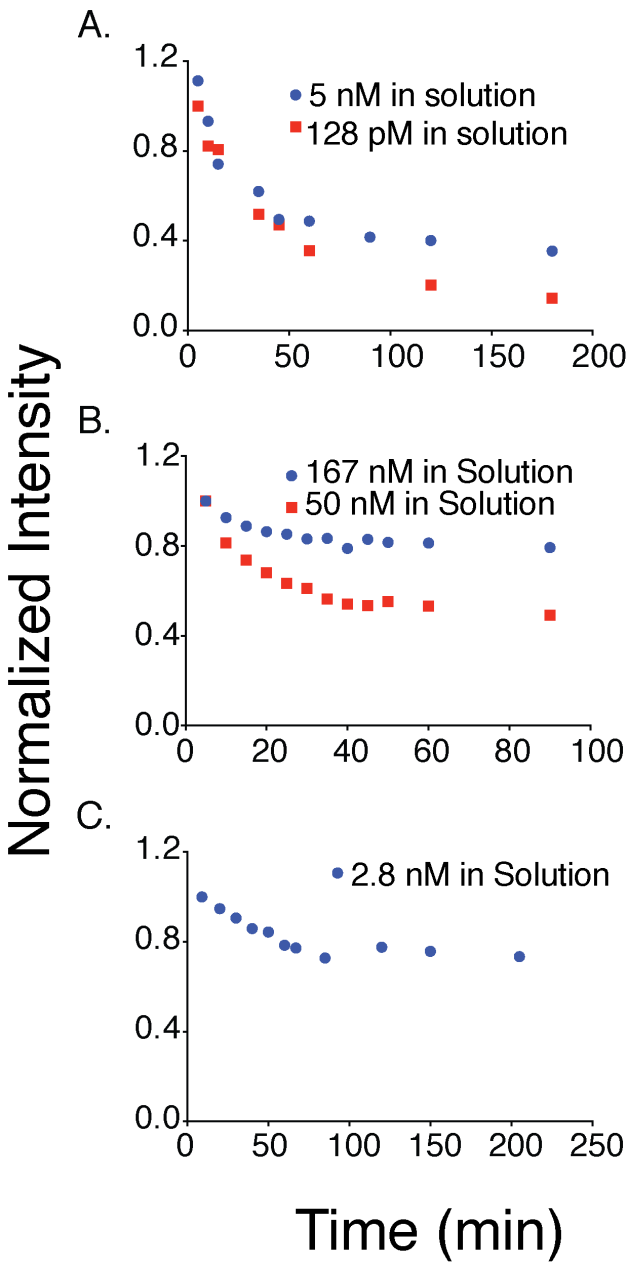

Figure 3.5. Controlling density of membrane bound His_8 p-Nephrin. Intensities of membrane bound Alexa-488 His_8 p-Nephrin were quantified after incubating 1 μM of the protein for 1 hour and then washing off excess His_8 p-Nephrin. Concentrations indicated in (A)-(B) are the concentrations in solution left after washing off excess protein. Y-axes represent the fraction of the intensity of Alexa-488 His_8 p-Nephrin at time zero after washing.

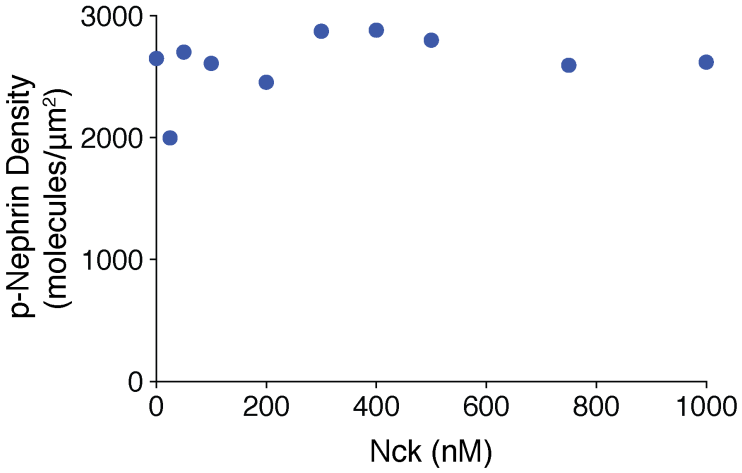

Figure 3.6. Quantification of average p-Nephrin density on the bilayer for every titration point shown in Figure 3.3 (A). Y-axis represents p-Nephrin density and x-axis represents the different Nck concentrations of the titration as in Figure 3.3 (A). Densities are averages of five different areas of each bilayer. Error bars representing standard deviations are smaller than the symbols.

A.

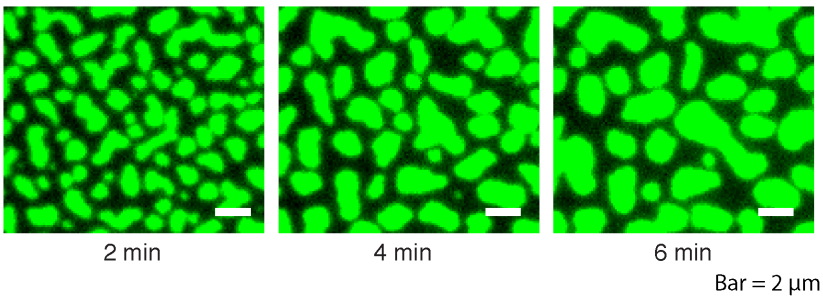

B.

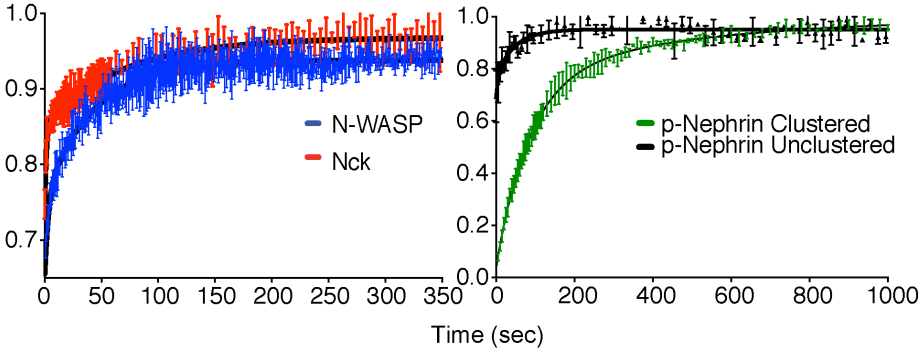

Molecule	τ-fast, sec (Percent Recovery)	τ-slow, sec (Percent Recovery)
N-WASP	2.6 s, (37%)	43 s, (63%)
Nck	1.6 s, (49%)	72 s, (51%)
p-Nephrin (clustered)	86 s, (76%)	526 s, (24%)
p-Nephrin (unclustered)	31 s	N/A (single exp)

Figure 3.7. Clusters are dynamic. A) Time-lapse TIRF imaging of bilayers containing fluorescent p-Nephrin after addition of 1 µM Nck and 1 µM N-WASP over a 10 minute interval. B) Fluorescence recovery after photobleaching of Nck and N-WASP (left panel), and p-Nephrin clustered and unclustered regions (right panel). FRAP experiments were peformed using Alexa-488 labeled p-Nephrin, Nck, or N-WASP. Lines show bi-exponential fits of the data, except the data for unclustered p-Nephrin, which was fit using a single-exponential. Bars represent standard deviation from three FRAP experiments on a single bilayer. Bottom table represents the data obtained from the exponential fits of the FRAP data.

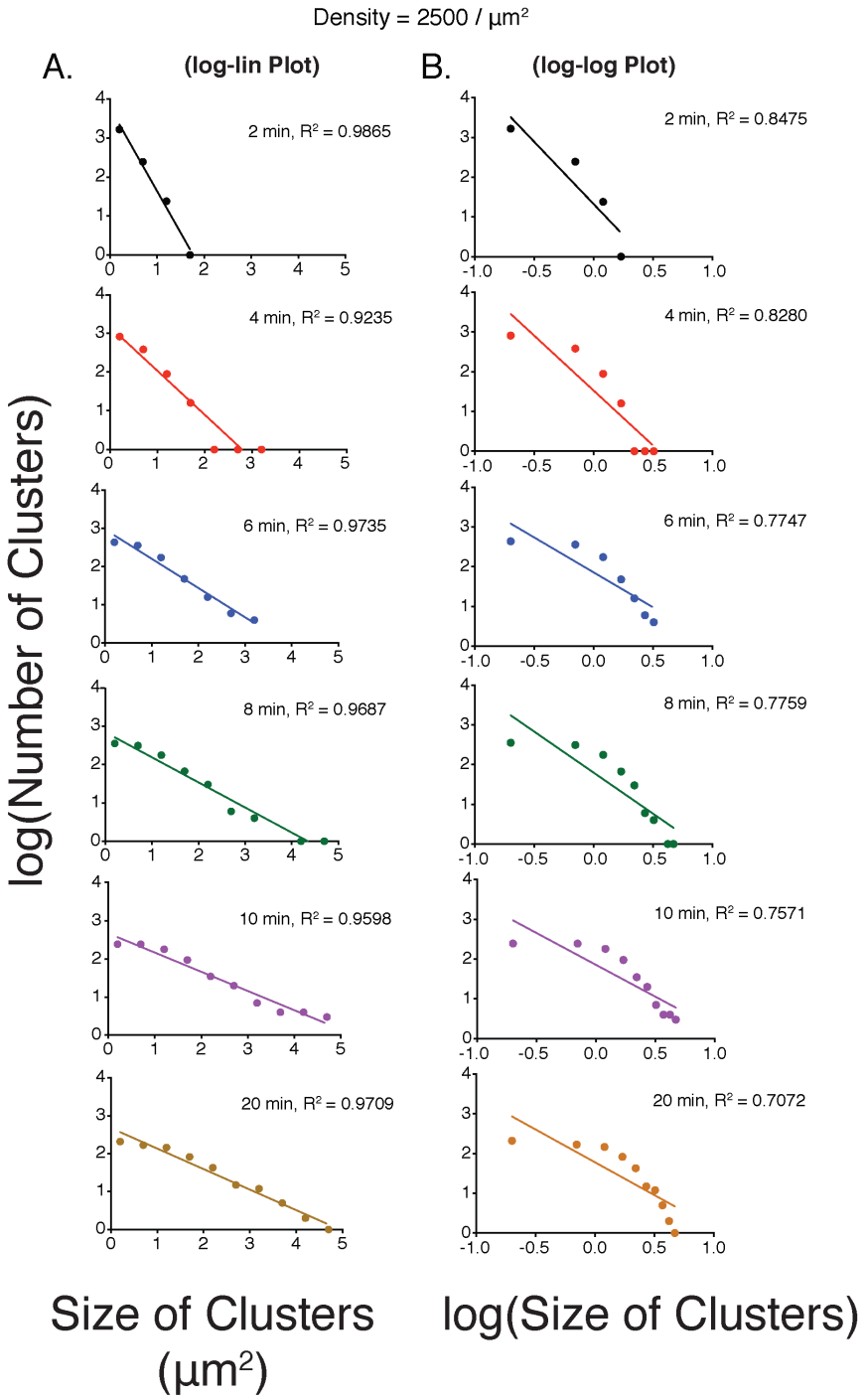

Figure 3.8. Cluster size-distribution analyses at different times suggest exponential behavior at lower densities. (A) Log-linear plot of cluster number vs size at p-Nephrin density of ~2500 µm^2, 1 µM Nck, and 1 µM N-WASP. The distributions are plotted for times between 2 and 20 min. (B) Log–log plot of the same data. Lines in (A and B) represent the best linear fits of the data. The better fits in (A) than (B) indicate that the data are better described by exponential than

power law functions. In other experiments (not shown), the sizes remain exponentially distributed to times as long as 60 min.

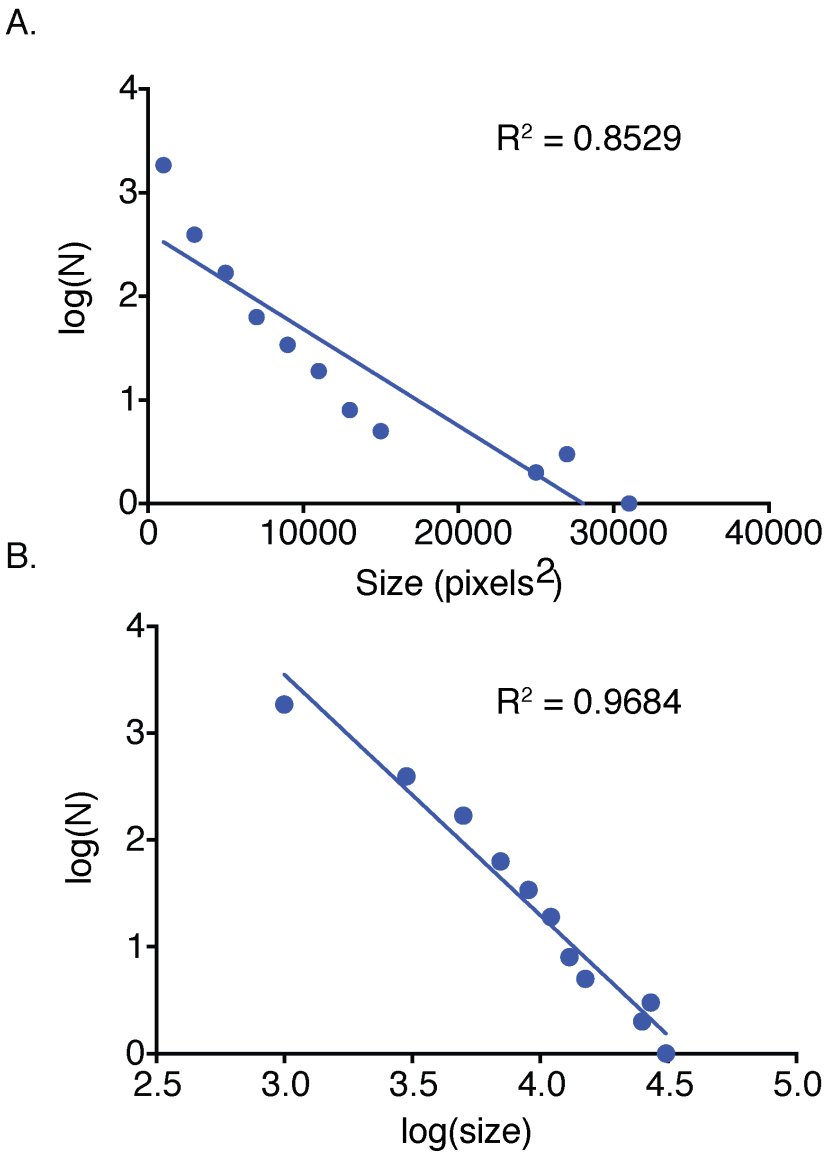

Figure 3.9. Cluster size-distribution analyses suggest power law behavior at higher densities. (A) Log-linear plot of the size distribution of clusters at a Nephrin density of ~4000 μm^2, 1 µM Nck, and 1 µM N-WASP, recorded 60 min after clustering was initiated. (B) Log–log plot of the size distribution of clusters at a Nephrin density of ~4000 μm^2, 1 µM Nck, and 1 µM N-WASP. Lines in (A and B) represent the best linear fits of the data. The better fits in (B) than (A) indicate that power law better describes the data than exponential functions (contrast with Figure 3.8).

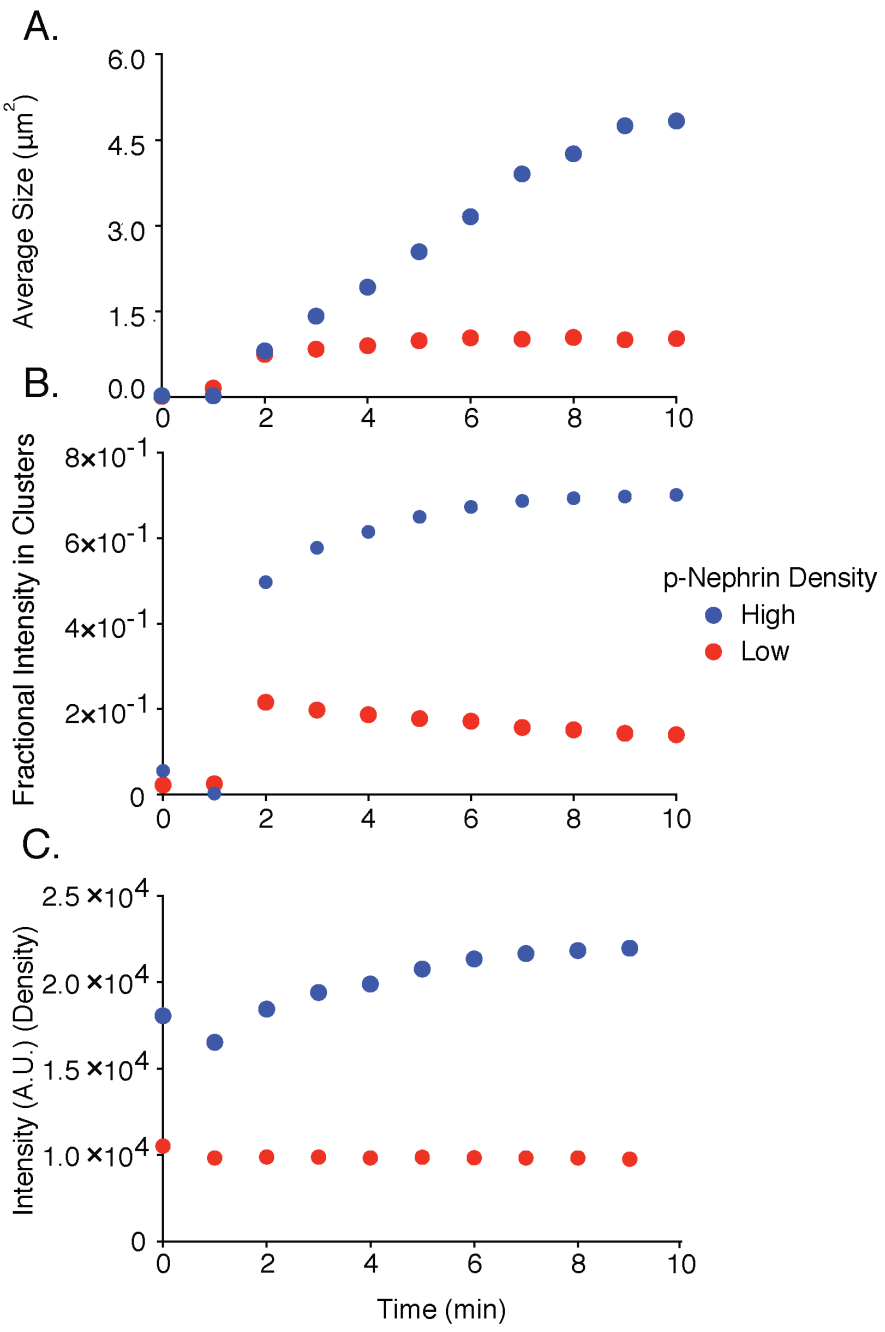

Figure 3.10. Average cluster size is dependent on molecular density. Samples contained either low (~2000 molecules/μm^2, red dots) or high (~3500 molecules/μm^2, blue dots) density of p-Nephrin. Clustering was initiated by addition of 1 μM Nck and 1 μM N-WASP. Images were taken every minute. (A) Average cluster size, (B) the fractional intensity in clusters.

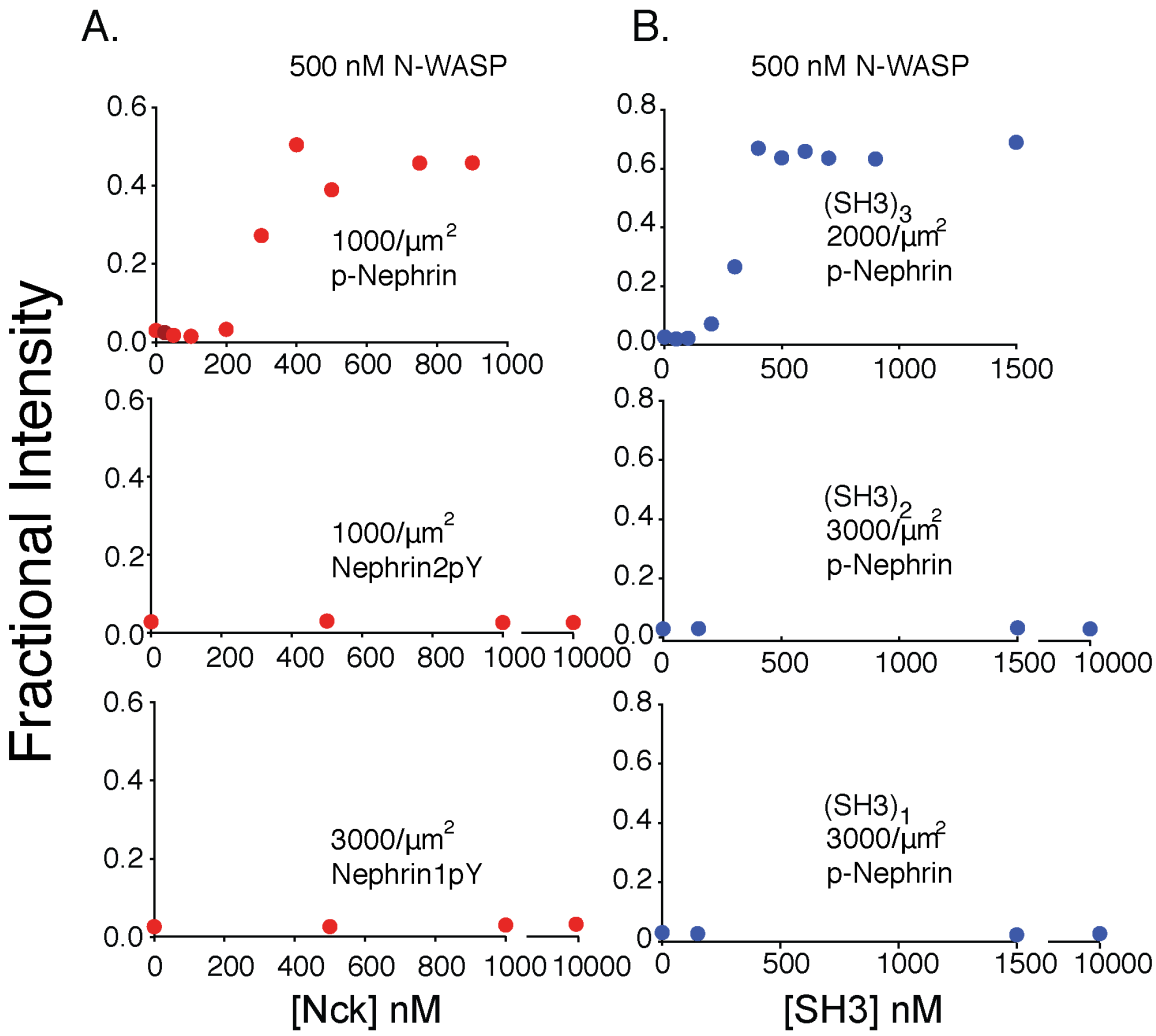

Figure 3.11. Clustering is dependent upon the valency of the interacting motifs. Plots show fractional intensity of fluorescent Nephrin proteins in clusters as a function of Nck protein concentrations for 500 nM N-WASP. (A) Top, middle, and bottom panels show data for p-Nephrin 3pY, 2pY, and 1pY, respectively. For these concentrations of N-WASP and Nck, only Nephrin 3pY shows clustering. At 2 μM N-WASP, Nephrin 2pY also clusters when Nck is added (Figure 4—figure supplement 1). (B) Top, middle, and bottom panels show data for p-Nephrin plus engineered Nck proteins containing 3, 2, or 1 repeat of the second SH3 domain of Nck. For these concentrations/densities of N-WASP/p-Nephrin, only the $(SH3)_3$ protein can induce clustering. At 5 μM N-WASP, $(SH3)_3$ also induces clustering. Note that the x-axis is Nck concentration in panel (A) but total SH3 domain concentration in panel (B).

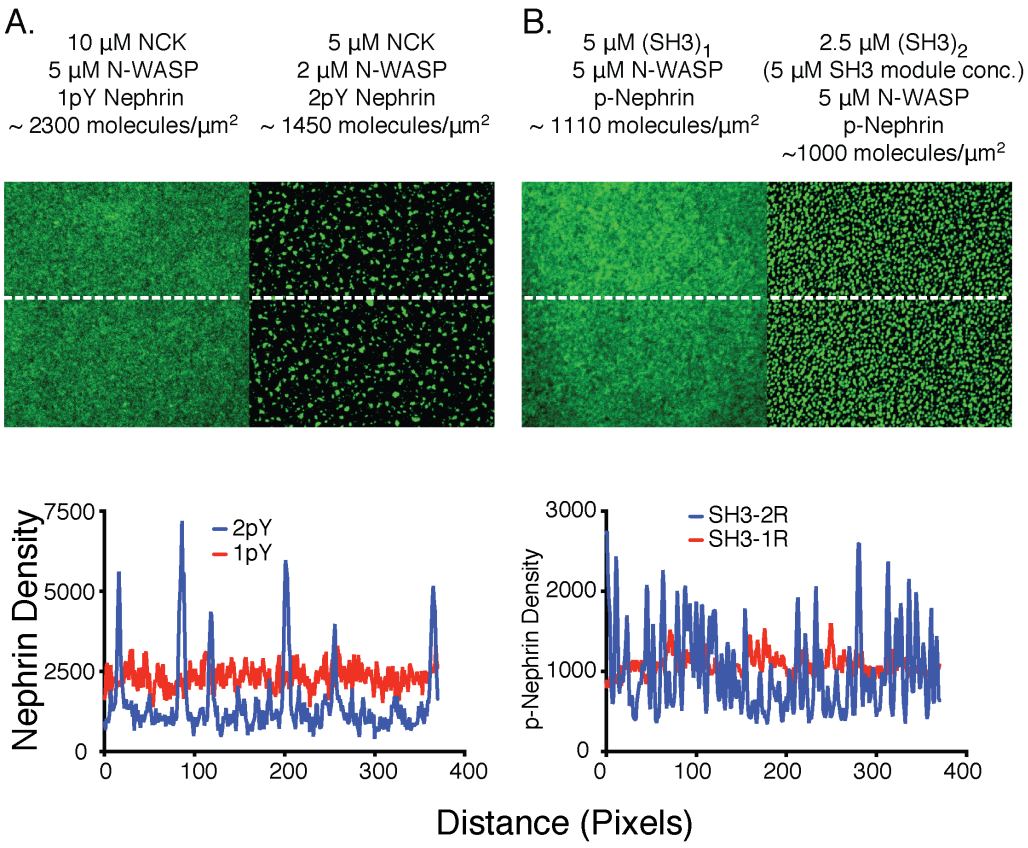

Figure 3.12. Di-valent molecules are stronger clustering agents than mono-valent molecules. (A) In the presence of 5 µM Nck and 2 µM N-WASP, p-Nephrin 2pY forms clusters (right panel). Even in the presence of 10 µM Nck and 5 µM N-WASP, p-Nephrin 1pY does not form clusters (left panel). Bottom: line-scan of images in the top panels, with locations indicated by dotted lines. (B) At 5 µM N-WASP, 2.5 µM $(SH3)_2$ (5 µM SH3 module concentration) produces p-Nephrin clusters (right panel), whereas $(SH3)_1$ does not (left panel). Bottom: line-scan of images in the top panels, with locations indicated by dotted lines.

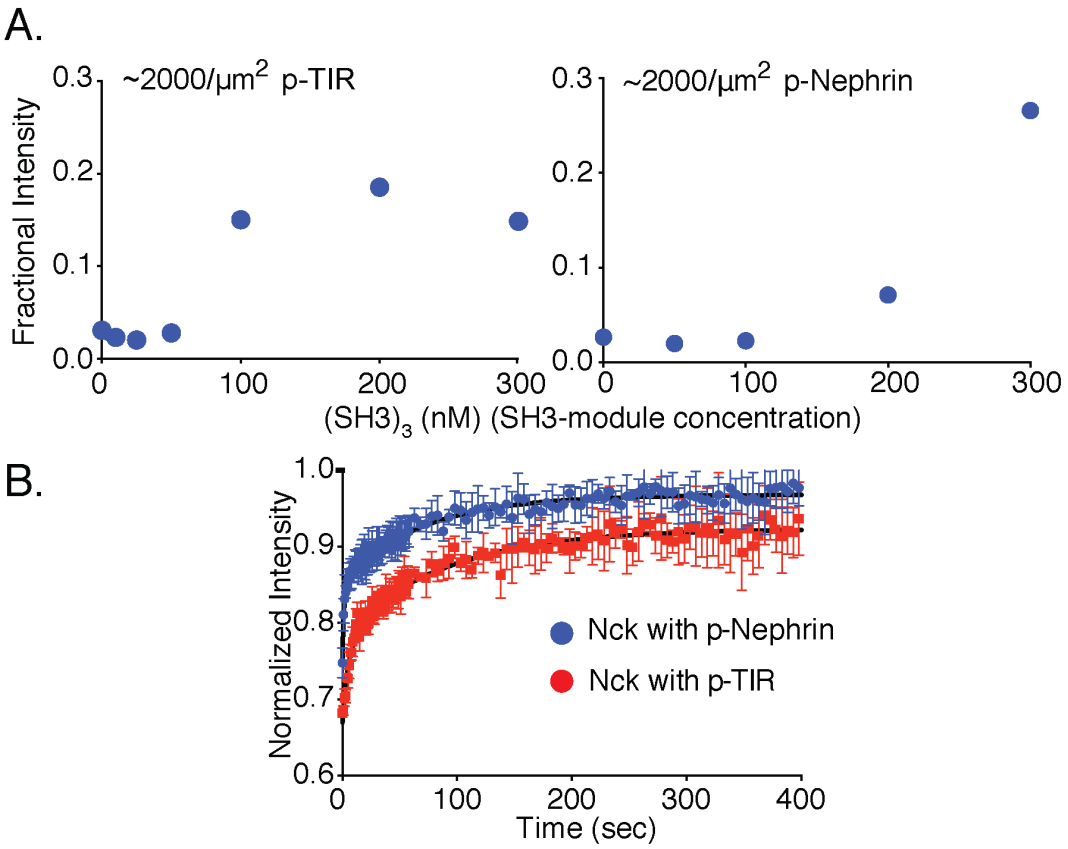

	τ (fast) (sec)	τ (slow)(sec)	R^2	Plateau	Y-intercept
Nck with p-TIR	6.5	89.5	0.87	0.92	0.66
Nck with p-Nephrin	1.6	73.2	0.82	0.97	0.75

Figure 3.13. Molecular affinities affect macroscopic clustering. (A) Fractional intensity of fluorescent pTyr proteins in clusters as a function of SH3 (module) concentrations for 500 nM N-WASP. Left and right panels show data for a p-TIR and p-Nephrin, whose pTyr motifs bind the SH2 domain of Nck with K_D values of 40 nM and 370 nM, respectively. (B) Fluorescence recovery after photobleaching (FRAP) for Alexa488-labeled Nck in p-Nephrin clusters (blue) and p-TIR clusters (red). Nck recovers more slowly (larger τ), can be bleached more strongly (Y-intercept) and recovers to a lower value (plateau) with p-TIR than with p-Nephrin, all indicating slower dynamics in clusters with the higher affinity SH2 binding partner. The bars represent standard deviation from three FRAP experiments on a single bilayer.

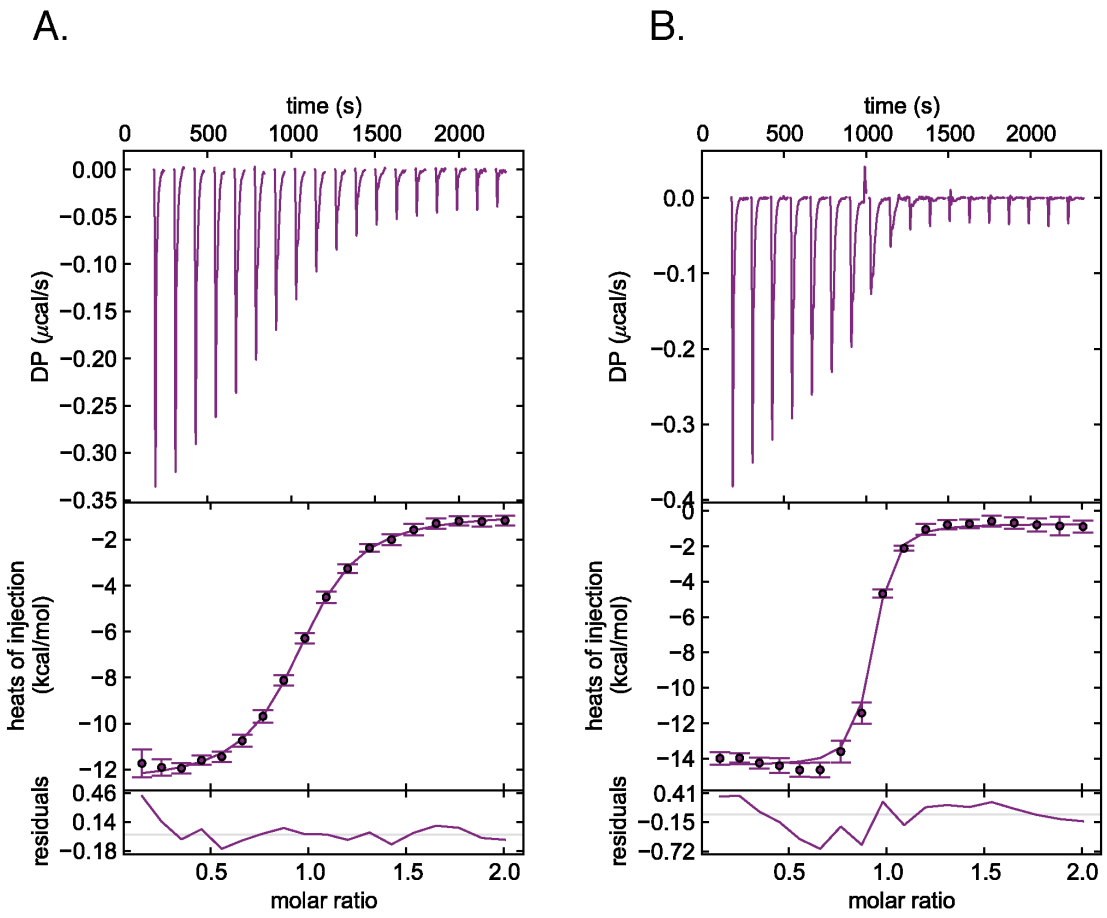

K_d = 0.37624 µM
ΔH = -11.68 kcal/mol
Incompetent Fraction p-Nephrin = 0.063
Incompetent Fraction Nck = 0

K_d = 0.03959 µM
ΔH = -13.67 kcal/mol
Incompetent Fraction p-TIR= 0.115
Incompetent Fraction Nck = 0

Figure 3.14. Measurement of the affinity of Nck for p-TIR and p-Nephrin. Isothermal titration calorimetry analysis of Nck binding to p-Nephrin and p-TIR. Nck (150 µM) in the syringe was titrated into 5 µM of either (A) p-Nephrin (3pY) or (B) p-TIR (3pY). Both datasets could be fit well to a three-site binding model with a single affinity for Nck. In the p-Nephrin and p-TIR titrations, ~6% and ~11% of the proteins, respectively, were found to be incompetent to bind Nck.

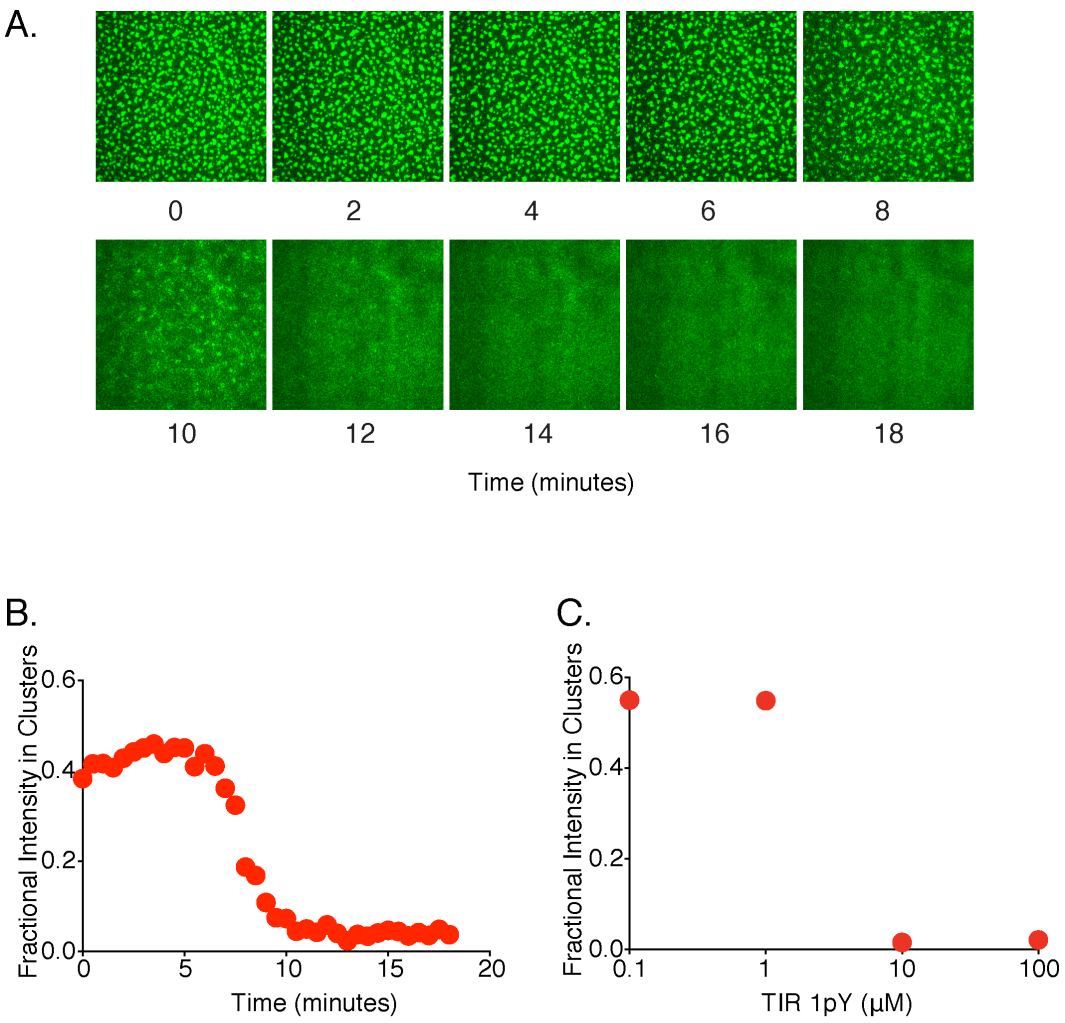

Figure 3.15. Monovalent pTyr peptide can eliminate clusters. (A) Time course following addition of 10 μM of a monovalent pTyr peptide derived from TIR (with K_D of 40 nM for the Nck SH2 domain) to clusters formed from p-Nephrin /$(SH3)_3$/N-WASP. (B) Time course of the fractional p-Nephrin intensity in clusters after addition of the TIR peptide. (C) Equilibrium fractional intensity of the p-Nephrin clusters as a function of p-TIR peptide concentration, performed in the presence of 1 μM $(SH3)_3$ and 500 nM N-WASP.

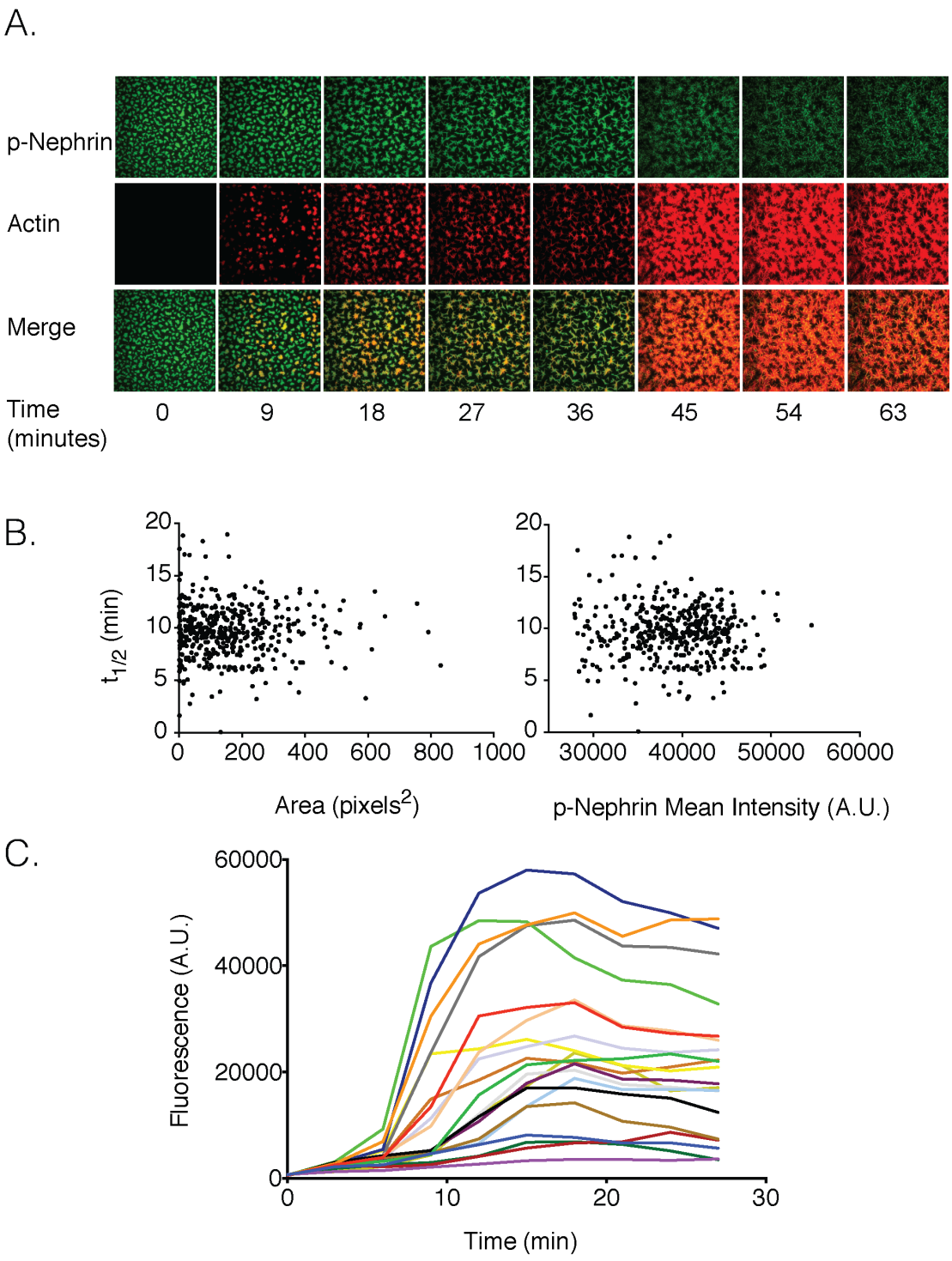

Figure 3.16. Actin assembles specifically on p-Nephrin/Nck/N-WASP clusters. (A) Alexa488-labeled p-Nephrin (2200 molecules/ μm^2) was clustered by addition of 2 μM N-WASP and 1 μM Nck. Images show time course of p-

Nephrin (top row), actin (middle row) and merge (bottom row) after addition of 10 nM Arp2/3 complex and 1 μM actin (10% rhodamine labeled). (B) Half-times of actin assembly as a function of surface area (left-panel) and p-Nephrin intensity (right-panel) in individual clusters. Half-times were calculated using the data for the first 27 min of the time-lapse. (C) Fluorescence of rhodamine-actin on individual clusters as a function of time for 20 representative clusters. Individual curves represent average intensity across an individual cluster.

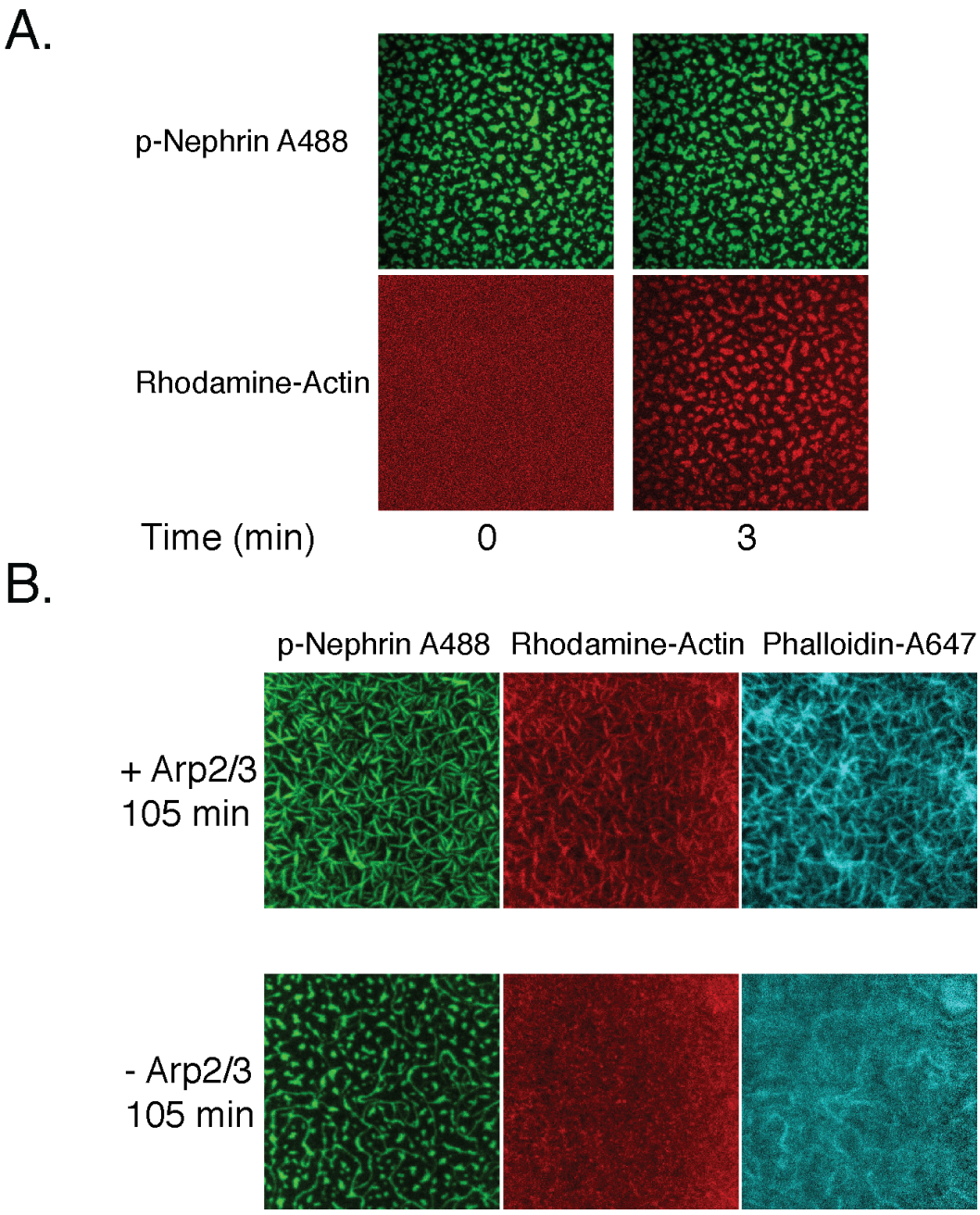

Figure 3.17. Actin localizes to and assembles on the clusters in an Arp2/3 dependent manner. (A) Images of clusters formed by p-Nephrin (2173 molecules/μm^2 on the supported lipid bilayer) plus soluble 1 μM Nck, 2 μM N-WASP, 10 nM Arp2/3 complex, and 1 μM actin (10% rhodamine labeled) at 0 and 3 min. Top panels show p-Nephrin (Alexa 488 labeled), bottom panels show fluorescence for rhodamine-actin. Note that the actin images are contrast-enhanced relative to those in Figure 7A to illustrate weak, but relatively uniform actin recruitment to the p-Nephrin clusters at 3 min. (B) Actin assembly reactions as in panel (A), except that of the lower row lacks the Arp2/3 complex, imaged at 105 min after actin addition. Left, middle, and right panels show p-Nephrin-

Alexa488, rhodamine-actin, and phalloidin-647 staining, respectively. In the bottom row phalloidin stains only the morphologically elongated structures, suggesting that the actin filaments are formed only in the re-shaped structures on the membrane.

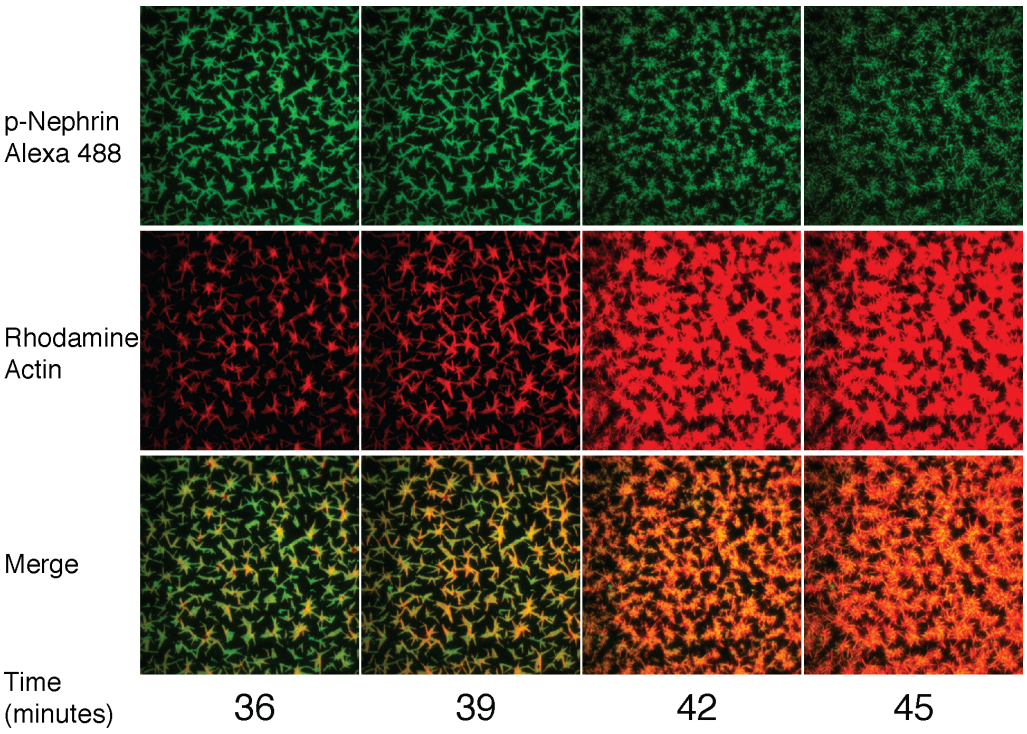

Figure 3.18. Actin assembly reorganizes p-Nephrin clusters. Enlarged actin assembly images from Figure 3.19, including more time points between 36 and 45 min. Top, middle, and bottom rows show p-Nephrin Alexa488, rhodamine-actin and merged colors, respectively.

Chapter 4. A Conserved Interdomain Linker Promotes Phase Separation of the Multivalent Adaptor Protein Nck

Sudeep Banjade[1,2], Qiong Wu[1], Anuradha Mittal[3], William Peeples[1,2], Rohit V. Pappu[3] and Michael K. Rosen[1,2]

[1]Department of Biophysics, UT Southwestern Medical Center, Dallas, TX, USA

[2]Howard Hughes Medical Institute, UT Southwestern Medical Center, Dallas, TX, USA

[3]Department of Biomedical Engineering and Center for Biological Systems Engineering, Washington University in St. Louis, St. Louis, Missouri, USA

Note: This is an earlier version of a manuscript submitted to *PNAS*. The NMR experiments contained here were done in collaboration with Dr. Qiong Wu. Dr. Qiong Wu and Dr. Michael Rosen performed the sequential assignments. William B. Peeples performed the polySUMO-polySIM experiment. Rohit Pappu and Anuradha Mittal computationally analyzed the linker-domain interactions in Nck. The manuscript was written by myself and Dr. Rosen.

Abstract

The organization of membranes and cytosol of eukaryotic cells can be controlled through phase separation of lipids, proteins and nucleic acids. Collective interactions of multivalent molecules mediated by modular binding domains can induce gelation and phase separation in several cytosolic and membrane-associated systems. The adaptor protein Nck has three SH3 domains, which bind multiple proline-rich segments in the actin regulatory protein N-WASP, and an SH2 domain that binds to multiple phosphotyrosine sites in the adhesion protein Nephrin, leading to phase separation. Here we show that the 50-residue linker between the first two SH3 domains of Nck enhances phase separation of Nck/N-WASP/Nephrin assemblies. Two linear motifs within this element, as well as its overall positively charged character, are important for this effect. The linker increases the driving force for self-assembly of Nck, likely through weak interactions with the second SH3 domain, and this appears to promote phase separation. The linker sequence is highly conserved, suggesting that the sequence determinants of the driving forces for phase separation may be generally important to Nck functions. Our studies demonstrate that linker regions between modular domains can contribute to the driving forces for self-assembly and phase separation of multivalent proteins.

Significance Statement

Many eukaryotic proteins are composed of tandem arrays of modular domains, which bind peptide ligands that also often appear in tandem arrays. The inter-domain linkers in such systems are often considered merely passive elements that flexibly connect the functional domains. Interactions between such multivalent molecules cause polymerization and concomitant phase separation, behaviors thought to be important in micron scale cellular organization. Here we show that in the multivalent signaling protein Nck, weak interactions of an inter-domain linker play a significant role in self-assembly and phase separation with ligands N-WASP and phosphorylated Nephrin. Our results suggest that high affinity interactions of modular domains may generally act synergistically with weak interactions of interdomain linkers to promote phase separation.

Introduction

Eukaryotic cells are compartmentalized into different organelles, which have specific functions. Membrane-bounded organelles, such as the endoplasmic reticulum and vacuoles have been studied extensively and their functions are relatively well understood. Non-membrane bound organelles also exist in cells. These include P-granules, Cajal bodies, PML bodies, Paraspeckles, the Nucleolus, etc. (Spector, 2006). Recently, many of these non-membrane bound structures have been proposed to form via liquid-liquid demixing phase-transitions of their constituent molecules (protein, DNA and RNA) (Hyman &

Simons, 2012). For example, germline P-granules and the nucleolus show liquid-like properties including droplet fusion, fission and shearing, and dissolve and condense in a fashion reminiscent of a phase separation process (Brangwynne et al, 2009; Brangwynne et al, 2011; Wang et al, 2014a). Similarly, stress granules also condense and dissolve, sequestering the family of DYRK kinases (Wippich et al, 2013). Organelles such as the centrosome have also been studied through the lens of phase separation theory (Zwicker et al, 2014).

A molecular understanding of the physical properties that promote formation of new phases is important to understanding the nature, function and regulation of non-membrane bound organelles. We recently showed that multivalent proteins can interact with multivalent ligands to form high order oligomers/polymers in aqueous solution that phase separate and give rise to liquid droplets. The constituent proteins are highly concentrated in these droplets (~100 fold) (Li et al, 2012). This phenomenon appears to be general for multivalent proteins; we have observed it for both natural and engineered systems involving both protein-protein and protein-RNA interactions ((Li et al, 2012) and unpublished data). When one of the interacting species is tethered to a membrane, multivalent polymerization and phase separation can also result in formation of analogous dynamic, two-dimensional puncta (Banjade & Rosen, 2014). A recent study demonstrated a similar multivalency-based behavior based on constituents of the mRNA decapping machinery (Fromm et al, 2014). In that work, interactions

between high valency helical leucine-like motifs and the oligomeric LSm protein caused the formation of a separate liquid phase.

These studies have emphasized the formation of large oligomers through the interactions of structured domains. These domains bind their ligands through well-defined molecular interfaces, with relatively high affinity (K_D ~1-100 μM) through specific interactions to form discrete structures. The connection of the domains by flexible tethers has been regarded largely as a mechanism to achieve multivalency and promote dynamics in the ligand-induced three-dimensional polymers. In other studies, however, unstructured regions of proteins, particularly those composed of low-complexity amino acid sequences, have been found to promote phase separation in vitro and in cells (Han et al, 2012; Kato et al, 2012; Martino et al, 2000; Mayer, 2001) and to promote association with RNA granules (Gilks et al, 2004; Han et al, 2012; Kato et al, 2012; Ramaswami et al, 2013). These unstructured elements can self-associate, leading to both liquid droplets (Nott et al, 2015) and solid hydrogels (Han et al, 2012; Kato et al, 2012), the former being apparently isotropic and latter being enriched in amyloid-like fibers. These studies highlight the importance of unstructured regions in the molecular self-assembly leading to formation of phase separated structures in cells.

The adaptor protein Nck and its orthologs function in signaling pathways that control diverse cellular processes including axon guidance, cell movement, cell-cell fusion, stress responses, and maintenance of cell-cell adhesions (Antoku et al, 2008; Bladt et al, 2003; Buday et al, 2002; Cowan & Henkemeyer, 2001; Garrity et al, 1996; Jones et al, 2006). In many cases these responses are coupled to the polymerization of actin through Nck/N-WASP/Arp2/3 complex pathways (Campellone et al, 2004; Ditlev et al, 2012; Eden et al, 2002; Gruenheid et al, 2001; Rohatgi et al, 2001; Weisswange et al, 2009). Nck is composed of an SH2 domain and three SH3 domains; the former binds pTyr in pYDEV sequence motifs and the latter bind a variety of proline-rich motifs (PRMs) (Mayer, 2001; Mayer & Eck, 1995; Ren et al, 1993). These modules are connected by linkers ranging from 24 to 50 residues that are predicted based on amino acid sequence to be intrinsically disordered (Rivera et al, 2004; Takeuchi et al, 2010). NMR studies of Nck2 indicate that the linkers are mostly disordered in that protein, although a portion of the linker between the first and second SH3 domains weakly interacts with the latter domain (Takeuchi et al, 2010). We have demonstrated that Nck phase separates upon interaction with PRMs in its ligand, N-WASP, and that this process occurs at lower concentrations in the presence of the pTyr ligand, phosphorylated Nephrin (p-Nephrin) (Banjade & Rosen, 2014; Li et al, 2012). Phase separation is dependent upon the number of pTyr motifs in p-Nephrin and SH3 domains in Nck.

Other than the NMR study above, potential functions of the linkers in Nck have not been examined to our knowledge. The linkers are typically viewed simply as passive, flexible tethers between the SH2 and SH3 domains. In this study we demonstrate that the linker between the first and second SH3 domains of Nck can affect the phase separation behavior of p-Nephrin/Nck/N-WASP oligomers. The linker consists of a basic N-terminal element and an acidic C-terminal element. The basic element promotes phase separation of Nck assemblies through two short linear motifs, as well as its overall positively charged character. This effect correlates with increased self-assembly of Nck, which NMR analyses suggest may be mediated by weak interactions of the linear motifs with the second SH3 domain. Our combined data suggest that weak interactions of the linker act synergistically with higher affinity interactions of the modular domains (SH3-PRM and SH2-pTyr) to promote oligomerization and consequently phase separation. Given that the sequence compositions and lengths of the linkers in different adaptor proteins are highly variable, the designs of these disordered regions may help specify when and where phase separation occurs in biological multivalent systems.

Results

The Linker between the First and Second SH3 Domains Can Promote Phase Separation of Nck Constructs

The three SH3 domains of Nck share 27 to 30 % pairwise amino acid sequence identity to each other. Previous studies have suggested that the different domains have different binding specificities for proline rich motifs (PRMs) (Gout et al, 1993; Musacchio et al, 1994; Ren et al, 1993; Yu et al, 1994). In order to eliminate these differences and isolate valency as the examined parameter, our recent investigation of two-dimensional phase separation of the p-Nephrin/Nck/N-WASP system utilized engineered, Nck-like proteins containing tandem repeats of the second Nck SH3 domain. This work demonstrated that phase separation is dependent on both the number of SH3 domains in Nck and the number of pTyr sites in p-Nephrin, supporting the idea that phase separation is driven by polymerization of the multivalent species (Figure 4.1a) (Banjade & Rosen, 2014).

Here, we began by asking how differences between the three SH3 domains in natural Nck might add complexity to this simple model. To test for specific roles of the different SH3 domains, we engineered a series of Nck truncation mutants containing only two SH3 domains (plus the SH2 domain), and examined their ability to phase separate in the presence of N-WASP (plus 7.5 μM triply-phosphorylated Nephrin (p-Nephrin) in all phase separation experiments hereafter, except where explicitly noted). We term the SH3 domains of Nck S1,

S2 and S3, from N- to C-terminal. We term the linkers between these domains L1 and L2, respectively, and the linker between S3 and the SH2 domain, L3 (Figure 4.1b).

We varied the concentration of an N-WASP fragment containing the basic, proline-rich and VCA regions of the protein (named simply N-WASP hereafter) and the various Nck proteins. Varying full length Nck and N-WASP in concert (i.e., moving along the diagonal of the phase diagram), phase separation is observed at 5 μM of both proteins (Figure 4.3a, Figure 4.2; note that in the complete phase diagram, phase separation is observed with as little as 5 μM Nck and 1 μM N-WASP (Li et al, 2012)). With the divalent molecules S1-L1-S2-L3-SH2 and S1-L1-S3-L3-SH2, phase separation is observed at 20 μM concentration plus 20 μM N-WASP (Figure 4.3 b,c). The increase in the concentration required for phase separation with loss of S3 or S2, respectively, is consistent with the valency dependence observed previously with the engineered Nck-like proteins (Banjade & Rosen, 2014). Further, the data suggest that S2 and S3 make similar contributions to phase separation since exchanging them produces identical behavior. However, to our surprise, the divalent molecule S2-L2-S3-L3-SH2 does not phase separate even up to a concentration of 250 μM plus 250 μM N-WASP (Figure 4.3d). Thus, the three divalent molecules are not equivalent in their phase separation behaviors.

To examine whether different binding specificities of the SH3 domains could account for these observations, we measured the affinities of each domain for a panel of PRM peptides derived from N-WASP by NMR spectroscopy. We analyzed 12 peptides consisting of individual PRMs, and also three peptides containing two PRMs (Figure 4.4). In each case, we titrated unlabeled peptide into ^{15}N-labeled SH3 domain and fit the ^{1}H and ^{15}N chemical shifts of the domain, measured in ^{1}H/^{15}N HSQC spectra, to a single-affinity binding isotherm. The dissociation constants (K_D's) for the binding of S1 binding to the individual PRMs ranged from 255 μM to 1080 μM, with some too weak to measure (K_D > 1080 μM); the diPRM constructs had apparent K_D values greater than or equal to 720 μM, suggesting negative cooperativity compared to some of the individual PRM peptides (Figure 4.4a). S2 had dissociation constants ≥150 μM against the single PRMs and ≥ 64 μM for the diPRMs (Figure 4.4b). S3 had behavior similar to S2, with K_D values against individual PRMs ≥ 220 μM and against diPRMs ≥ 67 μM (Figure 4.4c). In general, S2 and S3 had similar patterns of affinities for the various peptides, and typically bound with higher affinity than did S1. The similar affinity patterns of S2 and S3 toward the PRMs are also consistent with the identical phase separation behaviors of S1-L1-S2-L3-SH2 and S1-L1-S3-L3-SH2. However, the binding affinities appear insufficient to explain the absence of phase separation by S2-L2-S3-L3-SH2, since S2 and S3 bind better than S1 to virtually every peptide.

Another difference between constructs that phase separate and those that do not was the presence and absence of L1, respectively (Figure 4.3). Therefore, we added the L1 motif to the inactive divalent construct resulting in L1-S2-L2-S3-L3-SH2. This construct phase separated at 30 μM concentration plus 30 μM N-WASP (Figure 4.5 a and b). Thus, L1 was able to impart the ability to phase separate to an inactive di-SH3 protein. An L1-only peptide does not phase separate at concentrations as high as 2 mM (not shown) suggesting that the effect of the linker is synergistic with multivalent interactions of the SH3 domains of Nck with the PRMs of N-WASP.

A Positively Charged Element in L1 Promotes Phase Separation

The sequence of L1 shows a striking distribution of charges, with a highly basic N-terminus and a highly acidic C-terminus (Figure 4.5 a). All but one of its ten basic residues lie within its N-terminal half and all but one of its six acidic residues lie within its C-terminal half. This distribution is conserved over evolution from fish to humans, and also in Nck2.

To begin understanding how L1 promotes phase separation, we initially examined several L1-S2-L2-S3-L3-SH2 constructs lacking portions of the linker. A construct lacking the first 17 residues of the N-terminal basic region (ΔL1-S2-L2-S3-L3-SH2), did not phase separate up to 250 μM concentration plus 250 μM of N-WASP (Figure 4.5c). Mutation of three lysines in this region to glutamic acid

(L1K/E-S2-L2-S3-L3-SH2) or deletion of the central KVKRK motif (L1ΔKVKRK-S2-L2-S3-L3-SH2) had similarly deleterious effects on phase separation (Figure 4.5 c and d, respectively). However, replacing the C-terminal 25 amino acids with an uncharged $(GGSA)_3$ linker did not affect phase separation, producing liquid droplets at 30 μM concentration plus 30 μM N-WASP (L1ΔCT-S2-L2-S3-L3-SH2, Figure 4.5e). Thus, in the context of the di-SH3 proteins two regions of L1 appear to be most important to promoting phase separation, the 17 N-terminal residues and the central KVKRK motif.

In systems composed of disordered, linear binding motifs, the amino acid sequence context of those motifs (i.e. the flanking regions) can influence their interactions with ligands. Since basic elements within the N-terminus are important for phase separation, we asked whether the degree of positive charge in L1 could affect phase separation (Figure 4.6a). Increasing the overall positive charge in L1 (L1basic, Figure 4.6b) or increasing the positive charge density in the N-terminal element (L1addcharge and L1D/R) decreased the phase separation concentration to 10 or 20 μM di-SH3 protein plus 10 μM or 20 μM N-WASP (Figure 4.6 c and d, respectively). Shuffling charged residues throughout L1 (L1charge-shuffle) or all residues in the C-terminal segment (L1c30shuffle), both of which perturb the central KVKRK motif, also severely impair phase separation (Figure 4.6 e and f, respectively). The combined mutagenesis data suggest a model in which two motifs, the N-terminal 17 residues and the KVKRK

motif, as well as the overall positive charge in the sequence are responsible for the promotion of phase separation by L1.

We also observed parallel effects of L1 perturbations in full-length Nck. In experiments performed in the presence of 7.5 μM p-Nephrin, Nck (WT) induces phase separation at 5 μM concentration plus 5 μM N-WASP (Figure 4.7b). A construct where L1 is replaced with a $(Gly\text{-}Gly\text{-}Ser\text{-}Ala)_{10}$ linker (Nck(L1ggsa10)) requires 40 μM concentration plus 40 μM N-WASP to phase separate (Figure 4.7c). Deletion of 15 residues from the N-terminus of L1 (Nck ΔL1b) shifts the phase separation boundary to 20 μM concentration plus 20 μM N-WASP (Figure 4.7d), as does shuffling the entire L1 sequence (Nck L1shuffle, Figure 4.7d). Therefore, the enhancement of phase separation by L1 occurs consistently across a wide range of di-SH3 and full-length Nck proteins, and depends on the degree and density of positive charge in the sequence. A summary of the constructs examined here and their phase separation behaviors is presented in Figure 4.8.

L1 Promotes Self-Assembly of Nck

We focus the remainder of our analysis on the mechanism by which L1 promotes phase separation. We used isothermal titration calorimetry to compare the affinity of L1-S2-L2-S3-L3-SH2 and L1chargeshuffle-S2-L2-S3-L3-SH2 for N-WASP. Although this experiment is complicated by the presence of multiple SH3

domains and multiple PRMs in the respective partners, a simple 1:1 model of the binding isotherms yielded essentially identical apparent K_D values of 54 μM and 58 μM for L1-S2-L2-S3-L3-SH2 and L1chargeshuffle-S2-L2-S3-L3-SH2, respectively (Figure 4.9a). These affinities are also not higher than those of the individual SH3 domains for the di-PRM peptides (Figure 4.4). Together, the calorimetry and NMR data suggest that L1 does not substantially increase the affinity of the di-SH3 proteins for N-WASP. Thus, the difference in phase separation behavior of these constructs is not due to differential ability to bind N-WASP. Further, as shown in Figure 4.10 a and b, the ability of L1 to promote phase separation does not require p-Nephrin, suggesting also that the effect is also not due to increased affinity of the Nck SH2 domain for pTyr motifs. Thus, L1 does not appear to act by enhancing modular SH3-PRM or SH2-pTyr interactions.

We next asked whether L1 might promote self-association of Nck. We used dynamic light scattering (DLS) to measure the diffusion coefficients of the di-SH3 proteins as a function of concentration (Figure 4.9b). The construct containing L1 (L1-S2-L2-S2-L3-SH2) showed decreasing diffusion coefficients as concentration increased from 1 mg/mL to 25 mg/mL (27.6 μM to 690.9 μM). Over this same concentration range, the construct lacking L1 (S2-L2-S2-L3-SH2), showed a smaller decrease. These data indicate that the Nck constructs can weakly self-associate, and that L1 enhances this effect.

To further assess self-association mediated by electrostatic interactions involving L1, we used DLS to analyze diSH3 proteins containing either wild type L1 or L1chargeshuffle at various salt concentrations. We measured the diffusion coefficients of these proteins at 15 mg/mL (414.5 μM) in buffer containing 150 to 750 mM KCl (Figure 4.11). At lower KCl concentrations (150 and 250 mM), the L1-S2-L2-S3-L3-SH2 protein shows lower diffusion coefficients than the L1chargeshuffle-S2-L2-S3-L3-SH2 protein, suggesting higher degree of self-association in the wild-type L1 containing protein. The diffusion coefficient of the wild-type construct increases significantly as the salt concentration is raised, and this is consistent with disruption of intermolecular electrostatic interactions. At KCl concentrations higher than 500 mM, the diffusion coefficient of the wild-type construct equals that of the charge shuffled mutant, which is less sensitive to salt than the wild type. The combined data suggest that L1 has a propensity to enhance Nck self-association due to electrostatic interactions. These interactions are weakened either by the screening in high salt or by the screening that is encoded by shuffling the charge, thus weakening the linear charge density. We note that the concentrations used in the DLS experiments are appreciably higher than those required for phase separation, indicating that the enhancement of association due to L1 is very weak. Nevertheless, when acting in concert with multivalent SH3-PRM interactions, such weak effects are evidently significant.

We previously showed that dimerization, or more generally oligomerization, of N-WASP increases activity toward the Arp2/3 complex, due to the presence of two binding sites for the N-WASP VCA region on the Arp2/3 complex (Padrick et al, 2008; Padrick et al, 2011). We asked if the weak self-association of L1 in the presence of multivalent SH3-PRM interactions could also increase the activity of N-WASP in Arp2/3-mediated pyrene-actin assembly assays (Figure 4.9c) (Doolittle et al, 2013a). In such assays, the fluorescence of pyrene-labeled actin increases upon incorporation of the protein into filaments, such that changes in fluorescence report on the kinetics of filament formation. Addition of 5 μM S2-L2-S3-L3-SH2 to assays containing 50 nM N-WASP, 50 nM Arp2/3 complex and 2 μM actin (5% pyrene labeled) had no effect of the kinetics of actin assembly. However, the addition of 5 μM L1-S2-L2-S3-L3-SH2 decreased the lag time and increased the rate of assembly, indicating higher N-WASP activity (Figure 4.9c). These experiments were performed without Nephrin, in conditions where phase separation does not occur. Furthermore, the construct we use does not include the GBD region of N-WASP, and therefore the increase in activity toward the Arp2/3 complex is not due to regulation of autoinhibition of N-WASP (Padrick & Rosen, 2010). These data are consistent with the idea that the L1 linker enhances the self-association of Nck/N-WASP complexes.

Overall, the correlation between stronger self-association and the promotion of phase separation among the di-SH3 constructs examined here (S2-L2-S3-L3-

SH2 ~ L1chargeshuffle-S2-L2-S3-L3-SH2 < L1-S2-L2-S3-L3-SH2) suggests that these properties are causally related. Thus, weak self-association of Nck through positively charged elements in L1 could act cooperatively with stronger SH3-PRM and SH2-pTyr interactions, to promote phase separation in the p-Nephrin/Nck/N-WASP system.

The effect of enhancement in phase separation by L1 also occurs, although to a lesser degree, in an independent system of multivalent proteins. A protein consisting of five SUMO domains fused to five SUMO Interaction Motifs (SIMs) through a $(GGS)_4$ linker ($SUMO_5$-SIM_5) phase separates at 12 μM. However, a protein in which $SUMO_5$ and SIM_5 are connected by L1 ($SUMO_5$-L1-SIM_5) phase separates at 4 μM. However a protein in which L1 is replaced with L1chargeshuffle phase separates at 10 μM, quite similar to the construct containing a $(GGS)_4$ linker ($SUMO_5$-L1chargeshuffle-SIM_5, Figure 4.12). Thus, the effects of L1 are not specific to the p-Nephrin/Nck/N-WASP system. Rather, the linker can act autonomously to promote the phase separation of multivalent proteins. This observation suggests that the charged blocks of residues can non-specifically interact with charges on the surfaces of other protein partners, but when the acidic and basic residues are shuffled to decrease the local charge density they cannot. In this regard, it is probably important that like S2 and S3 of Nck, both $SUMO_5$ and SIM_5 are acidic (pI = 5.34 and 4.07, respectively), and that SUMO structures show a prominent acidic surface patch, which could enable

favorable interactions with the basic element of L1. In the context of multivalent binding, these weak interactions could produce an enhancement in assembly of these complexes.

L1 Can Bind the Second SH3 Domain of Nck

To learn how L1 might promote self-assembly of Nck, we examined $^{1}H/^{15}N$ TROSY (Transverse Relaxation-Optimized SpectroscopY) spectra of several ^{15}N-labeled Nck proteins. The spectrum of L1-S2-L2-S3-L3-SH2 shows a large number of well dispersed resonances, indicative of folded domains, as well as a series of intense, poorly dispersed resonances, representing disordered, dynamic residues (Figure 4.13 and Figure 4.15). Deletion of L1, which eliminates 48 backbone amides of the protein, causes the disappearance of 36 resonances, all of which are in the poorly dispersed region (^{1}H chemical shifts between 7.8 and 8.7 ppm). The disparity between residues and resonances lost suggests that 12 residues in L1 are undergoing chemical exchange, and thus have highly broadened/missing resonances in the L1-S2-L2-S3-L3-SH2 spectrum. Of the 36 disappearing amide resonances, seven gave only very weak signals in three-dimensional triple resonance experiments, suggesting that they too were undergoing chemical exchange, for a total of 19 such resonances. We were able to obtain definitive chemical shift assignments for 24 of the remaining 29 amides that disappeared upon truncation of L1. As shown in Figure 4.14, these correspond to residues Leu71-G78 and most of residues P84 to Y105. These

assignments suggest that the broadened/absent resonances likely correspond to the N-terminus of L1, K59-N70, as well as the K79-K83 motif, and thus that these regions are likely in chemical exchange. Notably, these regions correspond well to the elements of L1 that promote phase separation (Figure 4.5).

In addition to eliminating many crosspeaks, loss of L1 also causes shifts in 18 backbone crosspeaks of lower intensity, 15 of which are in the well dispersed regions of the spectrum (^{1}H chemical shifts < 7.8 and > 8.7 ppm) (Figure 4.14). Three tryptophan sidechain crosspeaks shift as well. Overlaying the spectrum of the isolated second SH3 domain reveals that all of these shifting crosspeaks correspond to this domain (Figure 4.13b and Figure 4.15a). Assignment of these shifting resonances shows that they localize to one face of the domain (Figure 4.15b). They are at highest density near one end of the canonical PRM binding site. Notably, the highly acidic RT loop is located near the center of the affected region, and all five of its residues are affected (E120-R121-E122-D123-E124, Figure 4.15). The simplest explanation for these data is that in L1-S2-L2-S3-L3-SH2, the immediate N-terminus and perhaps the KVKRK motif of L1 bind the second SH3 domain near the acidic RT loop, in or near the PRM binding site, while other regions of the linker are disordered. It is unclear from the data how populated the SH3-bound state of L1 is, and thus how strong the interaction is. However, a previous NMR study of Nck2, which is 69% identical to Nck1, also reported binding of a basic element in L1 to S2, and measured an interaction *in*

trans with K_D ~ 1.7 mM (Takeuchi et al, 2010). Further our ITC data (Figure 4.9) do not indicate that L1 competes strongly for PRM binding. Thus, it is likely that the interaction is weak in Nck1 as well. Given this propensity of L1 and S2 to bind each other, it is likely that at high concentrations in solution, or in the context of p-Nephrin/Nck/N-WASP assemblies where multiple Nck proteins are held in close approximation, these weak interactions promote Nck self-assembly and consequently phase separation. We recognize that if L1 interacts with the PRM binding site, this interaction could increase the apparent valency of Nck (by enabling multiple molecules to come together), but at the expense of total free SH3 concentration in solution. Nevertheless, the overall effects on the size and solubility of the oligomers could still act to promote phase separation.

Discussion

Phase separation of biological molecules into distinct liquid-like structures provides a potentially general mechanism for the formation and regulation of non-membrane-bounded compartments in cells. We and others have shown that liquid-liquid demixing (phase separation), can be promoted by the oligomerization/polymerization of multivalent proteins and their multivalent ligands, as well as by disordered polypeptide chains (Han et al, 2012; Kato et al, 2012; Li et al, 2012; Martino et al, 2000; Meyer et al, 2001; Nott TJ, 2015 in press; Schmidt & Gorlich, 2015). In the former case, relatively strong, specific interactions between modular elements (K_D = 1-100 μM for individual module-

module binding) can lead to assembly of large, dynamic oligomers or polymers (Benedek, 1982; Flory, 1953; Li et al, 2012). In both cases, relatively weak, non-specific interactions can provide the driving force for phase separation (Flory, 1953; Ken A. Dill, 2010). For some disordered chains, phase separation is followed by or occurs concomitantly with formation of amyloid-like filaments (Han et al, 2012; Kato et al, 2012). In modular systems, the large size of module-mediated oligomers should enhance the interactions that lead to demixing, analogous to the increase in the Flory-Huggins Chi parameter with an increase in polymer length (Flory, 1953). Theoretical models have been developed to describe how strong interactions quantified by a binding affinity and weak interactions quantified by second- and third-order Virial coefficients can work together to promote concomitant molecular assembly and phase separation (Alexander N. Semenov, 1998).

Here we have used the behavior of Nck and its ligands p-Nephrin and N-WASP to experimentally examine the interplay between modular domain interactions and the properties of interdomain linkers. We have found that the linker between the first and second SH3 domains of Nck can promote phase separation of multivalent assemblies with N-WASP and p-Nephrin. This effect is seen for both di-SH3 and tri-SH3 Nck constructs, and in complexes with N-WASP alone and those containing all three proteins. This property of the linker results from two sequence motifs, the N-terminal 17 residues and the central KVKRK motif, as

well as the basic character of the surrounding sequence context. For several constructs, the enhancement of phase separation correlates with an increased ability to promote weak Nck self-association, but not with higher affinity Nck-N-WASP or Nck-p-Nephrin binding. Thus, increased self-association of Nck may be the mechanism by which the linker promotes phase separation of Nck/N-WASP and pNephrin/Nck/N-WASP complexes. NMR analyses and atomistic simulation provide a potential structural mechanism for self-association, by revealing weak binding of L1 to the second SH3 domain of Nck. The correspondence of the sequence motifs in L1 that bind the SH3 domain (Figure 4.13) with those that promote phase separation (Fig. 4), as well as the acidic character of the interaction site on the SH3 domain (Figure 4.15b) and the importance of the overall basic character of L1 in promoting phase separation (Figure 4.6), support the idea that L1-SH3 interactions provide the mechanism for L1 to promote phase separation. At high concentrations this interaction may also occur in trans, which could enable self-binding. We note that L1 also enhances phase separation in the S1-L1-S3-SH2 and polySUMO-polySIM systems, which obviously lack the second Nck SH3 domain. Nevertheless, both of these other proteins also contain highly acidic domains (S3, SUMO and SIM), and we speculate that these could also bind weakly to the basic element of L1, leading to self-assembly and phase separation.

ClustalW analysis of ~50 Nck sequences reveals that the protein is highly conserved from fish to mammals, with average pairwise identity to human Nck1 of ~95% across the entire sequence. The average pairwise identify in the linker (94.9 %; Figure 4.16) is comparable to that in the three SH3 domains (95.1%, 95.7%, and 94.8%, respectively), and the SH2 domain (97.3 %), and slightly higher than that in the L2 and L3 linkers (89.5% and 86.3 %, respectively). The strong conservation of the linkers is unusual for multidomain proteins, suggesting that the properties of these elements in Nck are functionally important, perhaps through a general role of self-assembly and phase separation in Nck pathways. In this regard, it is notable that a large number of reported Nck ligands have three or more predicted or demonstrated pTyr binding sites for the Nck SH2 domain (Lettau et al, 2009; Obenauer et al, 2003), which would enable them to promote polymerization and phase separation analogously to p-Nephrin.

Furthermore, proteomic analyses have determined that several serines and threonines in the basic region of L1 can be phosphorylated in cells (Dephoure et al, 2008; Mayya et al, 2009). The importance of basic N-terminal region in the behavior of L1 suggests that these phosphorylation events could be used to regulate the phase separation of Nck assemblies, as the phosphorylation of the N-terminal residues would likely be inhibitory towards self-association of Nck. To our knowledge, Nck phosphorylation has not yet been examined in the context of

localization/assembly or biological function of the protein. Such analyses will be needed to test these potential regulatory mechanisms in the future.

Even a cursory analysis of the interdomain linkers of different adaptor proteins demonstrates wide variability in lengths and sequence compositions. Our findings here suggest that adaptors containing linkers with blocks of charges may be more prone to phase separate than those with more evenly distributed charges. Interactions between opposite charges could occur between linkers and structured domains, two different linkers, or even between charged surfaces of structured elements. Such linker properties are not essential for phase separation, however, as we have found that the adaptor protein Grb2, which has only very short, charge-neutral interdomain linkers, can phase-separate on lipid bilayers through interactions with its multivalent ligands, SOS and phosphorylated Lat (Su *et al.*, in preparation). Nevertheless, the nature of the linkers is expected to influence the propensity to phase separate, along with features such as module-module binding affinity, avidity effects and module valency (Li et al, 2012) and could provide additional mechanisms of regulation. Fine-tuning of these properties likely specifies which multivalent molecules are capable of forming supramolecular polymers and phase separating *in vivo*. Bioinformatics studies, based on these ideas, may be helpful in predicting molecules and pathways that could function and be regulated through phase separation.

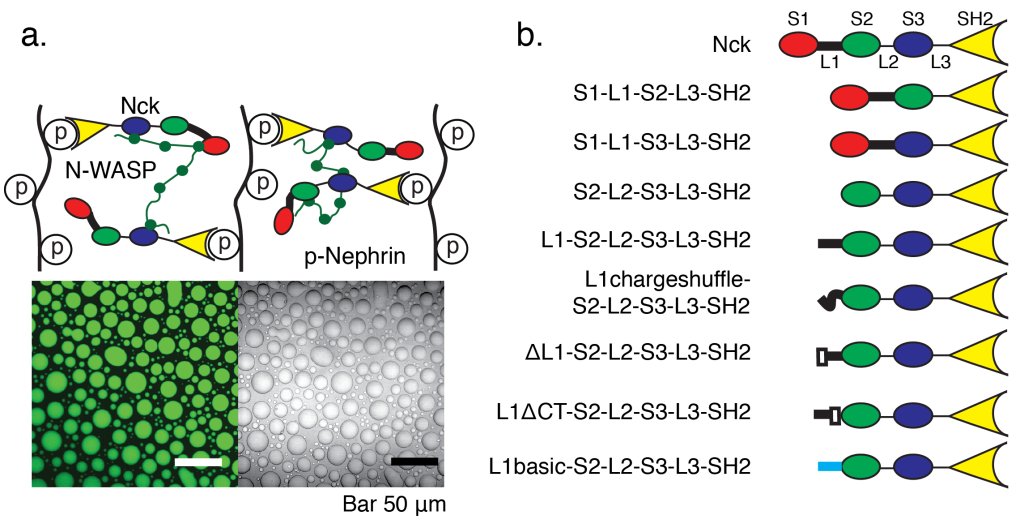

Figure 4.1. Multivalent interactions in adaptor proteins drive phase separation. (a) Model of the interaction of the multivalent proteins p-Nephrin, Nck and N-WASP (top-panel). Upon mixing 3 μM p-Nephrin, 2 μM N-WASP (10 % Alexa488-labeled) and 10 μM Nck, micron-scale droplets can be visualized by fluorescence (left) and differential interference contrast (right) microscopies. (b) A few constructs based on Nck used in this study.

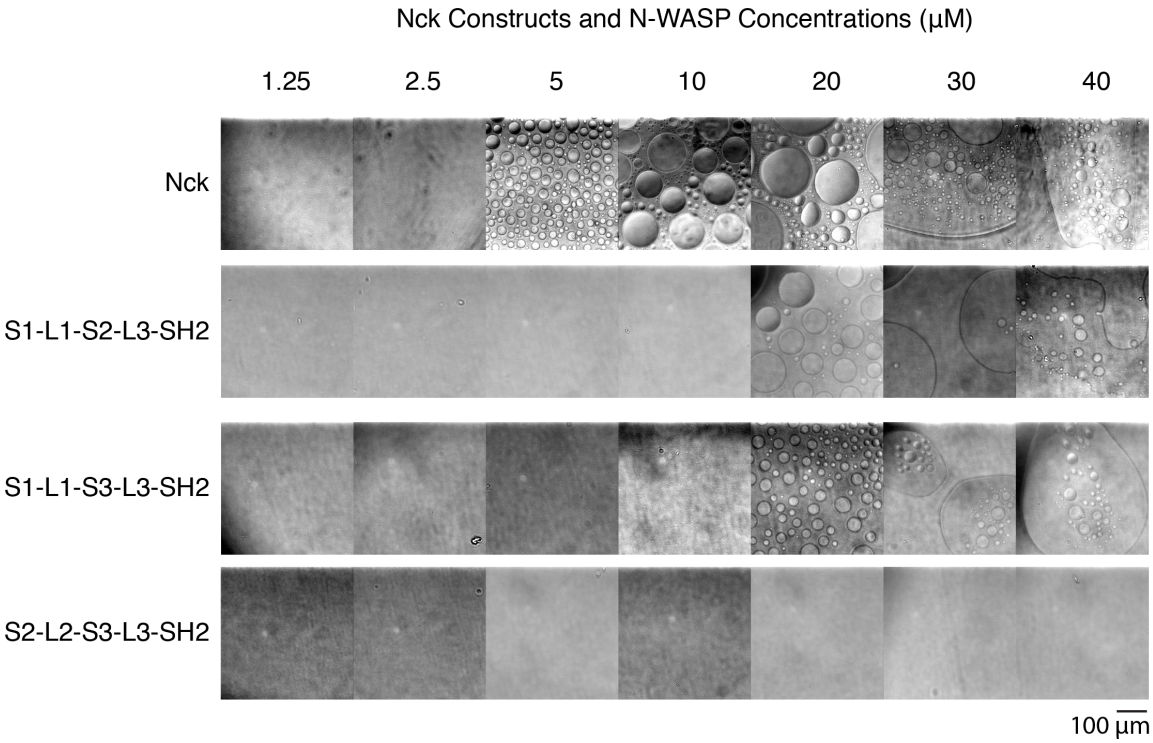

Figure 4.2. Di-valent Nck SH3 proteins do not phase separate equally. Bright-field microscope images showing the formation of droplets as a concentration of the different proteins indicated on the left. These data are represented as red dots for phase separation and blue dots for absence of phase separation in Fig. 2. Scale bar is 100 μm.

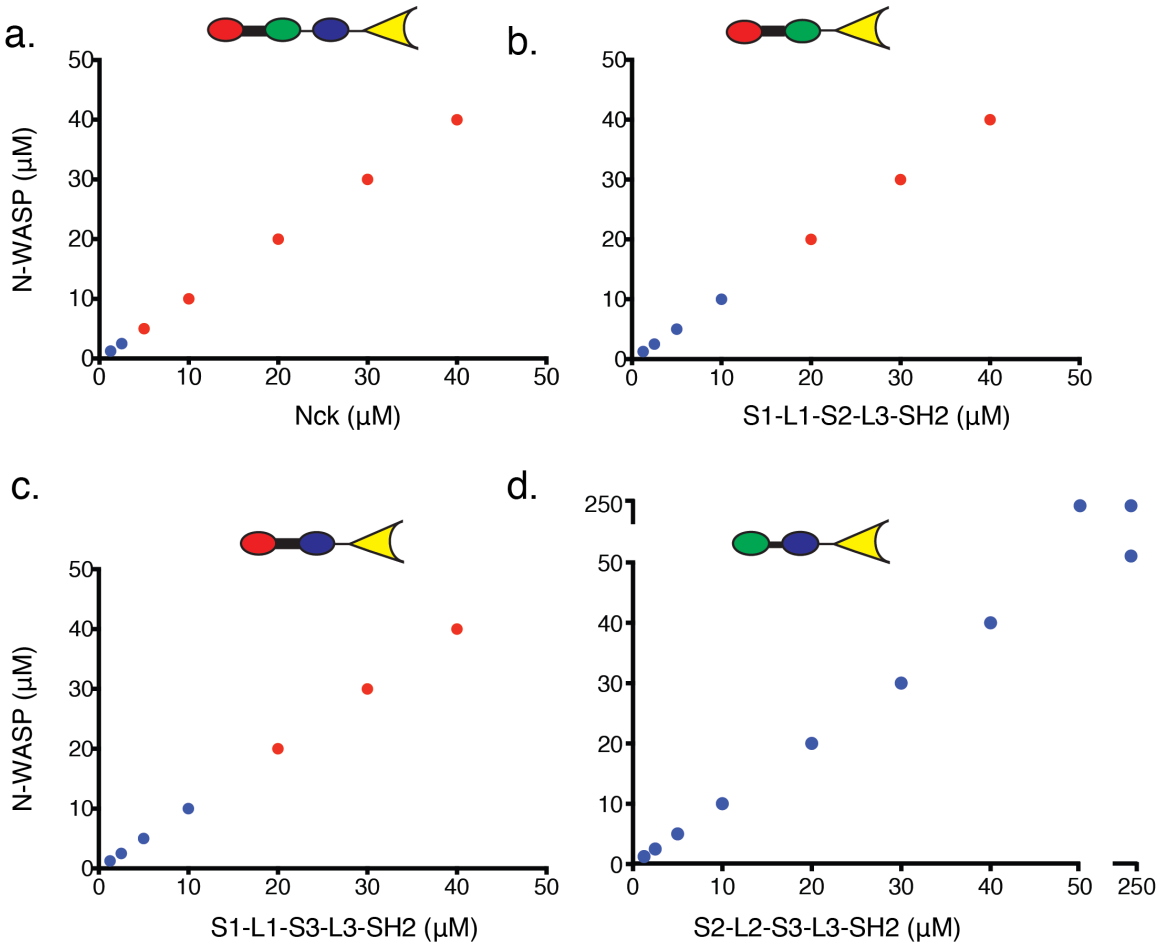

Figure 4.3. Different di-SH3 fragments of Nck are not equivalent in their phase separation properties. Phase separation of N-WASP and Nck proteins in the presence of 7.5 μM p-Nephrin. Red and blue symbols indicate phase separation and no phase separation, respectively. (a)-(d), data for Nck, S1-L1-S2-L3-SH2, S1-L1-S3-L3-SH2 and S2-L2-S3-L3-SH2, respectively.

a.

PRM	SH3-1 Kd (μM)	diPRM	SH3-2 Kd(μM)
1	> 1 mM	diPRM-1	720 +/- 97
2	> 1 mM		
3	420 +/- 22.1		
4	> 1 mM	diPRM-2	~ 1500
5	N.B.		
6	1080 +/- 94		
7	> 1 mM		
8	255 +/- 20.7	diPRM-3	~ 900
9	700		
10	> 1 mM		
11	346+/- 24.1		
12	N.B.		

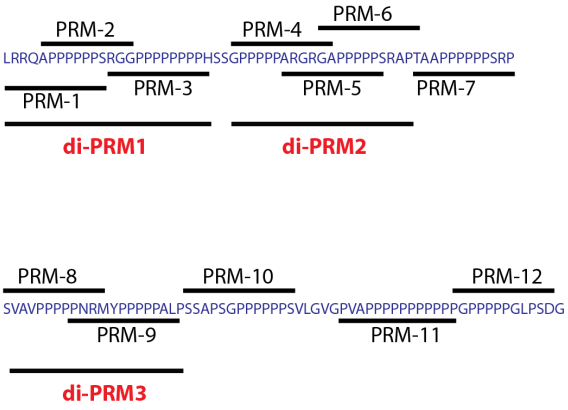

b.

PRM	SH3-2 Kd (μM)	diPRM	SH3-2 Kd(μM)
1	235 +/- 16	diPRM-1	88 +/- 38
2	348 +/- 24		
3	N.B.		
4	147 +/- 4	diPRM-2	64 +/- 8
5	295 +/- 23		
6	295 +/- 23		
7	701 +/- 70		
8	199 +/- 8	diPRM-3	160 +/- 19
9	N.B.		
10	N.B.		
11	N.B.		
12	N.B.		

c.

PRM	SH3-3 Kd (μM)	diPRM	SH3-3 Kd(μM)
1	231 +/- 36	diPRM-1	114 +/- 28
2	289 +/- 42		
3	1650 +/- 115		
4	222 +/- 29	diPRM-2	67 +/- 6
5	527 +/- 84		
6	~ 800		
7	N.B.		
8	~ 1 mM	diPRM-3	~ 1 mM
9	>> 1 mM		
10	>> 1 mM		
11	>> 1 mM		
12	>> 1 mM		

Figure 4.4. Affinities of the individual Nck SH3 domains for PRMs in N-WASP. Affinities of the different PRM's divided as shown in the top-right panel for the S1 (a), S2 (b) and S3 (c) domains, as measured by NMR spectroscopy.

a.

L1(wild type)	KNSARKASIVKNLKDTLGIGKVKRKPSVPDSASPADDSFVDPGERLYDLN
ΔL1	GIGKVKRKPSVPDSASPADDSFVDPGERLYDLN
L1K/E	KNSAREASIVENLEDTLGIGKVKRKPSVPDSASPADDSFVDPGERLYDLN
L1Δ(KVKRK)	KNSADKASIVDNLKDTLGIG--GS-PSVPKSASPADKSFVKPGERLYDLN
L1ΔCT	KNSARKASIVKNLKDTLGIGKVKRKGGSAGGSAGGSA

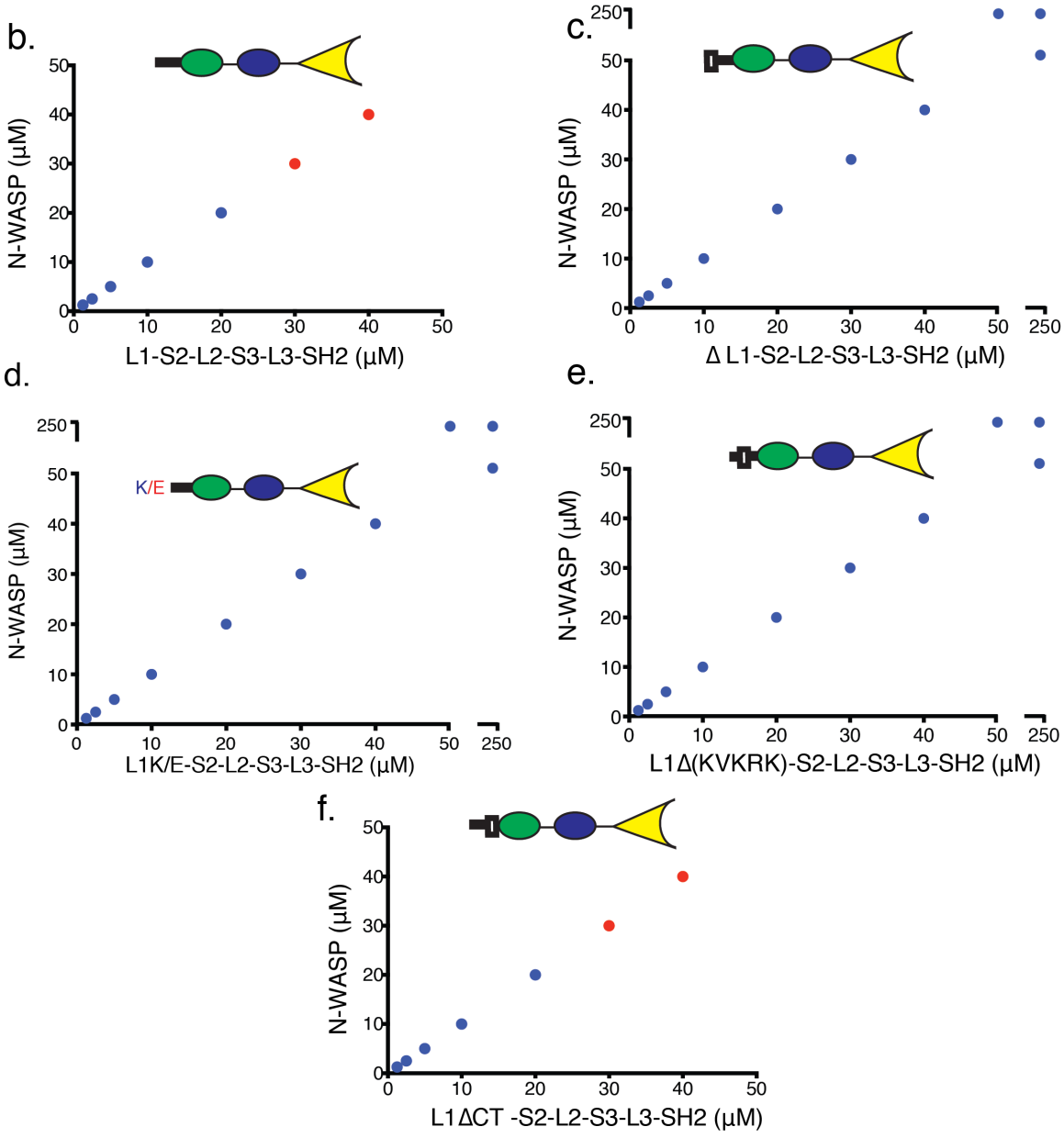

Figure 4.5. L1 promotes phase separation of a di-SH3 protein through a basic N-terminal element. (a) Sequences of L1 used in experiments shown in (b) – (g). (b) – (g) Phase separation experiments were performed in the presence

of 7.5 μM p-Nephrin. Red and blue symbols indicate phase separation and no phase separation, respectively.

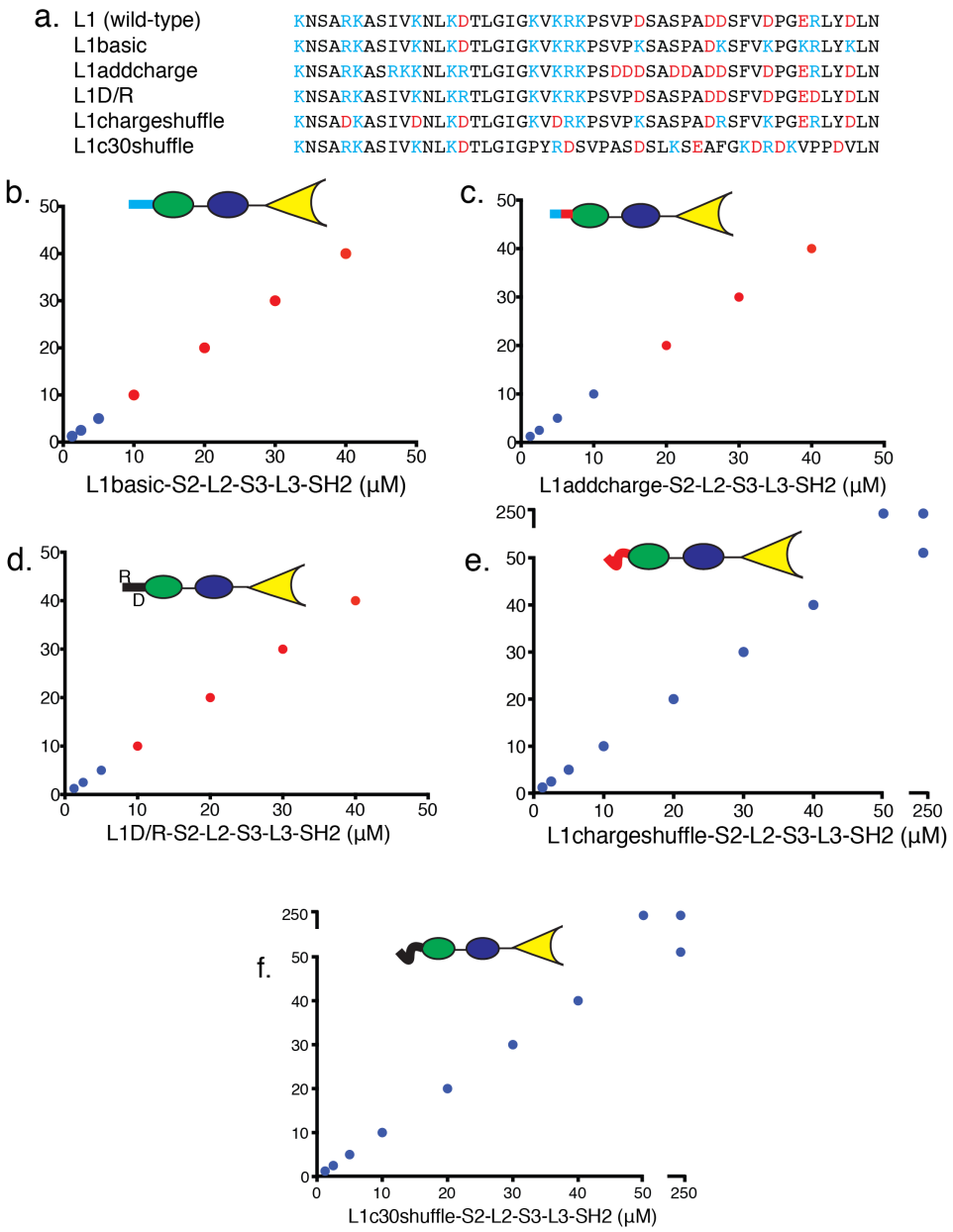

Figure 4.6. Basic region of L1 promotes phase separation of di-SH3 Nck constructs. (a) Sequence of L1 elements in L1-S2-L2-S3-L3-SH2 constructs used in panels (b)-(f). (b)-(f) Phase separation experiments were performed with the indicated di-SH3 proteins and N-WASP, in the presence of 7.5 μM p-Nephrin.

Red and blue symbols indicate phase separation and no phase separation, respectively.

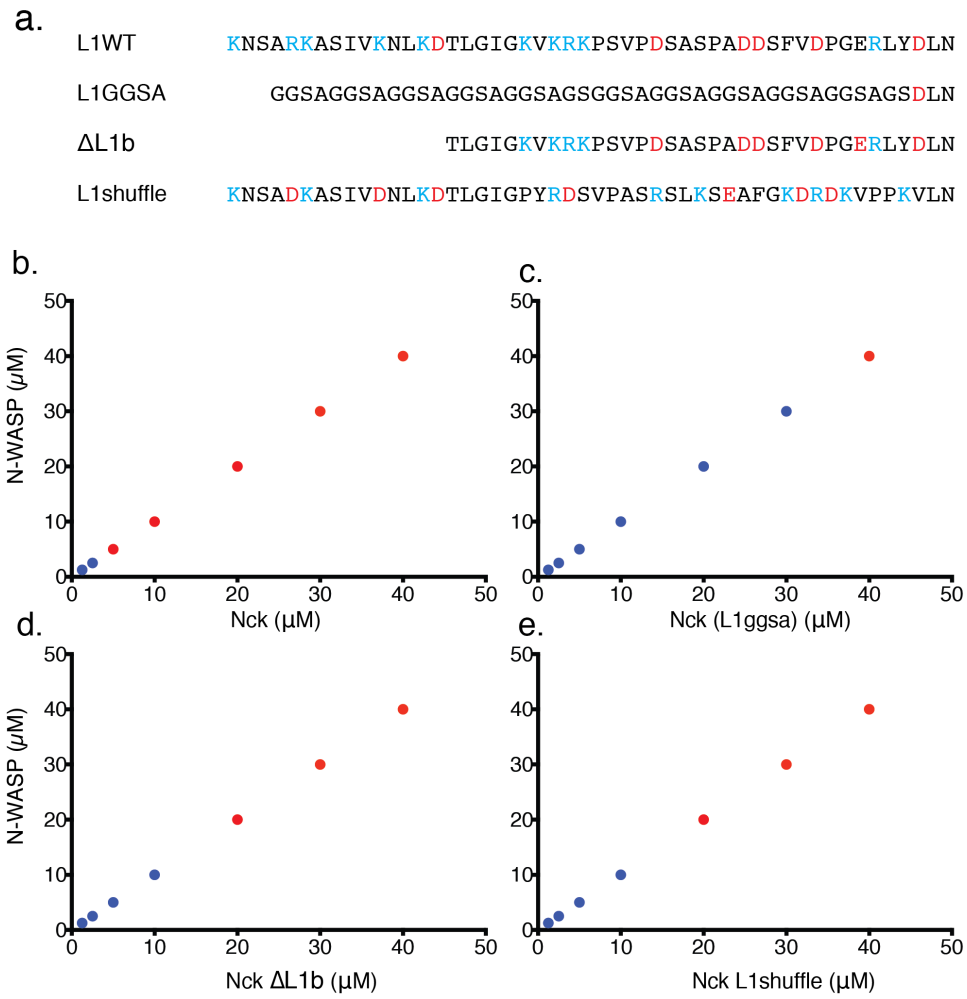

Figure 4.7. L1 affects phase separation of full-length Nck proteins. (a) Sequence of L1 elements in full length Nck constructs used in panels (b)-(f). (b-f) Phase separation experiments with Nck constructs in the presence of N-WASP and 7.5 μM p-Nephrin. Red and blue symbols indicate phase separation and no phase separation, respectively.

Construct	Sequence	Note	Phase Separation Concentration
L1 (wild-type)	KNSARKASIVKNLKDTLGIGKVKRKPSVPDSASPADDSFVDPGERLYDLN	WT	30 μM
ΔL1	GIGKVKRKPSVPDSASPADDSFVDPGERLYDLN	delete N-term 20 AA	>250 μM
L1KtoE	KNSAREASIVENLEDTLGIGKVKRKPSVPDSASPADDSFVDPGERLYDLN	mutate three N-term K's to E's	>250 μM
L1(ΔKVKRK)	KNSARKASIVKNLKDTLGIG-GS--PSVPDSASPADDSFVDPGERLYDLN	delete KVKRK	>250 μM
L1ΔCT	KNSARKASIVKNLKDTLGIGKVKRKGGSAGGSAGGSA	replace C-term 25 AA with $(GGSA)_3$	30 μM
L1basic	KNSARKASIVKNLKDTLGIGKVKRKPSVPKSASPADKSFVKPGKRLYKLN	mutate C term acidic's to K's	10 μM
L1addcharge	KNSARKASRKKNLKRTLGIGKVKRKPSDDDSADDADDSFVDPGERLYDLN	add basic residues N-term and acidic residues C-term	20 μM
L1D/R	KNSARKASIVKNLKRTLGIGKVKRKPSVPDSASPADDSFVDPGEDLYDLN	swap N-term D with C-term R	10 μM
L1charge-shuffle	KNSADKASIVDNLKDTLGIGKVDRKPSVPKSASPADRSFVKPGERLYDLN	shuffle only charged residues	>250 μM
L1c30shuffle	KNSARKASIVKNLKDTLGIGPYRDSVPASDSLKSEAFGKDRDKVPPDVLN	shuffle C-term 30 AA	>250 μM

Figure 4.8. Summary of L1 mutations used in the di-SH3 constructs. The minimum concentration at which phase separation of each construct was observed is listed.

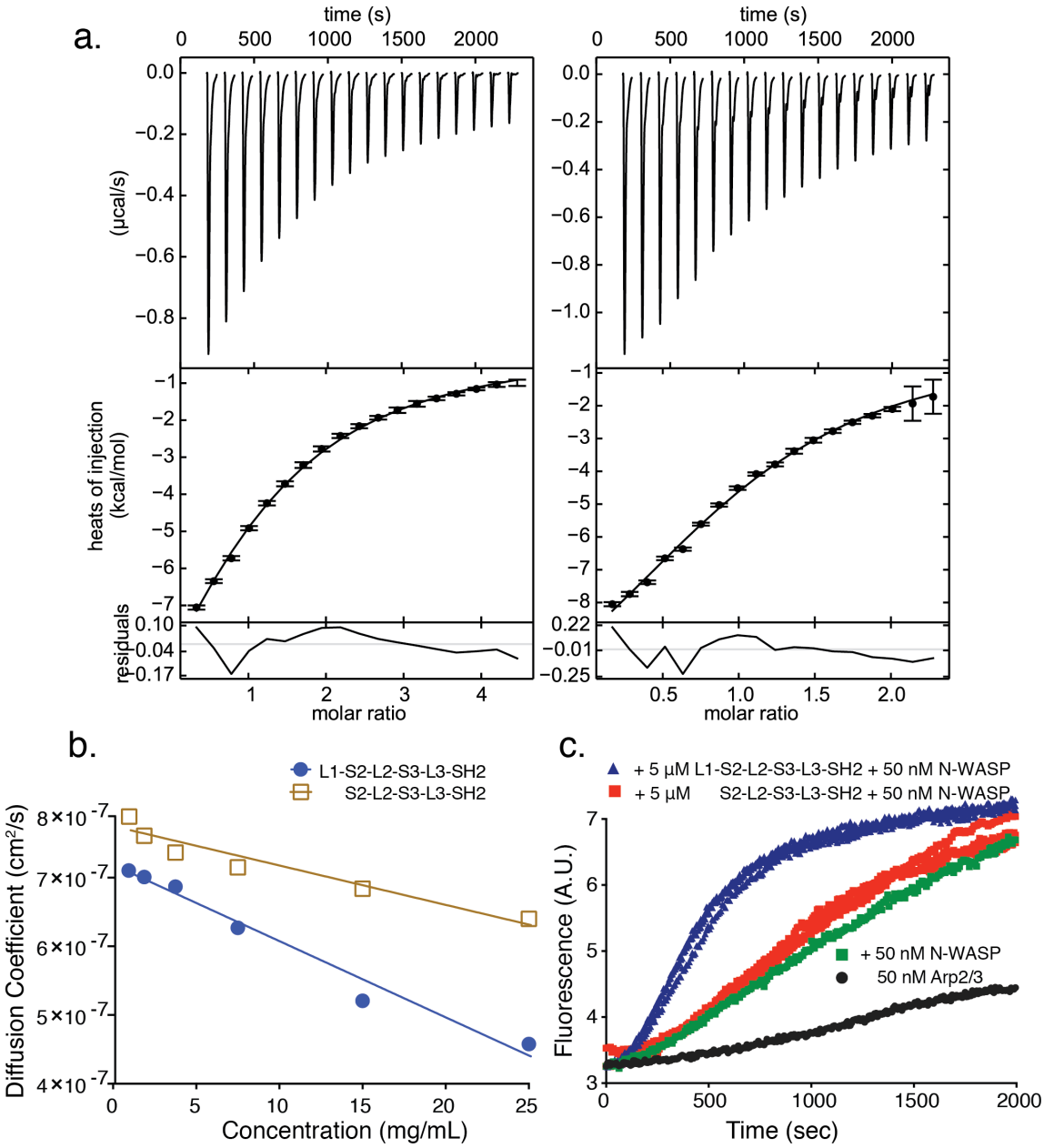

Figure 4.9. L1 promotes self-association of di-SH3 proteins, but does not substantially alter binding to N-WASP. (a) Isothermal titration calorimetry analysis of the binding of L1-S2-L2-S3-L3-SH2 or L1chargeshuffle-S2-L2-S3-L3-SH2 to N-WASP. Left: 1.1 mM of L1-S2-L2-S3-L3-SH2 was titrated to 100 µM N-WASP; right: 1.1 mM L1chargeshuffle-S2-L2-S3-L3-SH2 was titrated to 50 µM of N-WASP, thereby giving different molar ratios in the x-axis. Upper, middle and bottom panels show heats of injection, single-site fit to integrated heats, and residuals of the fit, respectively. (b) Diffusion coefficients of L1-S2-L2-S3-L3-SH2, brown squares, and S2-L2-S3-L3-SH2, blue circles at different concentrations, measured by dynamic light scattering. (c) Pyrene-actin assembly assays contained 2 µM actin (5 % pyrene-labeled) and 50 nM Arp2/3 complex (black),

plus: 50 nM N-WASP (green), 50 nM N-WASP and 5 μM S2-L2-S3-L3-SH2 (red) or 50 nM N-WASP and 5 μM L1-S2-L2-S3-L3-SH2. Data for S2-L2-S3-L3-SH2 and L1-S2-L2-S3-L3-SH2 reflect three replicates.

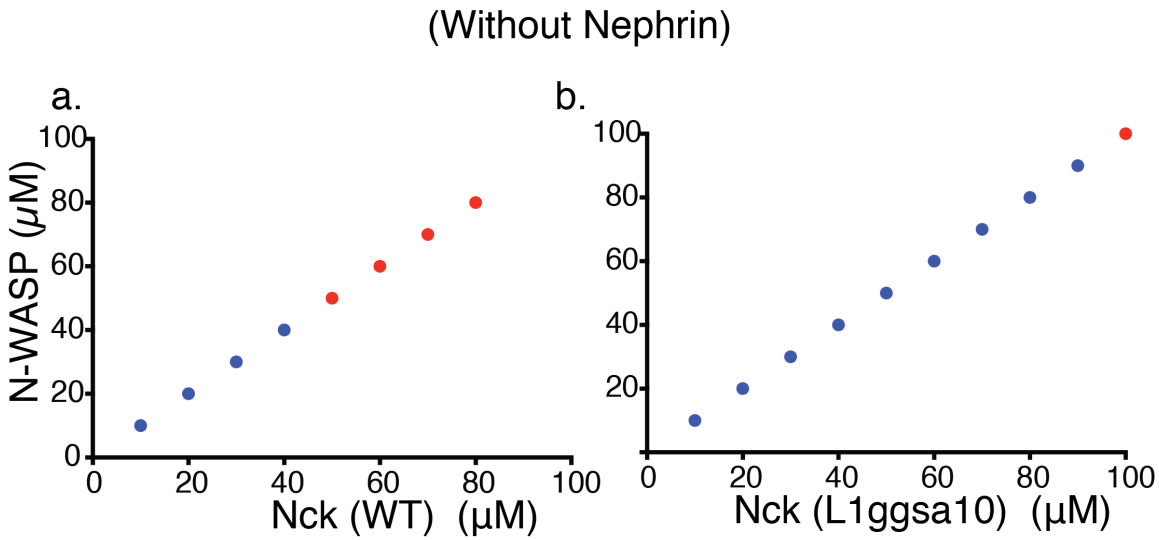

Figure 4.10. L1 affects phase separation in Nck in the absence of Nephrin. Phase separation experiments with Nck constructs in the presence of N-WASP without Nephrin, for a) Nck and b) NckL1ggsa10. Red and blue symbols indicate phase separation and no phase separation, respectively.

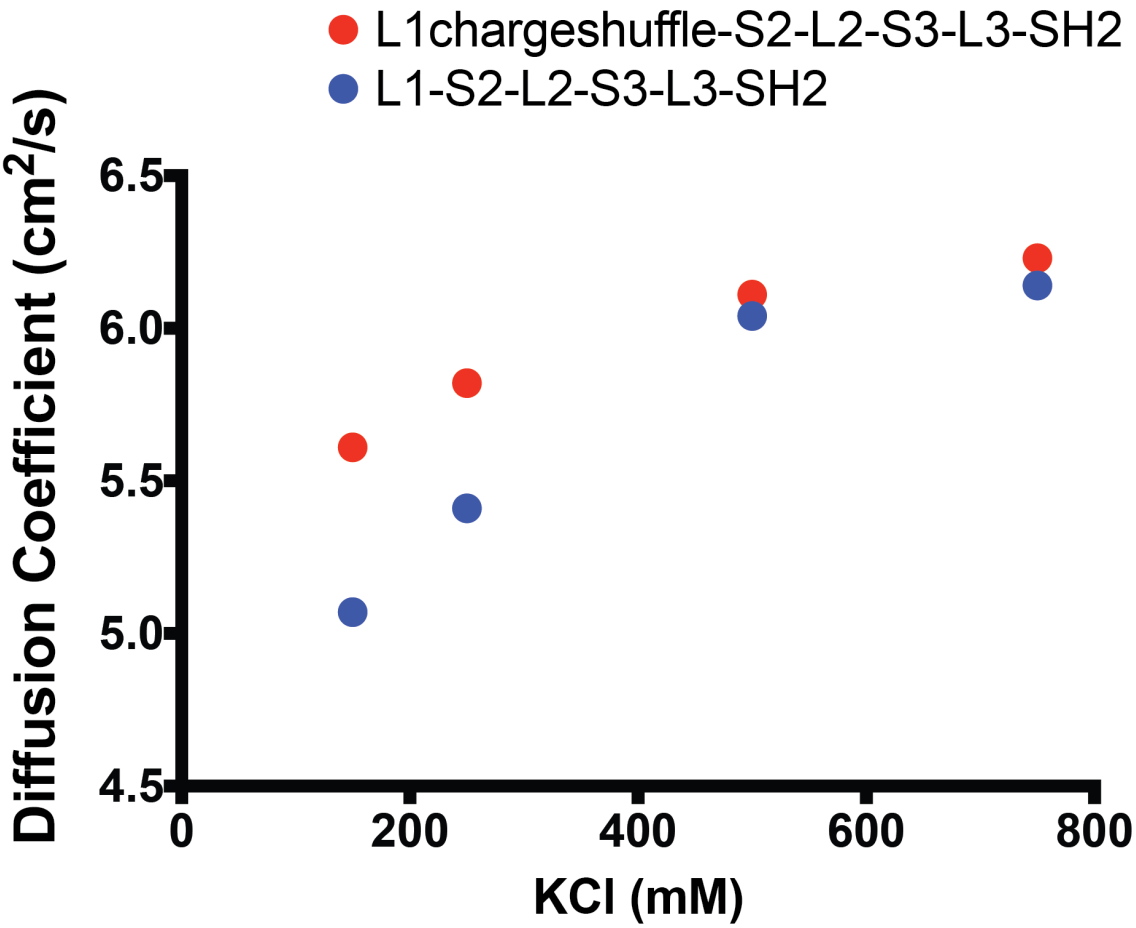

Figure 4.11. L1 promotes self-association via electrostatic interactions. Dynamic light scattering (DLS) experiments with L1-S2-L2-S3-L3-SH2 and L1chargeshuffle-S2-L2-S3-L3-SH2 constructs. Diffusion coefficients obtained from dynamic light scattering measurements at different KCl concentrations. Blue circles represent L1-S2-L2-S3-L3-SH2 and red circles represent L1chargeshuffle-S2-L2-S3-L3-SH2.

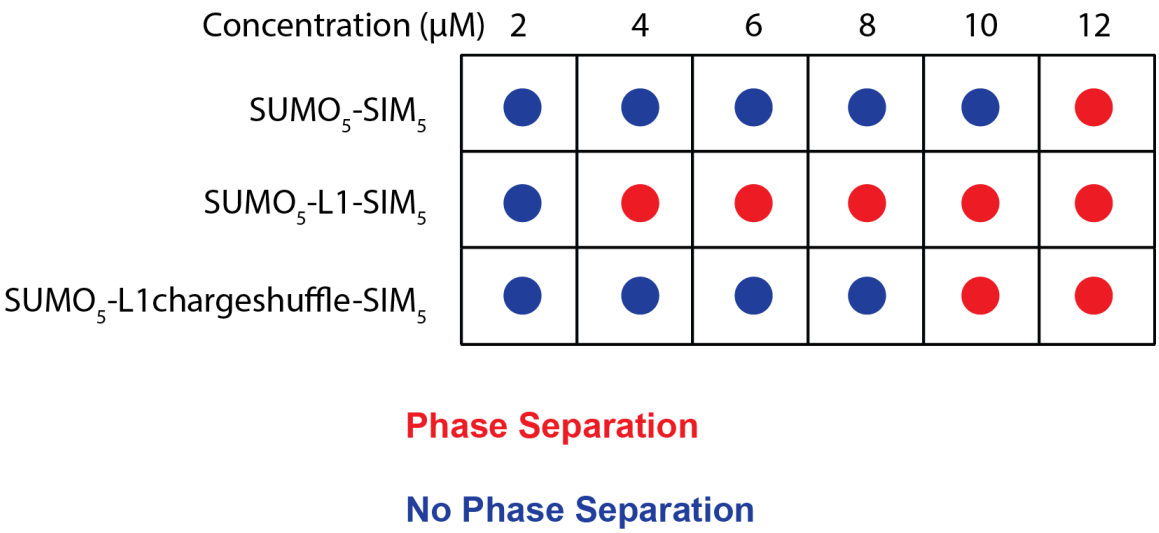

Figure 4.12. L1 enhances phase separation of PolySUMO-PolySIM proteins. (a) Phase separation (red dots) or no phase separation (blue dots) observed using $SUMO_5$-SIM_5, $SUMO_5$-L1-SIM_5, and $SUMO_5$-L1chargeshuffle-SIM_5 proteins.

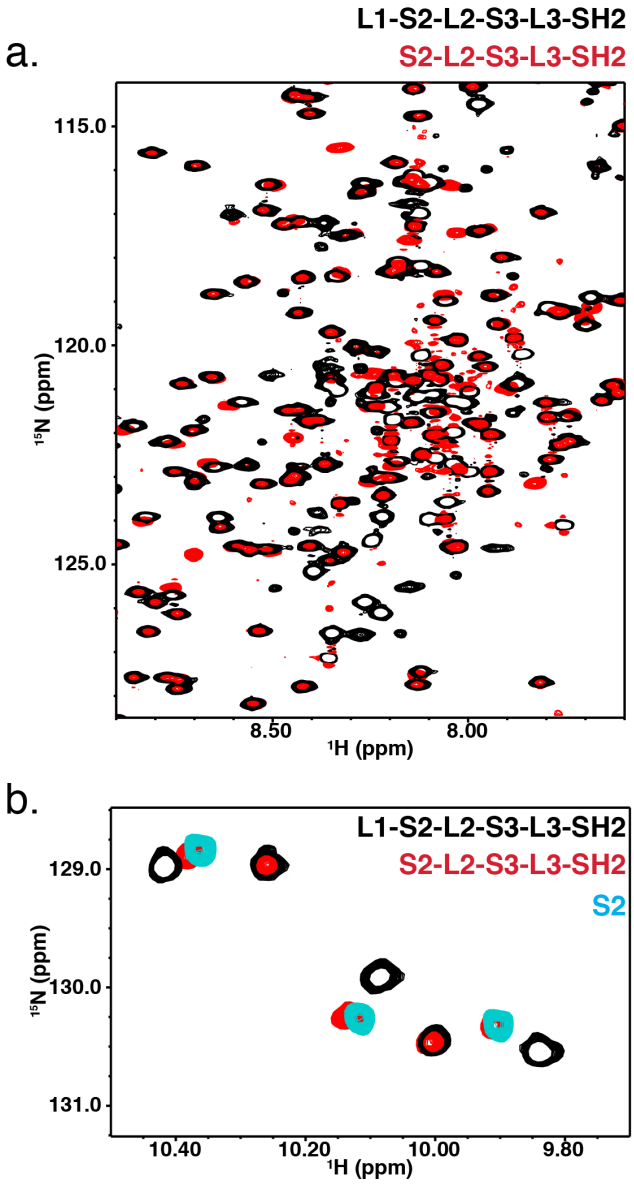

Figure 4.13. L1 is partially disordered, but also binds the second SH3 domain. (a) Overlaid $^{1}H/^{15}N$ TROSY spectra of 250 μM U-[^{15}N] labeled L1-S2-L2-S3-L3-SH2 (black) and 250 μM S2-L2-S3-L3-SH2 (red). (b) Overlaid tryptophan indole region of $^{1}H/^{15}N$ TROSY spectra of L1-S2-L2-S3-L3-SH2 (black), 250 μM S2-L2-S3-L3-SH2 (red) and 310 μM S2 (blue).

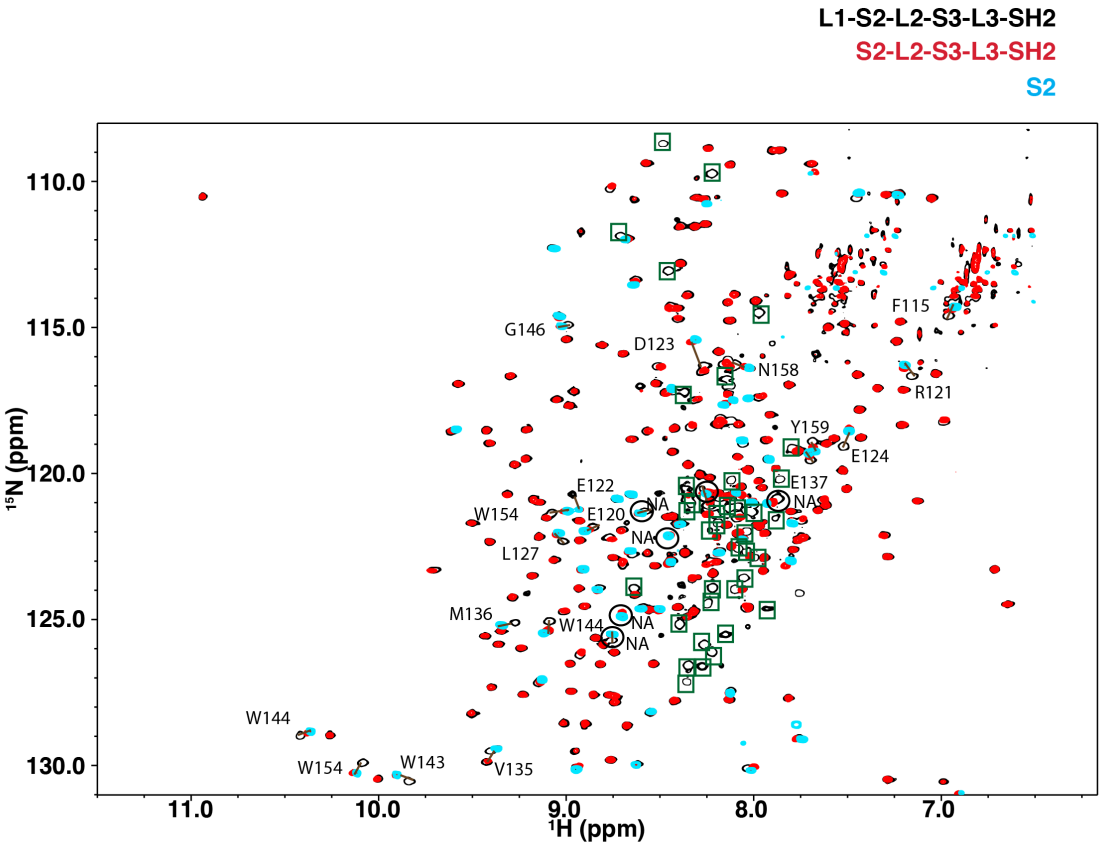

Figure 4.14. L1 binds to regions of S2. (a) ^{1}H-^{15}N TROSY spectra of 250 μM L1-S2-L2-S3-L3-SH2 (black), 250 μM S2-L2-S3-L3-SH2 (red) and 310 μM S2-L2-S3-L3-SH2 (blue). Boxes indicate resonances in the L1-S2-L2-S3-L3-SH2 spectrum that have no counterparts in the S2-L2-S3-L3-SH2 spectrum, and thus represent amides in L1. Green boxes indicate crosspeaks assigned to the indicated residues in L1 (bold text); magenta boxes indicate unassigned resonances from L1. Non-bold text indicates assignments for crosspeaks that shift between L1-S2-L2-S3-L3-SH2 and S2-L2-S3-L3-SH2. Lines connect likely counterpart peaks in the two spectra. Unassigned crosspeaks that shift between the two spectra are circled and indicated with NA. (b) Chemical shift assignments for the L1 element of the L1-S2-S3-SH2 protein. Red = backbone ^{1}H, ^{15}N, ^{13}Ca and ^{13}Cb assigned. Magenta = only ^{13}Ca and ^{13}Cb assigned. Black = unassigned.

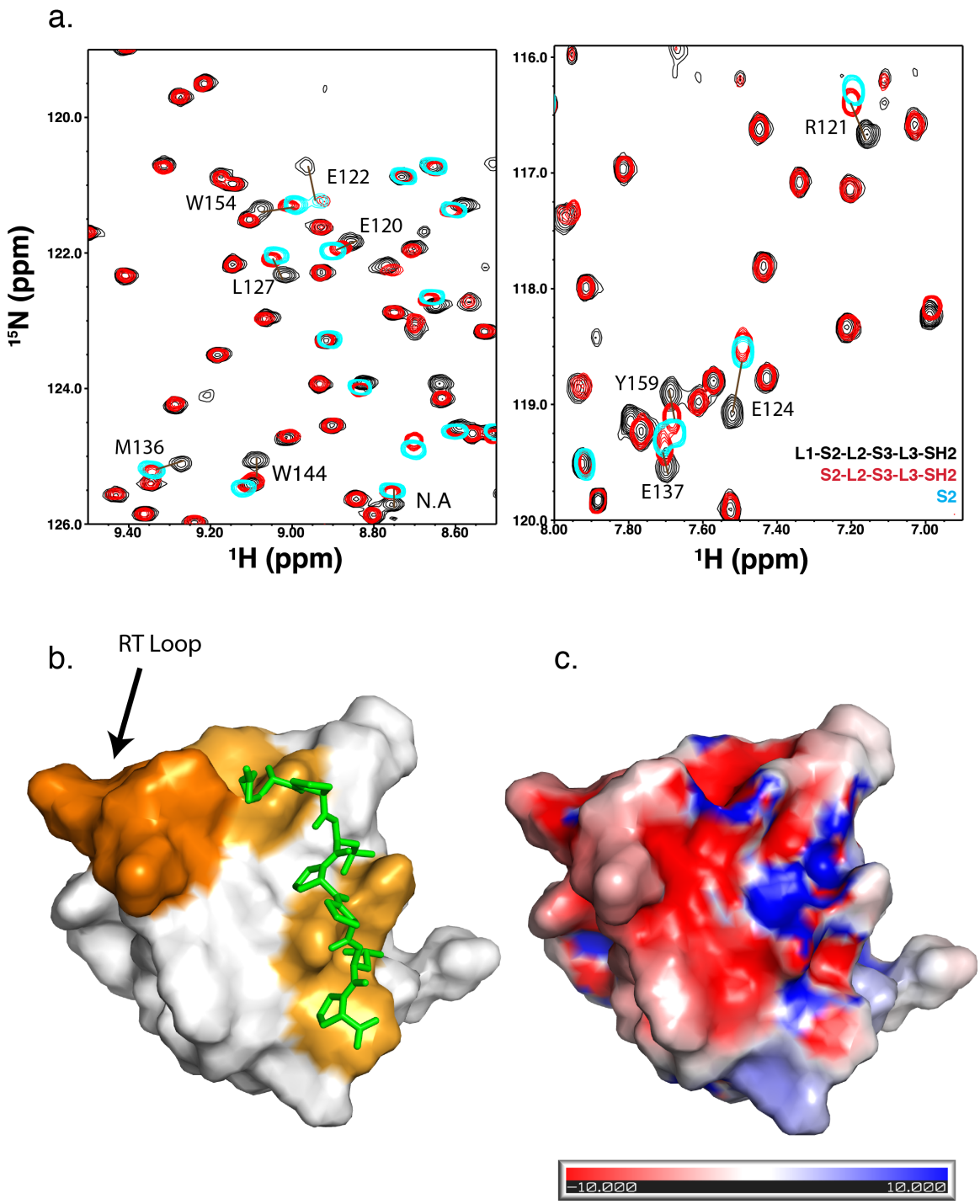

Figure 4.15. L1 binds to regions of S2. (a) ^{1}H-^{15}N TROSY spectra of L1-S2-L2-S3-L3-SH2 (black), S2-L2-S3-L3-SH2 (red) and S2 (blue), enlarging two regions from **Figure 4.14**. (b) Second Nck SH3 domain structure (PDB ID 2JS0) indicating regions of the domain that show changes in chemical shift in the L1-S2-L2-S3-L3-SH2 protein compared to S2-L2-S3-L3-SH2 (orange). A PRM peptide taken from the structure of the Grb2 C-terminal SH3 domain (aligned with

the Nck SH3 domain, but not shown) and its proline-rich peptide ligand (PDB 1IO6) is shown as green sticks. (c) Electrostatic surface potential of S2 as calculated using the APBS plugin in Pymol.

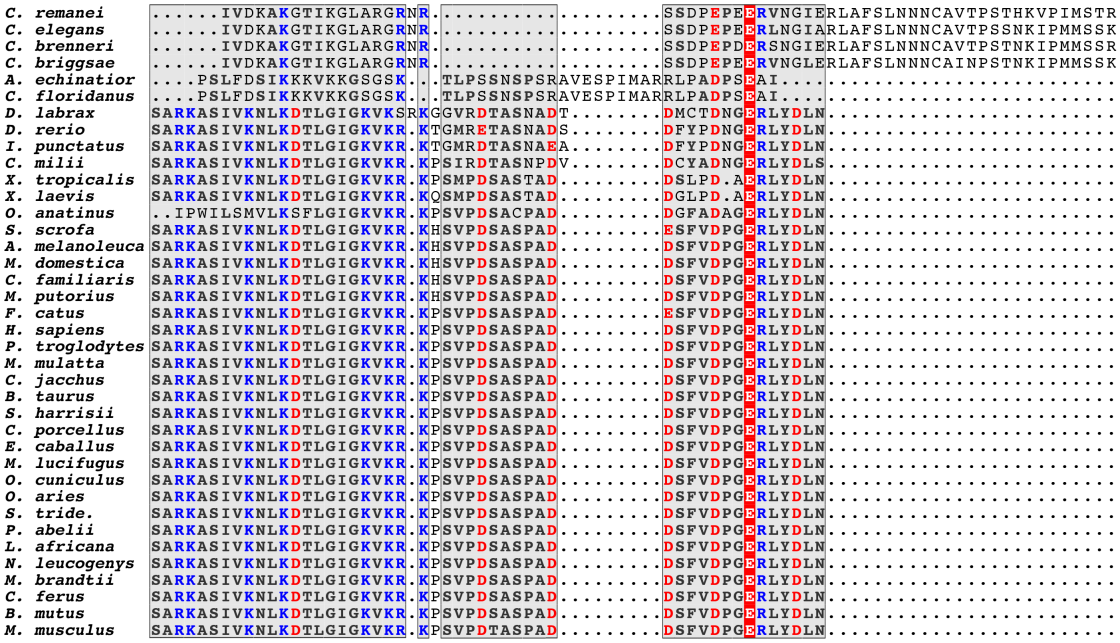

Figure 4.16. L1 is highly conserved. Sequence alignment of the linker L1 region in Nck1 generated by ESPript (Robert & Gouet, 2014). Conserved charged residues are colored blue for basic residues and red for acidic residues.

Chapter 5. Conclusions

In my graduate work, I studied how multivalent proteins interact with their multivalent ligands to produce macroscopic structures. Existence of multivalent proteins in signaling systems had been known for many years, but multivalency was primarily thought to exist in biology to enhance avidity effects. The idea that these properties in biological proteins could be used to enable formation of polymerized macroscopic structures was novel, despite the presence of theoretical studies. Furthermore, in many 2D and 3D systems, macroscopic clustered structures had been observed. My thesis work allowed these two areas of multivalent interactions and clustering of proteins to be combined. Using novel biochemical approaches of phase separation in 2D and 3D, I studied how multivalency-induced phase transitions affected formation of macroscopic structures and studied the biochemical activities of the proteins that form these structures. Importantly, before my work, only distinct mechanisms of clustering were defined for 2D and 3D systems. My work demonstrates that the same mechanism of multivalency-induced polymerization and phase separation can occur both in 2D and 3D.

The primary findings of my graduate work were:

1. Phase separation of multivalent molecules induces sharp change in their biochemical activity (Chapter 2).
2. Multivalent proteins form clusters on a 2D surface that can be understood through the concept of phase separation (Chapter 3).
3. An unstructured inter-domain linker in the multivalent adaptor protein Nck enhances its self-assembly through interaction with the structured domains to promote phase separation (Chapter 4).

Due to the widespread presence of multivalent proteins in biology (Chapter 2), and because phase separation seems to be an important mechanism of organizing cellular components, these findings promise to have broad corollaries.

However, many important questions remain unanswered. How is formation of these structures controlled in a cellular environment? Are there specific mechanisms that allow the control of the sizes and density of these structures in cells? In the context of a cellular environment, what are the minimum components necessary to induce the formation of such structures?

In my studies, I used the integral membrane protein Nephrin and its partners as a model system. Nephrin has a large extracellular region with multiple IgG domains. As observed in the cadherin literature, the extracellular region of different adhesion proteins are known to be involved in the formation of clustered

structures. It will be interesting to study the effect of having the large extracellular region on clustering of Nephrin with its multivalent partners Nck and N-WASP. For this purpose a reconstitution (either cell-free using GUVs or cellular based expressing full-length Nephrin) approach that displays adhered structures on the extracellular region and clustered structures in the intracellular region would be ideal. Mutations in the intracellular regions that lower the valency of phosphotyrosine motifs could be used to study the effect on adhesion/cluster formation of Nephrin. These studies would strengthen the hypothesis that intracellular components and clustering of proteins can stabilize adherence mediated by proteins at cell-cell contacts.

In the introduction to the thesis, I noted that a few different mechanisms exist to explain the formation of clustered structures in cells – gelation through low complexity sequences, association of lipids into lipid-rafts, formation of acto-myosin structures that induce formation of membrane receptor clusters, multivalent polymerization and phase separation, etc. It will be important to study specific systems keeping all of these potential mechanisms in mind. I hypothesize that these mechanisms cooperate with each other in specific contexts to control formation of macroscopic structures in cells. Despite the different molecular mechanisms, the macroscopic properties of clustering in various contexts (viscosities, density, size distributions, dynamics of molecules in and out of the clusters) could be similar, and perhaps functional studies would

benefit from experiments that correlate these macroscopic properties with function. Understanding specific molecular properties (valency and affinities of interacting motifs, specific protein sequences, distribution of particular amino acids in the interacting proteins, etc. that lead to changes in macroscopic properties) could then be related with function and generalizable to different biological systems.

Further studies are also required to study what advantages a phase-separated entity provides over random aggregation/clustering of molecules. Our data suggest that many of these phase-separated structures are dynamic in the timescale of seconds to minutes. Perhaps the advantage of phase separation into liquid like droplets is the rapid dynamic nature of these structures as opposed to a solid-like aggregated structure that is produced through non-specific interactions. On similar lines, perhaps multivalent interactions and polymerization provide a basis for specificity of formation of these structures in cells. I find it harder to imagine that a cell can control the formation of non-specifically interacting structures. Therefore I speculate that polymerization induced by multivalent interactions is a mechanism that cells use to nucleate new clustered structures in cells. A combination of biochemical reconstitution, cell based reconstitution and *in vivo* experiments are required to understand many of these remaining questions.

Materials and Methods

Protein Expression and Purification, Phosphorylation of Nephrin

Information on different constructs is provided in Table 2. Maltose binding protein (MBP)-tagged His_8-Nephrin and its mutants were expressed in BL21(DE3)T1R cells at 18 °C through overnight induction with 1 mM IPTG. Cells were collected by centrifugation and lysed by cell disruption (Emulsiflex-C5, Avestin) in 20 mM Tris pH 8, 20 mM imidazole, 150 mM NaCl, 5 mM βME, 0.01% NP-40, 10 % glycerol, 1 mM PMSF, 1 µg/mL Antipain, 1 mM Benzamidine and 1 µg/mL Leupeptin. The cleared lysate was applied to Ni-NTA agarose (Qiagen), washed with the lysis buffer containing 300 mM NaCl and 50 mM imidazole, and eluted with the same buffer but containing 150 mM NaCl and 300 mM imidazole. The MBP was removed with TEV protease treatment at 4 °C for 16 hours or at room-temperature for 2 hours. The protein was further purified using a Source 15Q column (GE Healthcare), evolved with a gradient of 150 → 300 mM NaCl in 20 mM Imidazole pH 8, 1 mM EDTA and 2 mM DTT, followed by an SD200 column (GE Healthcare) run in 25 mM Hepes pH 7.5, 150 mM NaCl, 1 mM $MgCl_2$, and 2 mM βME. Fractions containing His_8-Nephrin were concentrated using an using an Amicon Ultra 3 K concentrator (Millipore) and flash frozen in aliquots at -80 °C.

Nephrin proteins were phosphorylated at 30 °C with 20 nM Lck kinase overnight or with 500 nM Lck for 1 hour. The phosphorylation reaction was quenched with 10 mM EDTA. Kinase and incompletely phosphorylated Nephrin were removed using a source 15 Q column evolved with a gradient of 150 → 250 mM NaCl in 25 mM Hepes pH 7 and 2 mM βME. The phosphorylated product was further purified using an SD200 column (GE Healthcare) and labeled at its single cysteine residue with maleimide-Alexa 488 fluorophore (Invitrogen). The labeled protein was separated from unreacted fluorophore using a Source 15 Q column and a Hi-trap desalting column (GE Healthcare). Phosphorylation at one, two or three sites, for Nephrin1Y, Nephrin2Y or Nephrin3Y (see Table 2), respectively, was confirmed using mass-spectrometry.

GST-Nck and His_6-N-WASP were expressed in BL21(DE3)T1R cells at 18 °C through overnight induction with 1 mM IPTG. Cells expressing GST-Nck were collected by centrifugation and lysed by sonication in 20 mM Tris pH 8, 200 mM NaCl, 1 mM EDTA, 1 mM DTT, 1 mM PMSF, 1 μg/mL Antipain, 1 mM Benzamidine, 1 μg/mL Leupeptin and 1 μg/mL Pepstatin. The cleared lysate was applied to glutathione sepharose beads (GE) and washed with 10 column volumes of 200 mM NaCl, 20 mM Tris pH 8, 1 mM DTT and 1 mM EDTA. The GST tag was removed with TEV protease

treatment on the beads at 4 °C for 16 hours or at room-temperature for 2 hours. Cleaved Nck was collected by 20 column washes with 20 mM Imidazole pH 7 and 1 mM DTT, and applied to a Source 15 Q column using a gradient of 0 → 200 mM NaCl in 20 mM Imidazole pH 7, 1 mM DTT. Fractions containing Nck were pooled, concentrated using an Amicon Ultra 30K concentrator (Millipore), and passed through a Source 15 S column (GE), using a gradient of 0 → 200 mM NaCl in 20 mM Imidazole pH 7, 1 mM DTT. Fractions containing Nck were concentrated and run through an SD75 column (GE). Pooled fractions were concentrated and flash-frozen in 25 mM Hepes pH 7.5, 150 mM NaCl and 1 mM βME. The $(SH3)_1$, $(SH3)_2$ and $(SH3)_3$ proteins were purified in the same way, but excluding the Source 15 S column.

His_6-N-WASP expressing cells were collected by centrifugation and lysed by cell disruption (Emulsiflex-C5, Avestin) in 20 mM Imidazole pH 7, 300 mM KCl, 5 mM βME, 0.01% NP-40, 1 mM PMSF, 1 µg/mL Antipain, 1 mM Benzamidine and 1 µg/mL Leupeptin. The cleared lysate was applied to Ni-NTA agarose (Qiagen), washed with 300 mM KCl, 50 mM Imidazole pH 7, 5 mM βME and eluted with 100 mM KCl, 300 mM Imidazole pH 7 and 5 mM βME. The elute was further purified over a Source 15 Q column using a gradient of 250 → 450 mM NaCl in 20 mM Imidazole pH 7 and 1 mM DTT. The His_6-tag was removed by TEV protease at 4 °C for 16 hours or

at room-temperature for 2 hours. Cleaved N-WASP was then applied to a Source 15 S column using a gradient of 110 → 410 mM NaCl in 20 mM Imidazole pH 7, 1 mM DTT. Fractions containing N-WASP were concentrated using an Amicon Ultra 10 K concentrator (Millipore), passed through an SD200 column, concentrated and flash-frozen in 25 mM Hepes pH 7.5, 150 mM NaCl and 1 mM βME. N-WASP (BPVCA with single cysteine) and Nck (cysteine-modified, see Table 2) were labeled with Alexa488/568/647. For labeling purposes, the pure protein after Source15S was desalted into a buffer without reducing agent (25 mM Hepes pH 7, 150 mM NaCl), and reacted with a maleimide-conjugated fluorophore for 2 hours at room temperature. The reaction was quenched with DTT and the fluorophore was removed using a Source15Q and SD75/Hi-trap desalting columns.

His_6-Lck kinase was expressed from baculovirus in *Spodoptera frugiperta* (Sf9) cells. Cells were harvested in 50 mM Tris pH 7.5, 100 mM NaCl, 5 mM βME and 0.01 % NP-40, 1 mM PMSF, 1 µg/mL Antipain, 1 mM Benzamidine and 1 µg/mL Leupeptin. Cells were lysed by douncing on ice ~10 times. The cleared lysate was applied to Ni-NTA agarose beads equilibrated with 20 mM Tris pH 7.5, 500 mM NaCl, 20 mM Imidazole, 5 mM βME and 10 % glycerol (Buffer A), washed with Buffer A containing 1 M NaCl, and then eluted with Buffer A containing 200 mM Imidazole 7.5 and 100 mM NaCl. The elute was applied to a Source 15 Q

column using a gradient of 100 → 300 mM NaCl in 25 mM Hepes pH 7.5 and 2 mM βME. Collected fractions were concentrated (Amicon 10 K, Millipore) and applied to an SD75 column in 25 mM Hepes pH 7.5, 150 mM NaCl and 1 mM βME.

All N-WASP constructs (N-WASP GBD-P-VCA, N-WASPΔ, N-WASPΔP, N-WASP BPVCA) were expressed as His_6-tagged proteins. They were purified over Ni-NTA agarose, Mono Q/Source15 Q, Mono S/Source15 S and Superdex 75 or Superdex 200. TEV cleavage was done either before or after the anion exchange columns. All purified proteins were exchanged into 150 KMEI before use in assays.

Table 2. Information on the protein constructs used in this study

Proteins	Sequence Information	Notes
Nck	GHMAEEVVVVAKFDYVAQQEQELDIKKNERLWL LDDSKSWWRVRNSMNKTGFVPSNYVERKNSARK ASIVKNLKDTLGIGKVKRKPSVPDSASPADDSF VDPGERLYDLNMPAYVKFNYMAEREDELSLIKG TKVIVMEKCSDGWWRGSYNGQVGWFPSNYVTEE GDSPLGDHVGSLSEKLAAVVNNLNTGQVLHVVQ ALYPFSSSNDEELNFEKGDVMDVIEKPENDPEW WKCRKINGMVGLVPKNYVTVMQNNPLTSGLEPS PPQCDYIRPSLTGKFAGNPWYYGKVTRHQAEMA LNERGHEGDFLIRDSESSPNDFSVSLKAQGKNK HFKVQLKETVYCIGQRKFSTMEELVEHYKKAPI	Human, WT, residues 1-377

	FTSEQGEKLYLVKHLS	
N-WASP BPVCA	GSEFKEKKKGKAKKKRAPPPPPPSRGGPPPPPPPPHSSGPPPPPARGRGAPPPPPSRAPTAAPPPPPPSRPGVVVPPPPPNRMYPHPPPALPSSAPSGPPPPPPLSMAGSTAPPPPPPPPPPPGPPPPPGLPSDGDHQVPASSGNKAALLDQIREGAQLKKVEQNSRPVSCSGRDALLDQIRQGIQLKSVSDGQESTPPTPAPTSGIVGALMEVMQKRSKAIHSSDEDEDDDDEEDFEDDDEWED	Rat, residues 183-193 fused to 273-501
Nck (cysteine-modified)	GHMCMAEEVVVVAKFDYVAQQEQELDIKKNERLWLLDDSKSWWRVRNSMNKTGFVPSNYVERKNSARKASIVKNLKDTLGIGKVKRKPSVPDSASPADDSFVDPGERLYDLNMPAYVKFNYMAEREDELSLIKGTKVIVMEKSSDGWWRGSYNGQVGWFPSNYVTEEGDSPLGDHVGSLSEKLAAVVNNLNTGQVLHVVQALYPFSSSNDEELNFEKGDVMDVIEKPENDPEWWKARKINGMVGLVPKNYVTVMQNNPLTSGLEPSPPQSDYIRPSLTGKFAGNPWYYGKVTRHQAEMALNERGHEGDFLIRDSESSPNDFSVSLKAQGKNKHFKVQLKETVYSIGQRKFSTMEELVEHYKKAPIFTSEQGEKLYLVKHLS	Human, residues 1-377, with mutations: C139S, C232A, C266S, C340S
Nephrin3Y	GGSLEHHHHHHHHGGSCGGSGGSGGSGGSHLYDEVERTFPPSGAWGPLYDEVQMGPWDLHWPEDTFQDPRGIYDQVAGD	Human, residues 1174-1223, with mutations: Y1183F, Y1210F
Nephrin2Y	GGSLEHHHHHHHHGGSCGGSGGSGGSGGSHLFDEVERTFPPSGAWGPLYDEVQMGPWDLHWPEDTFQDPRGIYDQVAGD	Human, residues 1174-1223, with mutations:

		Y1176F, Y1183F, Y1210F
Nephrin1Y	GGSLEHHHHHHHHGGSCGGSGGSGGSGGSHLFD EVERTFPPSGAWGPLYDEVQMGPWDLHWPEDTF QDPRGIFDQVAGD	Human, residues 1174-1223, with mutations: Y1176F, Y1183F, Y1210F, Y1217F
TIR3Y	GGSLEHHHHHHHHGGSCGGSGGSGGSGGSHMHI YDEVAADPPPSGAWGHIYDEVAADPWDLHWPED TFQDPRHIYDEVAADP	Human Nephrin, with pTyr sites replaced by those in EPEC Tir protein (underlined)
$(SH3)_3$	GHMPAYVKFNYMAEREDELSLIKGTKVIVMEKS SDGWWRGSYNGQVGWFPSNYVTEEGDSPLSARK ASIVKNLKDTLGIGKVKRKPSVPDSASPADDSF VDPGERLYDLNMPAYVKFNYMAEREDELSLIKG TKVIVMEKSSDGWWRGSYNGQVGWFPSNYVTEE GDSPLSARKASIVKNLKDTLGIGKVKRKPSVPD SASPADDSFVDPGERLYDLNMPAYVKFNYMAER EDELSLIKGTKVIVMEKSSDGWWRGSYNGQVGW FPSNYVTEEGDSPLNNPLTSGLEPSPPQCDYIR PSLTGKFAGNPWYYGKVTRHQAEMALNERGHEG DFLIRDSESSPNDFSVSLKAQGKNKHFKVQLKE TVYCIGQRKFSTMEELVEHYKKAPIFTSEQGEK LYLVKHLS	Human, three repeats of the second Nck SH3 domain, plus the Nck SH2 domain
$(SH3)_2$	GHMPAYVKFNYMAEREDELSLIKGTKVIVMEKS SDGWWRGSYNGQVGWFPSNYVTEEGDSPLSARK ASIVKNLKDTLGIGKVKRKPSVPDSASPADDSF	Human, two repeats of the second Nck SH3

	VDPGERLYDLNMPAYVKFNYMAEREDELSLIKG TKVIVMEKSSDGWWRGSYNGQVGWFPSNYVTEE GDSPLNNPLTSGLEPSPPQCDYIRPSLTGKFAG NPWYYGKVTRHQAEMALNERGHEGDFLIRDSES SPNDFSVSLKAQGKNKHFKVQLKETVYCIGQRK FSTMEELVEHYKKAPIFTSEQGEKLYLVKHLS	domain, plus the Nck SH2 domain
$(SH3)_1$	GHMPAYVKFNYMAEREDELSLIKGTKVIVMEKS SDGWWRGSYNGQVGWFPSNYVTEEGDSPLNNPL TSGLEPSPPQCDYIRPSLTGKFAGNPWYYGKVT RHQAEMALNERGHEGDFLIRDSESSPNDFSVSL KAQGKNKHFKVQLKETVYCIGQRKFSTMEELVE HYKKAPIFTSEQGEKLYLVKHLS	Human, one repeat of the second Nck SH3 domain, plus the Nck SH2 domain
TIR-1pY	EEHIpYDEVAADPGGSWGGSC	N-terminal rhodamine labeled single pTyr motif from EPEC Tir protein
Lck	ANSLEPEPWFFKNLSRKDAERQLLAPGNTHGSF LIRESESTAGSFSLSVRDFDQNQGEVVKHYKIR NLDNGGFYISPRITFPGLHDLVRHYTNASDGLC TKLSRPCQTQKPQKPWWEDEWEVPRETLKLVER LGAGQFGEVWMGYYNGHTKVAVKSLKQGSMSPD AFLAEANLMKQLQHPRLVRLYAVVTQEPIYIIT EYMENGSLVDFLKTPSGIKLNVNKLLDMAAQIA EGMAFIEEQNYIHRDLRAANILVSDTLSCKIAD FGLARLIEDNEYTAREGAKFPIKWTAPEAINYG TFTIKSDVWSFGILLTEIVTHGRIPYPGMTNPE VIQNLERGYRMVRPDNCPEELYHLMMLCWKERP	Human, 119–509, Y505F

	EDRPTFDYLRSVLDDFFTATEGQFQPQP	
N-WASP (GBD-P-VCA)	193–501	Rat
N-WASPΔ (B-Crib-P)	183–239 + 273–396	Rat
N-WASP B-P-VCA	183–193 + 273–501	Rat
N-WASPΔP (GBD-VCA)	193–272–$(GGS)_2$– 396–501	Rat
$SH3_4$	GHMDLNMPAYVKFNYMAEREDELSLIKGTKVIVM EKSSDGWWRGSYNGQVGWFPSNYVTEEGDSPLAS GAGGSEGGGSEGGTSGATHM(DLNMPAYVKFNYM AEREDELSLIKGTKVIVMEKSSDGWWRGSYNGQV GWFPSNYVTEEGDSPLASGAGGSEGGGSEGGTSG AT)$_2$DLNMPAYVKFNYMAEREDELSLIKGTKVIV MEKSSDGWWRGSYNGQVGWFPSNYVTEEGDSPL	
$SH3_5$	GHM(DLNMPAYVKFNYMAEREDELSLIKGTKVIV MEKSSDGWWRGSYNGQVGWFPSNYVTEEGDSPLA SGAGGSEGGGSEGGTSGAT)$_2$HM(DLNMPAYVKF NYMAEREDELSLIKGTKVIVMEKSSDGWWRGSYN GQVGWFPSNYVTEEGDSPLASGAGGSEGGGSEGG TSGAT)$_2$DLNMPAYVKFNYMAEREDELSLIKGTK VIVMEKSSDGWWRGSYNGQVGWFPSNYVTEEGDS PL	
PRM_2	GHMKGGSWGGSKKKKTAPTPPKRSGGSGGSGGSG GSKKKKTAPTPPKRSGGSGSENLYFQ	
PRM_4	GHMKGGSWGGS(KKKKTAPTPPKRSGGSGGSGGS GGS)$_3$KKKKTAPTPPKRSGGSGSENLYFQ	

PRM_5	GHMKGGSWGGS(KKKKTAPTPPKRSGGSGGSGGSGGS)$_4$KKKKTAPTPPKRSGGSGSENLYFQ	
N-WASP (BPVCA)	GHMGSEFKEKKKGKAKKKRAPPPPPPSRGGPPPPPPPPHSSGPPPPPARGRGAPPPPPSRAPTAAPPPPPPSRPGVVVPPPPPNRMYPHPPPALPSSAPSGPPPPPPLSMAGSTAPPPPPPPPPPGPPPPPGLPSDGDHQVPASSGNKAALLDQIREGAQLKKVEQNSRPVSCSGRDALLDQIRQGIQLKSVSDGQESTPPTPAPTSGIVGALMEVMQKRSKAIHSSDEDEDDDDEEDFEDDDEWED	Rat, residues 183-193 fused to 273-501
Nephrin 3Y	GHMHLYDEVERTFPPSGAWGPLYDEVQMGPWDLHWPEDTFQDPRGIYDQVAGD	Human, residues 1174-1223, Y1183F, Y1210F
Nck	GHMAEEVVVVAKFDYVAQQEQELDIKKNERLWLLDDSKSWWRVRNSMNKTGFVPSNYVERKNSARKASIVKNLKDTLGIGKVKRKPSVPDSASPADDSFVDPGERLYDLNMPAYVKFNYMAEREDELSLIKGTKVIVMEKCSDGWWRGSYNGQVGWFPSNYVTEEGDSPLGDHVGSLSEKLAAVVNNLNTGQVLHVVQALYPFSSSNDEELNFEKGDVMDVIEKPENDPEWWKCRKINGMVGLVPKNYVTVMQNNPLTSGLEPSPPQCDYIRPSLTGKFAGNPWYYGKVTRHQAEMALNERGHEGDFLIRDSESSPNDFSVSLKAQGKNKHFKVQLKETVYCIGQRKFSTMEELVEHYKKAPIFTSEQGEKLYLVKHLS	Human, residues 1-377; S1-Red, S2-Green, S3-Blue,SH2-Brown
Lck	ANSLEPEPWFFKNLSRKDAERQLLAPGNTHGSFLIRESESTAGSFSLSVRDFDQNQGEVVKHYKIRNLDNGGFYISPRITFPGLHDLVRHYTNASDGLCTKL	Human, 119–509, Y505F

	SRPCQTQKPQKPWWEDEWEVPRETLKLVERLGAG QFGEVWMGYYNGHTKVAVKSLKQGSMSPDAFLAE ANLMKQLQHPRLVRLYAVVTQEPIYIITEYMENG SLVDFLKTPSGIKLNVNKLLDMAAQIAEGMAFIE EQNYIHRDLRAANILVSDTLSCKIADFGLARLIE DNEYTAREGAKFPIKWTAPEAINYGTFTIKSDVW SFGILLTEIVTHGRIPYPGMTNPEVIQNLERGYR MVRPDNCPEELYHLMMLCWKERPEDRPTFDYLRS VLDDFFTATEGQFQPQP	
S1-L1-S2-L3-SH2	GHMAEEVVVVAKFDYVAQQEQELDIKKNERLWLL DDSKSWWRVRNSMNKTGFVPSNYVERKNSARKAS IVKNLKDTLGIGKVKRKPSVPDSASPADDSFVDP GERLYDLNMPAYVKFNYMAEREDELSLIKGTKVI VMEKSSDGWWRGSYNGQVGWFPSNYVTEEGDSPL NNPLTSGLEPSPPQSDYIRPSLTGKFAGNPWYYG KVTRHQAEMALNERGHEGDFLIRDSESSPNDFSV SLKAQGKNKHFKVQLKETVYSIGQRKFSTMEELV EHYKKAPIFTSEQGEKLYLVKHLS	Missing S3 domain; Residues1-170, 252- 377, C139S, C266S, C340S
S1-L1-S3-L3-SH2	GHMAEEVVVVAKFDYVAQQEQELDIKKNERLWLL DDSKSWWRVRNSMNKTGFVPSNYVERKNSARKAS IVKNLKDTLGIGKVKRKPSVPDSASPADDSFVDP GERLYDLNVLHVVQALYPFSSSNDEELNFEKGDV MDVIEKPENDPEWWKCRKINGMVGLVPKNYVTVM QNNPLTSGLEPSPPQSDYIRPSLTGKFAGNPWYY GKVTRHQAEMALNERGHEGDFLIRDSESSPNDFS VSLKAQGKNKHFKVQLKETVYSIGQRKFSTMEEL VEHYKKAPIFTSEQGEKLYLVKHLS	Missing S2 domain; Residues 1-108, 191- 377, C266S, C340S
S2-L2-S3-L3-SH2	GHMDLNMPAYVKFNYMAEREDELSLIKGTKVIVM EKSSDGWWRGSYNGQVGWFPSNYVTEEGDSPLGD	di-SH3 construct lacking S1-L1;

	HVGSLSEKLAAVVNNLNTGQVLHVVQALYPFSSS NDEELNFEKGDVMDVIEKPENDPEWWKCRKINGM VGLVPKNYVTVMQNNPLTSGLEPSPPQSDYIRPS LTGKFAGNPWYYGKVTRHQAEMALNERGHEGDFL IRDSESSPNDFSVSLKAQGKNKHFKVQLKETVYS IGQRKFSTMEELVEHYKKAPIFTSEQGEKLYLVK HLS	Residues 106-377, C266S, C340S
L1-S2-L2-S3-L3- SH2	GHMKNSARKASIVKNLKDTLGIGKVKRKPSVPDS ASPADDSFVDPGERLYDLNMPAYVKFNYMAERED ELSLIKGTKVIVMEKSSDGWWRGSYNGQVGWFPS NYVTEEGDSPLGDHVGSLSEKLAAVVNNLNTGQV LHVVQALYPFSSSNDEELNFEKGDVMDVIEKPEN DPEWWKCRKINGMVGLVPKNYVTVMQNNPLTSGL EPSPPQSDYIRPSLTGKFAGNPWYYGKVTRHQAE MALNERGHEGDFLIRDSESSPNDFSVSLKAQGKN KHFKVQLKETVYSIGQRKFSTMEELVEHYKKAPI FTSEQGEKLYLVKHLS	Missing S1; Residues 59-377, C266S, C340S
L1chargeshuffle S2-L2-S3-L3-SH2	GHMKNSADKASIVDNLKDTLGIGKVDRKPSVPKS ASPADKSFVKPGERLYDLNMPAYVKFNYMAERED ELSLIKGTKVIVMEKSSDGWWRGSYNGQVGWFPS NYVTEEGDSPLGDHVGSLSEKLAAVVNNLNTGQV LHVVQALYPFSSSNDEELNFEKGDVMDVIEKPEN DPEWWKCRKINGMVGLVPKNYVTVMQNNPLTSGL EPSPPQSDYIRPSLTGKFAGNPWYYGKVTRHQAE MALNERGHEGDFLIRDSESSPNDFSVSLKAQGKN KHFKVQLKETVYSIGQRKFSTMEELVEHYKKAPI FTSEQGEKLYLVKHLS	Only the charges in the linker shuffled; Residues 59-377, C266S, C340S
L1non-	GHMKNSARKAVASKNLKDFLSVGKSKRKPGIPDS	Non-charged regions

chargeshuffle-S2-L2-S3-L3-SH2	IVPADDSTVDPGERLYDLNMPAYVKFNYMAEREDELSLIKGTKVIVMEKSSDGWWRGSYNGQVGWFPSNYVTEEGDSPLGDHVGSLSEKLAAVVNNLNTGQVLHVVQALYPFSSSNDEELNFEKGDVMDVIEKPENDPEWWKCRKINGMVGLVPKNYVTVMQNNPLTSGLEPSPPQSDYIRPSLTGKFAGNPWYYGKVTRHQAEMALNERGHEGDFLIRDSESSPNDFSVSLKAQGKNKHFKVQLKETVYSIGQRKFSTMEELVEHYKKAPIFTSEQGEKLYLVKHLS	of L1 shuffled (highlighted in green); Residues 59-377, C266S, C340S
ΔL1-S2-L2-S3-L3-SH2	GHMGIGKVKRKPSVPDSASPADDSFVDPGERLYDLNMPAYVKFNYMAEREDELSLIKGTKVIVMEKSSDGWWRGSYNGQVGWFPSNYVTEEGDSPLGDHVGSLSEKLAAVVNNLNTGQVLHVVQALYPFSSSNDEELNFEKGDVMDVIEKPENDPEWWKCRKINGMVGLVPKNYVTVMQNNPLTSGLEPSPPQSDYIRPSLTGKFAGNPWYYGKVTRHQAEMALNERGHEGDFLIRDSESSPNDFSVSLKAQGKNKHFKVQLKETVYSIGQRKFSTMEELVEHYKKAPIFTSEQGEKLYLVKHLS	di-SH3 Construct lacking 17 N-terminal L1 residues; Residues 76-377, C266S, C340S
L1ΔCT-S2-L2-S3-L3-SH2	GHMKNSARKASIVKNLKDTLGIGKVKRKGGSAGGSAGGSAMPAYVKFNYMAEREDELSLIKGTKVIVMEKSSDGWWRGSYNGQVGWFPSNYVTEEGDSPLGDHVGSLSEKLAAVVNNLNTGQVLHVVQALYPFSSSNDEELNFEKGDVMDVIEKPENDPEWWKCRKINGMVGLVPKNYVTVMQNNPLTSGLEPSPPQSDYIRPSLTGKFAGNPWYYGKVTRHQAEMALNERGHEGDFLIRDSESSPNDFSVSLKAQGKNKHFKVQLKETVYSIGQRKFSTMEELVEHYKKAPIFTSEQGEKLYLVKHLS	di-SH3 construct where 25 C-terminal L1 residues were replaced by a $(GGSA)_3$ linker; Residues 59-83,109-377, C266S, C340S

L1Δ(KVKRK)-S2-L2-S3-L3-SH2	GHMKNSARKASIVKNLKDTLGIG(GS)PSVPDSA SPADDSFVDPGERLYDLNMPAYVKFNYMAEREDE LSLIKGTKVIVMEKSSDGWWRGSYNGQVGWFPSN YVTEEGDSPLGDHVGSLSEKLAAVVNNLNTGQVL HVVQALYPFSSSNDEELNFEKGDVMDVIEKPEND PEWWKCRKINGMVGLVPKNYVTVMQNNPLTSGLE PSPPQSDYIRPSLTGKFAGNPWYYGKVTRHQAEM ALNERGHEGDFLIRDSESSPNDFSVSLKAQGKNK HFKVQLKETVYSIGQRKFSTMEELVEHYKKAPIF TSEQGEKLYLVKHLS	In L1, (KVKRK) replace with GS; Residues 59-78, 84-377, C266S, C340S
L1basic-S2-L2-S3-L3-SH2	GHMKNSARKASIVKNLKDTLGIGKVKRKPSVPKS ASPADKSFVKPGKRLYKLNMPAYVKFNYMAERED ELSLIKGTKVIVMEKSSDGWWRGSYNGQVGWFPS NYVTEEGDSPLGDHVGSLSEKLAAVVNNLNTGQV LHVVQALYPFSSSNDEELNFEKGDVMDVIEKPEN DPEWWKCRKINGMVGLVPKNYVTVMQNNPLTSGL EPSPPQSDYIRPSLTGKFAGNPWYYGKVTRHQAE MALNERGHEGDFLIRDSESSPNDFSVSLKAQGKN KHFKVQLKETVYSIGQRKFSTMEELVEHYKKAPI FTSEQGEKLYLVKHLS	L1 acidic residues mutated to K's; Residues 59-377, C266S, C340S
L1HM S2-L2-S3-L3-SH2	GHMKNSARKASNSKNSKDTLGIGKVKRKPSVPDS ASPADDSFVDPGERLYDLNMPAYVKFNYMAERED ELSLIKGTKVIVMEKSSDGWWRGSYNGQVGWFPS NYVTEEGDSPLGDHVGSLSEKLAAVVNNLNTGQV LHVVQALYPFSSSNDEELNFEKGDVMDVIEKPEN DPEWWKCRKINGMVGLVPKNYVTVMQNNPLTSGL EPSPPQSDYIRPSLTGKFAGNPWYYGKVTRHQAE MALNERGHEGDFLIRDSESSPNDFSVSLKAQGKN	Hydrophobic mutations in the linker (I to N, V to S, L to S); Residues 59-377, C266S, C340S

	KHFKVQLKETVYSIGQRKFSTMEELVEHYKKAPI FTSEQGEKLYLVKHLS	
L1K/E S2-L2-S3- L3-SH2	GHMKNSAREASIVENLEDTLGIGKVKRKPSVPDS ASPADDSFVDPGERLYDLNMPAYVKFNYMAERED ELSLIKGTKVIVMEKSSDGWWRGSYNGQVGWFPS NYVTEEGDSPLGDHVGSLSEKLAAVVNNLNTGQV LHVVQALYPFSSSNDEELNFEKGDVMDVIEKPEN DPEWWKCRKINGMVGLVPKNYVTVMQNNPLTSGL EPSPPQSDYIRPSLTGKFAGNPWYYGKVTRHQAE MALNERGHEGDFLIRDSESSPNDFSVSLKAQGKN KHFKVQLKETVYSIGQRKFSTMEELVEHYKKAPI FTSEQGEKLYLVKHLS	N-terminal charges mutated (K to E); Residues 59-377, C266S, C340S
L1D/Rswap-S2- L2-S3-L3-SH2	GHMKNSARKASIVKNLKRTLGIGKVKRKPSVPDS ASPADDSFVDPGEDLYDLNMPAYVKFNYMAERED ELSLIKGTKVIVMEKSSDGWWRGSYNGQVGWFPS NYVTEEGDSPLGDHVGSLSEKLAAVVNNLNTGQV LHVVQALYPFSSSNDEELNFEKGDVMDVIEKPEN DPEWWKCRKINGMVGLVPKNYVTVMQNNPLTSGL EPSPPQSDYIRPSLTGKFAGNPWYYGKVTRHQAE MALNERGHEGDFLIRDSESSPNDFSVSLKAQGKN KHFKVQLKETVYSIGQRKFSTMEELVEHYKKAPI FTSEQGEKLYLVKHLS	D to R swapped in linker to make N- terminus more basic and C-terminus more acidic; Residues 59- 377, C266S, C340S
Nck(L1ggsa10)	GHMAEEVVVVAKFDYVAQQEQELDIKKNERLWLL DDSKSWWRVRNSMNKTGFVPSNYVERGGSAGGSA GGSAGGSAGGSA GSGGSAGGSAGGSAGGSAGGSAGSDLNMPAYVKF NYMAEREDELSLIKGTKVIVMEKCSDGWWRGSYN GQVGWFPSNYVTEEGDSPLGDHVGSLSEKLAAVV	L1 replaced with a GGSA linker in full- length Nck; Residues 1-58, 109- 377

	NNLNTGQVLHVVQALYPFSSSNDEELNFEKGDVM DVIEKPENDPEWWKCRKINGMVGLVPKNYVTVMQ NNPLTSGLEPSPPQCDYIRPSLTGKFAGNPWYYG KVTRHQAEMALNERGHEGDFLIRDSESSPNDFSV SLKAQGKNKHFKVQLKETVYCIGQRKFSTMEELV EHYKKAPIFTSEQGEKLYLVKHLS	
Nck ΔL1b	GHMAEEVVVVAKFDYVAQQEQELDIKKNERLWLL DDSKSWWRVRNSMNKTGFVPSNYVERKNSGGSAG GSAGGSATLGIGKVKRKPSVPDSASPADDSFVDP GERLYDLNMPAYVKFNYMAEREDELSLIKGTKVI VMEKSSDGWWRGSYNGQVGWFPSNYVTEEGDSPL GDHVGSLSEKLAAVVNNLNTGQVLHVVQALYPFS SSNDEELNFEKGDVMDVIEKPENDPEWWKCRKIN GMVGLVPKNYVTVMQNNPLTSGLEPSPPQSDYIR PSLTGKFAGNPWYYGKVTRHQAEMALNERGHEGD FLIRDSESSPNDFSVSLKAQGKNKHFKVQLKETV YSIGQRKFSTMEELVEHYKKAPIFTSEQGEKLYL VKHLS	N-terminal 15 residues replaced with a GGSA linker, in full-length Nck; Residues 1-60, 74-377
Nck(L1shuffle)	GHMAEEVVVVAKFDYVAQQEQELDIKKNERLWLL DDSKSWWRVRNSMNKTGFVPSNYVERKNSADKAS IVDNLKDTLGIGPYRDSVPASRSLKSEAFGKDRD KVPPKVNMPAYVKFNYMAEREDELSLIKGTKVIV MEKCSDGWWRGSYNGQVGWFPSNYVTEEGDSPLG DHVGSLSEKLAAVVNNLNTGQVLHVVQALYPFSS SNDEELNFEKGDVMDVIEKPENDPEWWKCRKING MVGLVPKNYVTVMQNNPLTSGLEPSPPQCDYIRP SLTGKFAGNPWYYGKVTRHQAEMALNERGHEGDF LIRDSESSPNDFSVSLKAQGKNKHFKVQLKETVY	Residues in L1 shuffled in full-length Nck

	CIGQRKFSTMEELVEHYKKAPIFTSEQGEKLYLV KHLS	
SH3-1	GHMAEEVVVVAKFDYVAQQEQELDIKKNERLWLL DDSKSWWRVRNSMNKTGFVPSNYVERKNSAR	Residues 1-63
SH3-2	GHMDLNMPAYVKFNYMAEREDELSLIKGTKVIVM EKSSDGWWRGSYNGQVGWFPSNYVTEEGDSPL	Residues 106-168, C139S
SH3-3	GHMHVVQALYPFSSSNDEELNFEKGDVMDVIEKP ENDPEWWKCRKINGMVGLVPKNYVTVMQNNPLTS GL	Residues 193-259,
Isolated L1	GHMKNSARKASIVKNLKDTLGIGKVKRKPSVPDS ASPADDSFVDPGERLYDLN	Isolated L1; Residues 59-108
$(SUMO)_5$-$(SIM)_5$	GHMGGSWGGSMSEEKPKEGVKTENDHINLKVAGQ DGSVVQFKIKRHTPLSKLMKAYSERQGLSMRQIR FRFDGQPINETDTPAQLEMEDEDTIDVFQQQTVV GGSGGSGGSGGSMSEEKPKEGVKTENDHINLKVA GQDGSVVQFKIKRHTPLSKLMKAYSERQGLSMRQ IRFRFDGQPINETDTPAQLEMEDEDTIDVFQQQT VVGGSGGSGGSGGSMSEEKPKEGVKTENDHINLK VAGQDGSVVQFKIKRHTPLSKLMKAYSERQGLSM RQIRFRFDGQPINETDTPAQLEMEDEDTIDVFQQ QTVVGGSGGSGGSGGSMSEEKPKEGVKTENDHIN LKVAGQDGSVVQFKIKRHTPLSKLMKAYSERQGL SMRQIRFRFDGQPINETDTPAQLEMEDEDTIDVF QQQTVVGGSGGSGGSGGSMSEEKPKEGVKTENDH INLKVAGQDGSVVQFKIKRHTPLSKLMKAYSERQ GLSMRQIRFRFDGQPINETDTPAQLEMEDEDTID VFQQQTVVGGSGGSGGSWGGSKVDVIDLTIESSS DEEEDPPAKRGGSGGSGGSGGSKVDVIDLTIESS	SUMO is the human SUMO-3 isoform. Residues 1-92, C47S. SIM is from PIASx.

	SDEEEDPPAKRGGSGGSGGSGG SKVDVIDLTIESSSDEEEDPPAKRGGSGGSGGSG GSKVDVIDLTIESSSDEEEDPPAKRG GSGGSGGSGGSKVDVIDLTIESSSDEEEDPPAKR GGSCGRSENLYFQ	
$(SUMO)_5$-L1- $(SIM)_5$	GHMGGSWGGSMSEEKPKEGVKTENDHINLKVAGQ DGSVVQFKIKRHTPLSKLMKAYSERQGLSMRQIR FRFDGQPINETDTPAQLEMEDEDTIDVFQQQTVV GGSGGSGGSGGSMSEEKPKEGVKTENDHINLKVA GQDGSVVQFKIKRHTPLSKLMKAYSERQGLSMRQ IRFRFDGQPINETDTPAQLEMEDEDTIDVFQQQT VVGGSGGSGGSGGSMSEEKPKEGVKTENDHINLK VAGQDGSVVQFKIKRHTPLSKLMKAYSERQGLSM RQIRFRFDGQPINETDTPAQLEMEDEDTIDVFQQ QTVVGGSGGSGGSGGSMSEEKPKEGVKTENDHIN LKVAGQDGSVVQFKIKRHTPLSKLMKAYSERQGL SMRQIRFRFDGQPINETDTPAQLEMEDEDTIDVF QQQTVVGGSGGSGGSGGSMSEEKPKEGVKTENDH INLKVAGQDGSVVQFKIKRHTPLSKLMKAYSERQ GLSMRQIRFRFDGQPINETDTPAQLEMEDEDTID VFQQQTVVGGSGGSKNSARKASIVKNLKDTLGIG KVKRKPSVPDSASPADDSFVDPGERLYDLNRSGG SWGGSKVDVIDLTIESSSDEEE DPPAKRGGSGGSGGSGGSKVDVIDLTIESSSDEE EDPPAKRGGSGGSGGSGGSKVDVIDL TIESSSDEEEDPPAKRGGSGGSGGSGGSKVDVID LTIESSSDEEEDPPAKRGGSGGSGGS GGSKVDVIDLTIESSSDEEEDPPAKRGGSCGRSE	L1 added to $(SUMO)_5$-$(SIM)_5$

	NLYFQ	

Table 3. Purification details of different Nck mutants.

Construct	Step/Columns
S1-L1-S2-L3-SH2	GST (pH 8), TEV cleavage, Source15S (pH7.0, elutes ~ 170 mM NaCl), SD200
S1-L1-S3-L3-SH2	GST (pH 8), TEV cleavage, Source15S (pH 7.0, elutes ~ 130 mM NaCl), SD200
S2-L2-S3-L3-SH2	GST (pH 8), TEV cleavage, Source15Q (pH 7.0, elutes ~ 90 mM NaCl, SD200
L1-S2-L2-S3-L3-SH2	GST (pH 8), TEV cleavage, Source15Q (pH 7.0, elutes ~ 80 mM NaCl), SD200
L1chargeshuffle S2-L2-S3-L3-SH2	GST (pH 8), TEV cleavage, Source15Q (pH 8.0, elutes ~ 80 mM NaCl), SD200
L1non-chargeshuffle-S2-L2-S3-L3-SH2	GST (pH 8), TEV cleavage, Source15Q (pH 7.0, elutes ~ 90 mM NaCl), SD200
ΔL1-S2-L2-S3-L3-SH2	GST (pH 8), TEV cleavage, Source15Q (pH 7.0, elutes ~ 90 mM NaCl), SD200
L1ΔCT-S2-L2-S3-L3-SH2	GST (pH 8), TEV cleavage, Source15Q (pH 8.0, elutes ~ 60 mM NaCl), SD200
L1Δ(KVKRK)-S2-L2-S3-L3-SH2	GST (pH 8), TEV cleavage, Source15Q (pH 7.0, elutes ~ 100 mM NaCl), SD200
L1basic-S2-L2-S3-L3-SH2	GST (pH 8), TEV cleavage, precipitates at low salt after cleavage, raise salt to 200 KCl, Source15S (pH 7.0, elutes ~ broadly 250 - 290

	mM NaCl), SD200
L1HM S2-L2-S3-L3-SH2	GST (pH 8), TEV cleavage, Source15Q (pH 7.0, elutes ~ 80 mM NaCl), SD200
L1K/E S2-L2-S3-L3-SH2	GST (pH 8), TEV cleavage, Source15Q (pH 7.0, elutes ~ 130 mM NaCl), SD200
L1D/Rswap-S2-L2-S3-L3-SH2	GST (pH 8), TEV cleavage, Source15S (pH 7.0, elutes ~ 200 mM NaCl), SD200
Nck(L1ggsa10)	GST (pH 8), TEV cleavage, Source15Q (pH 7.0, elutes ~ 110 mM NaCl, SD200)
Nck ΔL1	GST (pH 8), TEV cleavage, Source15Q (pH 7.0, elutes ~ 110 mM NaCl, SD200
Nck(L1shuffle)	GST (pH 8), TEV cleavage, Source15Q (pH 7.0, elutes ~ 70 mM NaCl), SD200
Isolated L1 WT	GST (pH 8), TEV cleavage, Source15S (pH 7, elutes 250 mM NaCl), SD200

Cryo-Electron Microscopy

Carbon-coated copper grids were glow-discharged in an EMS-100 unit with a 40 mA current for 90 seconds. 100 μM SH3-5R was loaded onto the carbon-coated side of the grid, after which 100 μM of Abl PRM-5R was introduced (module concentrations), making a final volume of 4.0 uL. The mixture was immediately blotted for 6.5 s in a Mark III Vitrobot (Gatan, Inc.) before being plunged into liquid ethane. SH3-5R and PRM-5R below the critical concentrations (2.5 μM and

2.5 μM each) were incubated for a short period of time before being blotted and frozen in the same way. As controls, 250 μM SH3-5R or PRM-5R alone was prepared in a similar procedure. The experiments were performed in 150 KMEI buffer (150 mM KCl, 1 mM $MgCl_2$, 1 mM EGTA, 10 mM imidazole 7, 1 mM DTT). Frozen grids were stored in liquid nitrogen until EM examination. Imaging was performed under low-dose cryo conditions in a JEOL 2200FS FEG transmission electron microscope, using a 2K x 2K Tietz slowscan CCD camera. The dose rate was adjusted at ~20 electrons per square angstrom, and the defocus level varied from -1.0 to -3.0 microns. The magnification for the CCD was calibrated in a range of 30k to 100K, and the parameters were used in the software controller to obtain the right scale in the output images.

Competition Assay

SH3-5R and PRM-8R were mixed at various concentrations on a Corning flat-bottomed 96-well plate, either by themselves, with PRM(H)-1R (PRM from DLGAP having a K_d of 10 μM towards the second SH3 motif of Nck), or with PRM-1R (PRM from Abl, having a K_d of 350 μM). The affinities were measured using N-15 HSQC experiments. The experiments were performed in 150 KMEI buffer (150 mM KCl, 1 mM $MgCl_2$, 1 mM EGTA, 10 mM imidazole 7, 1 mM DTT). The solutions that underwent phase transition turned cloudy immediately. Phase-

transition was observed and ascertained via bright-field microscopy after a 12-hour incubation at room temperature.

Dynamic Light Scattering (DLS)

DLS experiments were performed in a Protein Solutions DynaPro instrument (Wyatt Technology). To collect enough volume of the droplet phase (> 25 μL), 850 μM SH3-5R was mixed with 850 μM PRM-8R to a final volume of 900 μL in 150 KMEI. The denser droplet phase (~25 μL) was collected via centrifugation at 16,000 g for 10 minutes at 4 ˚C. Scattering from the droplet was measured at 1000 s acquisition time at 10% laser power and 22˚C, for a total of 20 runs. In the titration experiment, SH3-5R was fixed at 850 μM and various concentrations of PRM-1R, PRM(H)-1R, PRM-2R and PRM-4R were added to it. Scattering measurements were performed in the same instrument at 100 s acquisition times at 30% laser power and 22˚C for a total of 20 runs. The solutions and buffers were centrifuged for 10 minutes at 16000 g and 4˚C before using for scattering measurements. The autocorrelation data were analyzed using the regularization method present in the Dynamics V6.4.3 software. Decay time, molecular weights and hydrodynamic radii were obtained using the curves for percent mass distribution. Calculation of the hydrodynamic radii assumes that the species present are hypothetical hard spheres. Molecular weights are calculated using these hydrodynamic radii and assuming that the particles are globular.

Supported Lipid Bilayers

Liposomes were prepared as follows. A mixture of 99% DOPC and 1% Ni^{2+}-NTA DOGS (Avanti Polar Lipids) was dried under argon, and further dried under vacuum overnight. The dried mixture was hydrated with MilliQ water for 3 hours. Buffer (25 mM Hepes 7.5, 150 mM NaCl, 1 mM $MgCl_2$) was added to the hydrated multi-lamellar vesicle solution. Small unilamellar vesicles (SUVs) were prepared by 21 passes through an extruder (Avanti) fitted with 80 nm, and again 7 times with a fresh 80 nm or 30 nm filter. In our hands, changing the filter and re-extruding produced more consistently homogeneous liposomes. SUVs made by this method were stored at 4 °C and used within 2 days of extrusion.

To make supported lipid bilayers, chambered glass coverslips (Lab-tek, Cat # 155409) were cleaned with 50% isopropanol, washed with Milli-Q water, and then incubated for 2 hours in 6 M NaOH. We found that cleaning the glass and using it within the few hours after cleaning was important to get consistent fluidity of the supported bilayers. Therefore, all experiments were performed within 8 hours of cleaning the glass substrate. After extensive further washes with Milli-Q water, 150 μl of room temperature SUV solution containing 0.5 to 1 mg/mL lipid was added to the coverslips and incubated for 10 minutes. Unadsorbed vesicles were

removed by a three-step wash totaling a 216-fold dilution. BSA, 0.1 % (Sigma A3294, protease-free) in 25 mM Hepes pH 7.5, 150 mM NaCl, 1 mM $MgCl_2$ was used to block the surface for 45 minutes, yielding a total solution volume of 200 μl. The surface was washed again with 25 mM Hepes pH 7.5, 150 mM NaCl, 1 mM $MgCl_2$ and 0.1 % BSA in two steps totaling a 36-fold dilution. His_8-p-Nephrin was added to the bilayer at 100 nM and incubated for 1 hour and washed twice totaling a 36-fold dilution. This procedure yielded 200 μl solution above the bilayer containing 2.8 nM His_8-p-Nephrin (assuming a negligible fraction of the total protein binds the bilayer). Subsequent experiments were performed after waiting 30 minutes to allow the His_8 attachment to the bilayer to stabilize. Precise control of the timing and dilution-factor of all wash steps was critical to obtaining consistent p-Nephrin densities on the bilayers (quantified as described below). All experiments were performed in 25 mM Hepes 7.5, 150 mM NaCl, 1 mM $MgCl_2$, 1 mM BME and 0.1% BSA.

Measurement of Nephrin Density on Supported Lipid Bilayers

The density of His_8-p-Nephrin on the supported lipid bilayers was quantified as previously described (Galush et al, 2008; Salaita et al, 2010). Briefly, SUVs containing fluorescent lipid (OG-DHPE, Invitrogen) were made as described above, and used to generate a standard curve of OG-

DHPE concentration versus fluorescence intensity on a Nikon Eclipse Ti microscope using a 20X objective focusing deep into the solution and away from the glass). The slope of the standard curve was denoted I-labeledSUV. Using the identical settings, a similar standard curve was made using His_8-p-Nephrin-Alexa488 in solution, with slope I-labeledprotein. I-labeledprotein was identical in the presence or absence of Ni-NTA-containing SUVs at 9.5 μM Ni-NTA concentration (minimum of 158-fold excess over His_8-p-Nephrin), showing that the His_8-p-Nephrin-Alexa488 fluorescence does not change upon binding lipid. The correction factor F, denoted by F = I-labeledprotein/I-labeledSUV, represents the intrinsic brightness of and sensitivity of the microscope for His_8-p-Nephrin-Alexa488 versus OG-DHPE. Since the OG and Alexa488 fluorophores have very similar excitation and emission spectra, F should be an instrument-independent parameter.

The SUVs containing OG-DHPE were combined in different ratios with non-fluorescent SUVs to make supported bilayers with OG-DHPE densities between 0.05 and 0.4 %. Assuming the surface area of the lipid head groups to be 69 $Å^2$ (Kucerka et al, 2005), this corresponded to OG-DHPE densities of 1430 to 11440 molecules/μm^2. A standard curve of bilayer fluorescence intensity on a Nikon Eclipse Ti microscope and a 100 X objective, versus fluorophore density was then generated from these

bilayers. To obtain the density of His_8-p-Nephrin-Alexa488 on the supported bilayers, the measured fluorescence intensity was first divided by F, and the result analyzed with the standard curve of bilayers with OG-DHPE. We note that this approach assumes that F is the same on the SLB as when His_8-p-Nephrin-Alexa488 and OG-DHPE are associated with SUVs in free solution.

To examine potential changes in Alexa488 fluorescence of as a function of p-Nephrin density, we generated supported bilayers as above 10% to 100% Alexa488-labeled p-Nephrin. Intensity remained linear up to ~ 60% labeling. Initial measurements suggested that the density change in p-Nephrin upon clustering is 4-fold. Therefore, we used p-Nephrin labeled with 15 % or less Alexa488 for all quantitative image analyses.

2D Critical Concentration Measurements

For critical concentration of clustering measurements, images were collected on a Nikon Eclipse Ti microscope equipped with an Andor iXon Ultra 897 EM-CCD camera, with a 100 X objective in epi-fluorescence mode. Background was collected with supported bilayers containing non-fluorescent lipids, and subtracted from all images before processing. Images were corrected for uneven illumination and detector sensitivity as previously described (Wu et al, 2008). Briefly, pixel intensities across a

homogeneous bilayer containing p-NephrinA488 were normalized to the maximum intensity of the image to obtain pixel-by-pixel correction factors (in a 0 to 1 range). Experimental images were then corrected by dividing by these factors.

Images were thresholded using the triangle algorithm in Image J. The fractional intensity of the clustered regions was then calculated by dividing the integrated intensity of the thresholded image by that of the nonthresholded image. Analyzing the clusters using the triangle algorithm or the Maximum Entropy algorithm yielded the same critical concentrations. Similar thresholding results were obtained using an iterative manual procedure to identify pixels with intensity greater than three standard deviations above the mean of the non-clustered regions. Thus, our calculation of fractional intensity in the clustered regions, and our consequent determination of critical concentration is not dependent on the method used to identify clusters.

Size Distribution and Spatial Distribution Analyses

For the size distribution and spatial distribution analyses, 512 by 512 pixel images were taken at 93 randomly selected areas of a sample with clusters made using p-NephrinA488, 1 μM Nck and 1 μM N-WASP. The

images were background corrected as described above, flattened using the rolling-ball method in ImageJ and thresholded using the triangle method. The clusters were binned according to size (excluding those at the image edges) and the distribution was fit to a single exponential using Graph-pad Prism. The size distributions in Figure 3b were determined similarly from single images obtained at each time point.

To analyze the spatial distribution of puncta, each thresholded image was divided into 25 boxes. In each box, the number of clusters was counted twice--excluding and including clusters at the edges. The average number of edge clusters was obtained from the difference in these values, averaged across all boxes in all images. To eliminate overcounting, for each box half of this value was subtracted from the number of clusters counted including edges. These data were plotted to obtain a frequency histogram using Graph-pad Prism, and fit to a Gaussian distribution.

Fluorescence Recovery After Photobleaching (FRAP)

FRAP was performed using a Nikon Eclipse Ti microscope equipped with an Andor iXon Ultra EM-CCD camera. A circle of 1 μm diameter was initially photobleached, and recovery followed for up to 1000 seconds. The images were corrected for drift using the Sift-Align plugin in Image J

(Schneider et al, 2012). Background photobleaching was obtained by imaging under the same conditions, excluding the laser illumination used for photobleaching. Background corrected images were normalized to the intensities of the pre-bleached images and fit to either a single or a double exponential using Graph-pad Prism. F-tests performed in Prism demonstrated that the double-exponential fits are most appropriate (p-values for all experiments were < 0.0001, see Table 4).

In the FRAP experiments, a glucose-oxidase scavenger system with trolox was used to reduce photobleaching during the recovery period. His_8-p-NephrinA488 dissociation from the membrane was monitored by the decrease in total fluorescence measured in TIRF mode following washes that afforded a final solution concentration of 2.8 nM (see Supported Lipid Bilayers section above). To limit the effect of photobleaching, the images at each time point were taken at a different area of the bilayer. The data were fit to a single exponential with time constant of 2080 s.

Table 4. Fitting Statistics for FRAP of Nephrin, Nck and N-WASP at Membrane Clusters

	p-Nephrin	Nck (with p-Nephrin)	Nck (with p-TIR)	N-WASP
Null hypothesis	Single Exp.	Single Exp.	Single Exp.	Single Exp.
Alternative hypothesis	Double Exp.	Double Exp.	Double Exp.	Double Exp.
P value	< 0.0001	< 0.0001	<0.0001	< 0.0001
Conclusion (alpha = 0.05)	Reject null hypothesis	Reject null hypothesis	Reject null hypothesis	Reject null hypothesis
Preferred model	Double Exp.	Double Exp.	Double Exp.	Double Exp.
F (DFn, DFd)	64.16 (2,282)	47.33 (2,635)	46.72 (2,379)	48.64 (2,379)

Actin Assembly Assays

Actin and Arp2/3 complex were purified from rabbit muscle and bovine thymus, respectively, using established methods (Doolittle et al, 2013a; Doolittle et al, 2013b). G-actin (1 μM, 10 % rhodamine labeled) was added to p-Nephrin clusters containing 1 µM Nck and 2 µM N-WASP, with or without 10 nM Arp2/3 complex. Images were collected in TIRF mode every 3 minutes.

For quantitative analysis, images were background corrected and thresholded as described above. In the p-Nephrin clusters the average intensities of p-Nephrin and rhodamine-actin were measured for times up

to 27 minutes. For each cluster, $t_{1/2}$ represents the time at which the average actin intensity reaches half its maximum value.

Isothermal Titration Calorimetry

ITC was performed using a VP-ITC 200 calorimeter (GE Healthcare). Before the experiment, the proteins were dialyzed in the same buffer (25 mM Hepes 7.5, 150 mM NaCl, 1 mM $MgCl_2$ and 2 mM TCEP). Nck at 150 μM in the syringe was titrated to either triply phosphorylated Nephrin or triply phosphorylated TIR. We assumed that all the three sites in Nephrin were of equal affinity. Isotherms were fit well using NITPIC and Sedphat (Houtman et al, 2007; Keller et al, 2012), assuming that all three pTyr sites in p-Nephrin have equal affinity for Nck.

Peptide Synthesis

PRM peptides were synthesized at the UTSW proteomics center. To facilitate absorbance measurements and concentration determination, a tryptophan a WGGS linker) was added at the N-terminus of the peptides that were used for affinity measurements with the SH3 domains.

References

Abdul-Manan N, Aghazadeh B, Liu GA, Majumdar A, Ouerfelli O, Siminovitch KA, Rosen MK (1999) Structure of Cdc42 in complex with the GTPase-binding domain of the 'Wiskott-Aldrich syndrome' protein. *Nature* **399:** 379-383

Alexander N. Semenov MR (1998) Thermoreversible Gelation in Solutions of Associative Polymers. 1. Statics. *Macromolecules* **31:** 1373-1385

Alley MR, Maddock JR, Shapiro L (1992) Polar localization of a bacterial chemoreceptor. *Genes & development* **6:** 825-836

Anderson RG, Jacobson K (2002) A role for lipid shells in targeting proteins to caveolae, rafts, and other lipid domains. *Science* **296:** 1821-1825

Angres B, Barth A, Nelson WJ (1996) Mechanism for transition from initial to stable cell-cell adhesion: kinetic analysis of E-cadherin-mediated adhesion using a quantitative adhesion assay. *The Journal of cell biology* **134:** 549-557

Antoku S, Saksela K, Rivera GM, Mayer BJ (2008) A crucial role in cell spreading for the interaction of Abl PxxP motifs with Crk and Nck adaptors. *Journal of cell science* **121:** 3071-3082

Ariotti N, Liang H, Xu Y, Zhang Y, Yonekubo Y, Inder K, Du G, Parton RG, Hancock JF, Plowman SJ (2010) Epidermal growth factor receptor activation remodels the plasma membrane lipid environment to induce nanocluster formation. *Molecular and cellular biology* **30:** 3795-3804

Banjade S, Rosen MK (2014) Phase transitions of multivalent proteins can promote clustering of membrane receptors. *eLife* **3**

Baum B, Georgiou M (2011) Dynamics of adherens junctions in epithelial establishment, maintenance, and remodeling. *The Journal of cell biology* **192:** 907-917

Benedek RJCaGB (1982) Equilibrium and Kinetic Theory of Polymerization and the Sol-Gel Transition. *J Phys Chem* **86:** 3696-3714

Berne BJP, R. (1976) *Dynamic Light Scattering*.

Bladt F, Aippersbach E, Gelkop S, Strasser GA, Nash P, Tafuri A, Gertler FB, Pawson T (2003) The murine Nck SH2/SH3 adaptors are important for the development of mesoderm-derived embryonic structures and for regulating the cellular actin network. *Molecular and cellular biology* **23:** 4586-4597

Blasutig IM, New LA, Thanabalasuriar A, Dayarathna TK, Goudreault M, Quaggin SE, Li SS, Gruenheid S, Jones N, Pawson T (2008) Phosphorylated YDXV motifs and Nck SH2/SH3 adaptors act cooperatively to induce actin reorganization. *Molecular and cellular biology* **28:** 2035-2046

Brangwynne CP, Eckmann CR, Courson DS, Rybarska A, Hoege C, Gharakhani J, Julicher F, Hyman AA (2009) Germline P granules are liquid droplets that localize by controlled dissolution/condensation. *Science* **324:** 1729-1732

Brangwynne CP, Mitchison TJ, Hyman AA (2011) Active liquid-like behavior of nucleoli determines their size and shape in Xenopus laevis oocytes. *Proceedings of the National Academy of Sciences of the United States of America* **108:** 4334-4339

Brasch J, Harrison OJ, Honig B, Shapiro L (2012) Thinking outside the cell: how cadherins drive adhesion. *Trends in cell biology* **22:** 299-310

Brieher WM, Yap AS, Gumbiner BM (1996) Lateral dimerization is required for the homophilic binding activity of C-cadherin. *The Journal of cell biology* **135:** 487-496

Brown DA, Crise B, Rose JK (1989) Mechanism of membrane anchoring affects polarized expression of two proteins in MDCK cells. *Science* **245:** 1499-1501

Brown DA, Rose JK (1992) Sorting of GPI-anchored proteins to glycolipid-enriched membrane subdomains during transport to the apical cell surface. *Cell* **68:** 533-544

Buday L, Wunderlich L, Tamas P (2002) The Nck family of adapter proteins: regulators of actin cytoskeleton. *Cellular signalling* **14:** 723-731

Bunnell SC, Hong DI, Kardon JR, Yamazaki T, McGlade CJ, Barr VA, Samelson LE (2002) T cell receptor ligation induces the formation of dynamically regulated signaling assemblies. *The Journal of cell biology* **158:** 1263-1275

Cajal SR (1903) Un sencillo metodo de coloracion seletiva del reticulo protoplasmatico y sus efectos en los diversos organos nerviosos de vertebrados e invertebrados. *Trab Lab Invest Biol (Madrid)* **2**

Campellone KG, Rankin S, Pawson T, Kirschner MW, Tipper DJ, Leong JM (2004) Clustering of Nck by a 12-residue Tir phosphopeptide is sufficient to trigger localized actin assembly. *The Journal of cell biology* **164:** 407-416

Carracedo A, Ito K, Pandolfi PP (2011) The nuclear bodies inside out: PML conquers the cytoplasm. *Current opinion in cell biology* **23:** 360-366

Chappuis-Flament S, Wong E, Hicks LD, Kay CM, Gumbiner BM (2001) Multiple cadherin extracellular repeats mediate homophilic binding and adhesion. *The Journal of cell biology* **154:** 231-243

Clayton AH, Orchard SG, Nice EC, Posner RG, Burgess AW (2008) Predominance of activated EGFR higher-order oligomers on the cell surface. *Growth factors* **26:** 316-324

Comrie WA, Babich A, Burkhardt JK (2015) F-actin flow drives affinity maturation and spatial organization of LFA-1 at the immunological synapse. *The Journal of cell biology* **208:** 475-491

Cooper JA, Qian H (2008) A mechanism for SRC kinase-dependent signaling by noncatalytic receptors. *Biochemistry* **47:** 5681-5688

Cooper JA, Walker SB, Pollard TD (1983) Pyrene actin: documentation of the validity of a sensitive assay for actin polymerization. *Journal of muscle research and cell motility* **4:** 253-262

Cowan CA, Henkemeyer M (2001) The SH2/SH3 adaptor Grb4 transduces B-ephrin reverse signals. *Nature* **413:** 174-179

Davis S, Gale NW, Aldrich TH, Maisonpierre PC, Lhotak V, Pawson T, Goldfarb M, Yancopoulos GD (1994) Ligands for EPH-related receptor tyrosine kinases that require membrane attachment or clustering for activity. *Science* **266:** 816-819

Davson HD, J.F. (1935) A contribution to the theory of permeability of thin films. *Journal of Cellular and Comparative Physiology* **5:** 495

de The H, Chomienne C, Lanotte M, Degos L, Dejean A (1990) The t(15;17) translocation of acute promyelocytic leukaemia fuses the retinoic acid receptor alpha gene to a novel transcribed locus. *Nature* **347:** 558-561

Dephoure N, Zhou C, Villen J, Beausoleil SA, Bakalarski CE, Elledge SJ, Gygi SP (2008) A quantitative atlas of mitotic phosphorylation. *Proceedings of the National Academy of Sciences of the United States of America* **105:** 10762-10767

Derry JM, Ochs HD, Francke U (1994) Isolation of a novel gene mutated in Wiskott-Aldrich syndrome. *Cell* **78:** 635-644

Ditlev JA, Michalski PJ, Huber G, Rivera GM, Mohler WA, Loew LM, Mayer BJ (2012) Stoichiometry of Nck-dependent actin polymerization in living cells. *The Journal of cell biology* **197:** 643-658

Doolittle LK, Rosen MK, Padrick SB (2013a) Measurement and analysis of in vitro actin polymerization. *Methods in molecular biology* **1046:** 273-293

Doolittle LK, Rosen MK, Padrick SB (2013b) Purification of Arp2/3 complex from Saccharomyces cerevisiae. *Methods in molecular biology* **1046:** 251-271

Douglass AD, Vale RD (2005) Single-molecule microscopy reveals plasma membrane microdomains created by protein-protein networks that exclude or trap signaling molecules in T cells. *Cell* **121:** 937-950

Eddy EM (1975) Germ plasm and the differentiation of the germ cell line. *International review of cytology* **43:** 229-280

Eden S, Rohatgi R, Podtelejnikov AV, Mann M, Kirschner MW (2002) Mechanism of regulation of WAVE1-induced actin nucleation by Rac1 and Nck. *Nature* **418:** 790-793

Edidin M (2003) The state of lipid rafts: from model membranes to cells. *Annual review of biophysics and biomolecular structure* **32:** 257-283

Engel K, Sasaki T, Wang Q, Kuriyan J (2013) A highly efficient peptide substrate for EGFR activates the kinase by inducing aggregation. *The Biochemical journal* **453:** 337-344

Flory PJ (1941) Molecular Size Distribution in Three Dimensional Polymers. I. Gelation. *JACS* **63:** 3083

Flory PJ (1953) *Principles of Polymer Chemistry*, 1 edn.

Fox AH, Lamond AI (2010) Paraspeckles. *Cold Spring Harbor perspectives in biology* **2:** a000687

Frey S, Gorlich D (2007) A saturated FG-repeat hydrogel can reproduce the permeability properties of nuclear pore complexes. *Cell* **130:** 512-523

Frey S, Richter RP, Gorlich D (2006) FG-rich repeats of nuclear pore proteins form a three-dimensional meshwork with hydrogel-like properties. *Science* **314:** 815-817

Fromm SA, Kamenz J, Noldeke ER, Neu A, Zocher G, Sprangers R (2014) In vitro reconstitution of a cellular phase-transition process that involves the mRNA decapping machinery. *Angewandte Chemie* **53:** 7354-7359

Fujimori T, Takeichi M (1993) Disruption of epithelial cell-cell adhesion by exogenous expression of a mutated nonfunctional N-cadherin. *Molecular biology of the cell* **4:** 37-47

Gall JG (2000) Cajal bodies: the first 100 years. *Annual review of cell and developmental biology* **16:** 273-300

Galush WJ, Nye JA, Groves JT (2008) Quantitative fluorescence microscopy using supported lipid bilayer standards. *Biophysical journal* **95:** 2512-2519

Garrity PA, Rao Y, Salecker I, McGlade J, Pawson T, Zipursky SL (1996) Drosophila photoreceptor axon guidance and targeting requires the dreadlocks SH2/SH3 adapter protein. *Cell* **85:** 639-650

Gerke P, Huber TB, Sellin L, Benzing T, Walz G (2003) Homodimerization and heterodimerization of the glomerular podocyte proteins nephrin and NEPH1. *Journal of the American Society of Nephrology : JASN* **14:** 918-926

Gilks N, Kedersha N, Ayodele M, Shen L, Stoecklin G, Dember LM, Anderson P (2004) Stress granule assembly is mediated by prion-like aggregation of TIA-1. *Molecular biology of the cell* **15:** 5383-5398

Goldberg RJ (1952) A Theory of Antibody—Antigen Reactions. I. Theory for Reactions of Multivalent Antigen with Bivalent and Univalent Antibody. *J Am Chem Soc* **74:** 5715-5725

Goldstein B, Perelson AS (1984) Equilibrium theory for the clustering of bivalent cell surface receptors by trivalent ligands. Application to histamine release from basophils. *Biophysical journal* **45:** 1109-1123

Goswami D, Gowrishankar K, Bilgrami S, Ghosh S, Raghupathy R, Chadda R, Vishwakarma R, Rao M, Mayor S (2008) Nanoclusters of GPI-anchored proteins are formed by cortical actin-driven activity. *Cell* **135:** 1085-1097

Gout I, Dhand R, Hiles ID, Fry MJ, Panayotou G, Das P, Truong O, Totty NF, Hsuan J, Booker GW, et al. (1993) The GTPase dynamin binds to and is activated by a subset of SH3 domains. *Cell* **75:** 25-36

Gowrishankar K, Ghosh S, Saha S, C R, Mayor S, Rao M (2012) Active remodeling of cortical actin regulates spatiotemporal organization of cell surface molecules. *Cell* **149:** 1353-1367

Grecco HE, Schmick M, Bastiaens PI (2011) Signaling from the living plasma membrane. *Cell* **144:** 897-909

Griffin EE, Odde DJ, Seydoux G (2011) Regulation of the MEX-5 gradient by a spatially segregated kinase/phosphatase cycle. *Cell* **146:** 955-968

Groves JT, Kuriyan J (2010) Molecular mechanisms in signal transduction at the membrane. *Nature structural & molecular biology* **17:** 659-665

Gruenheid S, DeVinney R, Bladt F, Goosney D, Gelkop S, Gish GD, Pawson T, Finlay BB (2001) Enteropathogenic E. coli Tir binds Nck to initiate actin pedestal formation in host cells. *Nature cell biology* **3:** 856-859

Han TW, Kato M, Xie S, Wu LC, Mirzaei H, Pei J, Chen M, Xie Y, Allen J, Xiao G, McKnight SL (2012) Cell-free formation of RNA granules: bound RNAs identify features and components of cellular assemblies. *Cell* **149:** 768-779

Hancock JF (2006) Lipid rafts: contentious only from simplistic standpoints. *Nature reviews Molecular cell biology* **7:** 456-462

Hansen SD, Kwiatkowski AV, Ouyang CY, Liu H, Pokutta S, Watkins SC, Volkmann N, Hanein D, Weis WI, Mullins RD, Nelson WJ (2013) alphaE-catenin actin-binding domain alters actin filament conformation and regulates binding of nucleation and disassembly factors. *Molecular biology of the cell* **24:** 3710-3720

Harder T, Simons K (1997) Caveolae, DIGs, and the dynamics of sphingolipid-cholesterol microdomains. *Current opinion in cell biology* **9:** 534-542

Harrison OJ, Jin X, Hong S, Bahna F, Ahlsen G, Brasch J, Wu Y, Vendome J, Felsovalyi K, Hampton CM, Troyanovsky RB, Ben-Shaul A, Frank J, Troyanovsky SM, Shapiro L, Honig B (2011) The extracellular architecture of adherens junctions revealed by crystal structures of type I cadherins. *Structure* **19:** 244-256

Himanen JP, Chumley MJ, Lackmann M, Li C, Barton WA, Jeffrey PD, Vearing C, Geleick D, Feldheim DA, Boyd AW, Henkemeyer M, Nikolov DB (2004) Repelling class discrimination: ephrin-A5 binds to and activates EphB2 receptor signaling. *Nature neuroscience* **7:** 501-509

Hong S, Troyanovsky RB, Troyanovsky SM (2013) Binding to F-actin guides cadherin cluster assembly, stability, and movement. *The Journal of cell biology* **201:** 131-143

Houtman JC, Brown PH, Bowden B, Yamaguchi H, Appella E, Samelson LE, Schuck P (2007) Studying multisite binary and ternary protein interactions by global analysis of isothermal titration calorimetry data in SEDPHAT: application to adaptor protein complexes in cell signaling. *Protein science : a publication of the Protein Society* **16:** 30-42

Hyman AA, Simons K (2012) Cell biology. Beyond oil and water--phase transitions in cells. *Science* **337:** 1047-1049

Jacobson K, Sheets ED, Simson R (1995) Revisiting the fluid mosaic model of membranes. *Science* **268:** 1441-1442

Jaffe SH, Friedlander DR, Matsuzaki F, Crossin KL, Cunningham BA, Edelman GM (1990) Differential effects of the cytoplasmic domains of cell adhesion molecules on cell aggregation and sorting-out. *Proceedings of the National Academy of Sciences of the United States of America* **87:** 3589-3593

James JR, Vale RD (2012) Biophysical mechanism of T-cell receptor triggering in a reconstituted system. *Nature* **487:** 64-69

Jin X, Walker MA, Felsovalyi K, Vendome J, Bahna F, Mannepalli S, Cosmanescu F, Ahlsen G, Honig B, Shapiro L (2012) Crystal structures of Drosophila N-cadherin ectodomain regions reveal a widely used class of Ca(2)+-free interdomain linkers. *Proceedings of the National Academy of Sciences of the United States of America* **109:** E127-134

Jones N, Blasutig IM, Eremina V, Ruston JM, Bladt F, Li H, Huang H, Larose L, Li SS, Takano T, Quaggin SE, Pawson T (2006) Nck adaptor proteins link nephrin to the actin cytoskeleton of kidney podocytes. *Nature* **440:** 818-823

Jones N, New LA, Fortino MA, Eremina V, Ruston J, Blasutig IM, Aoudjit L, Zou Y, Liu X, Yu GL, Takano T, Quaggin SE, Pawson T (2009) Nck proteins maintain the adult glomerular filtration barrier. *Journal of the American Society of Nephrology : JASN* **20:** 1533-1543

Kabouridis PS, Magee AI, Ley SC (1997) S-acylation of LCK protein tyrosine kinase is essential for its signalling function in T lymphocytes. *The EMBO journal* **16:** 4983-4998

Kato M, Han TW, Xie S, Shi K, Du X, Wu LC, Mirzaei H, Goldsmith EJ, Longgood J, Pei J, Grishin NV, Frantz DE, Schneider JW, Chen S, Li L, Sawaya MR, Eisenberg D, Tycko R, McKnight SL (2012) Cell-free formation of RNA granules: low complexity sequence domains form dynamic fibers within hydrogels. *Cell* **149:** 753-767

Keller S, Vargas C, Zhao H, Piszczek G, Brautigam CA, Schuck P (2012) High-precision isothermal titration calorimetry with automated peak-shape analysis. *Analytical chemistry* **84:** 5066-5073

Ken A. Dill SB (2010) *Molecular Driving Forces: Statistical Thermodynamics in Chemistry and Biology*, 2 edn.

Kim AS, Kakalis LT, Abdul-Manan N, Liu GA, Rosen MK (2000) Autoinhibition and activation mechanisms of the Wiskott-Aldrich syndrome protein. *Nature* **404:** 151-158

Kim KK, Yokota H, Kim SH (1999) Four-helical-bundle structure of the cytoplasmic domain of a serine chemotaxis receptor. *Nature* **400:** 787-792

Kouyama T, Mihashi K (1981) Fluorimetry study of N-(1-pyrenyl)iodoacetamide-labelled F-actin. Local structural change of actin protomer both on polymerization and on binding of heavy meromyosin. *European journal of biochemistry / FEBS* **114:** 33-38

Kucerka N, Tristram-Nagle S, Nagle JF (2005) Structure of fully hydrated fluid phase lipid bilayers with monounsaturated chains. *The Journal of membrane biology* **208:** 193-202

Labokha AA, Gradmann S, Frey S, Hulsmann BB, Urlaub H, Baldus M, Gorlich D (2013) Systematic analysis of barrier-forming FG hydrogels from Xenopus nuclear pore complexes. *The EMBO journal* **32:** 204-218

Laur OY, Klingelhofer J, Troyanovsky RB, Troyanovsky SM (2002) Both the dimerization and immunochemical properties of E-cadherin EC1 domain depend on Trp(156) residue. *Archives of biochemistry and biophysics* **400:** 141-147

Lemke G (1997) A coherent nomenclature for Eph receptors and their ligands. *Molecular and cellular neurosciences* **9:** 331-332

Lettau M, Pieper J, Janssen O (2009) Nck adapter proteins: functional versatility in T cells. *Cell communication and signaling : CCS* **7:** 1

Li H, Lemay S, Aoudjit L, Kawachi H, Takano T (2004) SRC-family kinase Fyn phosphorylates the cytoplasmic domain of nephrin and modulates its interaction with podocin. *Journal of the American Society of Nephrology : JASN* **15:** 3006-3015

Li JN, T.; Wu, C. (2010) The slow relaxation mode: from solutions to gel networks. *Polymer Journal* **42:** 609-625

Li P, Banjade S, Cheng HC, Kim S, Chen B, Guo L, Llaguno M, Hollingsworth JV, King DS, Banani SF, Russo PS, Jiang QX, Nixon BT, Rosen MK (2012) Phase transitions in the assembly of multivalent signalling proteins. *Nature* **483:** 336-340

Lillemeier BF, Mortelmaier MA, Forstner MB, Huppa JB, Groves JT, Davis MM (2010) TCR and Lat are expressed on separate protein islands on T cell membranes and concatenate during activation. *Nature immunology* **11:** 90-96

Lingwood D, Simons K (2010) Lipid rafts as a membrane-organizing principle. *Science* **327:** 46-50

Liu Y, Levit M, Lurz R, Surette MG, Stock JB (1997) Receptor-mediated protein kinase activation and the mechanism of transmembrane signaling in bacterial chemotaxis. *The EMBO journal* **16:** 7231-7240

Low MG (1989) The glycosyl-phosphatidylinositol anchor of membrane proteins. *Biochimica et biophysica acta* **988:** 427-454

Madania A, Dumoulin P, Grava S, Kitamoto H, Scharer-Brodbeck C, Soulard A, Moreau V, Winsor B (1999) The Saccharomyces cerevisiae homologue of human

Wiskott-Aldrich syndrome protein Las17p interacts with the Arp2/3 complex. *Molecular biology of the cell* **10:** 3521-3538

Maddock JR, Shapiro L (1993) Polar location of the chemoreceptor complex in the Escherichia coli cell. *Science* **259:** 1717-1723

Marquardt T, Shirasaki R, Ghosh S, Andrews SE, Carter N, Hunter T, Pfaff SL (2005) Coexpressed EphA receptors and ephrin-A ligands mediate opposing actions on growth cone navigation from distinct membrane domains. *Cell* **121:** 127-139

Martino M, Coviello A, Tamburro AM (2000) Synthesis and structural characterization of poly(LGGVG), an elastin-like polypeptide. *International journal of biological macromolecules* **27:** 59-64

Mayer BJ (2001) SH3 domains: complexity in moderation. *Journal of cell science* **114:** 1253-1263

Mayer BJ, Eck MJ (1995) SH3 domains. Minding your p's and q's. *Current biology : CB* **5:** 364-367

Mayor S, Maxfield FR (1995) Insolubility and redistribution of GPI-anchored proteins at the cell surface after detergent treatment. *Molecular biology of the cell* **6:** 929-944

Mayor S, Parton RG, Donaldson JG (2014) Clathrin-independent pathways of endocytosis. *Cold Spring Harbor perspectives in biology* **6**

Mayya V, Lundgren DH, Hwang SI, Rezaul K, Wu L, Eng JK, Rodionov V, Han DK (2009) Quantitative phosphoproteomic analysis of T cell receptor signaling reveals system-wide modulation of protein-protein interactions. *Science signaling* **2:** ra46

Meyer DE, Kong GA, Dewhirst MW, Zalutsky MR, Chilkoti A (2001) Targeting a genetically engineered elastin-like polypeptide to solid tumors by local hyperthermia. *Cancer research* **61:** 1548-1554

Musacchio A, Saraste M, Wilmanns M (1994) High-resolution crystal structures of tyrosine kinase SH3 domains complexed with proline-rich peptides. *Nature structural biology* **1:** 546-551

Nagafuchi A, Takeichi M (1988) Cell binding function of E-cadherin is regulated by the cytoplasmic domain. *The EMBO journal* **7:** 3679-3684

New LA, Keyvani Chahi A, Jones N (2013) Direct regulation of nephrin tyrosine phosphorylation by Nck adaptor proteins. *The Journal of biological chemistry* **288:** 1500-1510

Nikolov DB, Xu K, Himanen JP (2014) Homotypic receptor-receptor interactions regulating Eph signaling. *Cell adhesion & migration* **8:** 360-365

Nott TJ PE, Farber P, Jervis D, Fussner E, Plochowietz A, Craggs T, Bazett-Jones DP, Forman-Kay JP, Baldwin AJ, Pawson T (2015 in press) Phase transition of a disordered Nuage protein generates environmentally responsive membraneless organelles. *Molecular cell*

Nott TJ, Petsalaki E, Farber P, Jervis D, Fussner E, Plochowietz A, Craggs TD, Bazett-Jones DP, Pawson T, Forman-Kay JD, Baldwin AJ (2015) Phase transition of a disordered nuage protein generates environmentally responsive membraneless organelles. *Molecular cell* **57:** 936-947

Nye JA, Groves JT (2008) Kinetic control of histidine-tagged protein surface density on supported lipid bilayers. *Langmuir : the ACS journal of surfaces and colloids* **24:** 4145-4149

O'Leary DD, Wilkinson DG (1999) Eph receptors and ephrins in neural development. *Current opinion in neurobiology* **9:** 65-73

Obenauer JC, Cantley LC, Yaffe MB (2003) Scansite 2.0: Proteome-wide prediction of cell signaling interactions using short sequence motifs. *Nucleic acids research* **31:** 3635-3641

Ozawa M, Kobayashi W (2014) Cadherin cytoplasmic domains inhibit the cell surface localization of endogenous E-cadherin, blocking desmosome and tight junction formation and inducing cell dissociation. *PloS one* **9:** e105313

Padrick SB, Cheng HC, Ismail AM, Panchal SC, Doolittle LK, Kim S, Skehan BM, Umetani J, Brautigam CA, Leong JM, Rosen MK (2008) Hierarchical regulation of WASP/WAVE proteins. *Molecular cell* **32:** 426-438

Padrick SB, Doolittle LK, Brautigam CA, King DS, Rosen MK (2011) Arp2/3 complex is bound and activated by two WASP proteins. *Proceedings of the National Academy of Sciences of the United States of America* **108:** E472-479

Padrick SB, Rosen MK (2010) Physical mechanisms of signal integration by WASP family proteins. *Annual review of biochemistry* **79:** 707-735

Panyi G, Vamosi G, Bacso Z, Bagdany M, Bodnar A, Varga Z, Gaspar R, Matyus L, Damjanovich S (2004) Kv1.3 potassium channels are localized in the immunological synapse formed between cytotoxic and target cells. *Proceedings of the National Academy of Sciences of the United States of America* **101:** 1285-1290

Parker R, Sheth U (2007) P bodies and the control of mRNA translation and degradation. *Molecular cell* **25:** 635-646

Pasquale EB (2010) Eph receptors and ephrins in cancer: bidirectional signalling and beyond. *Nature reviews Cancer* **10:** 165-180

Pavenstadt H, Kriz W, Kretzler M (2003) Cell biology of the glomerular podocyte. *Physiological reviews* **83:** 253-307

Pawson T, Nash P (2003) Assembly of cell regulatory systems through protein interaction domains. *Science* **300:** 445-452

Pralle A, Keller P, Florin EL, Simons K, Horber JK (2000) Sphingolipid-cholesterol rafts diffuse as small entities in the plasma membrane of mammalian cells. *The Journal of cell biology* **148:** 997-1008

Ramaswami M, Taylor JP, Parker R (2013) Altered ribostasis: RNA-protein granules in degenerative disorders. *Cell* **154:** 727-736

Rao M, Mayor S (2005) Use of Forster's resonance energy transfer microscopy to study lipid rafts. *Biochimica et biophysica acta* **1746:** 221-233

Ren R, Mayer BJ, Cicchetti P, Baltimore D (1993) Identification of a ten-amino acid proline-rich SH3 binding site. *Science* **259:** 1157-1161

Renaud-Young M, Gallin WJ (2002) In the first extracellular domain of E-cadherin, heterophilic interactions, but not the conserved His-Ala-Val motif, are required for adhesion. *The Journal of biological chemistry* **277:** 39609-39616

Rimm DL, Koslov ER, Kebriaei P, Cianci CD, Morrow JS (1995) Alpha 1(E)-catenin is an actin-binding and -bundling protein mediating the attachment of F-actin to the membrane adhesion complex. *Proceedings of the National Academy of Sciences of the United States of America* **92:** 8813-8817

Ritter R (1890) Die Entwicklung der Geschlechtsorgane und des Darmes bei Chiromomus. *Zeit furr Wiss Zool Bd* **50:** 408-427

Rivera GM, Briceno CA, Takeshima F, Snapper SB, Mayer BJ (2004) Inducible clustering of membrane-targeted SH3 domains of the adaptor protein Nck triggers localized actin polymerization. *Current biology : CB* **14:** 11-22

Robert X, Gouet P (2014) Deciphering key features in protein structures with the new ENDscript server. *Nucleic acids research* **42:** W320-324

Rohatgi R, Nollau P, Ho HY, Kirschner MW, Mayer BJ (2001) Nck and phosphatidylinositol 4,5-bisphosphate synergistically activate actin polymerization through the N-WASP-Arp2/3 pathway. *The Journal of biological chemistry* **276:** 26448-26452

Rothberg KG, Ying YS, Kamen BA, Anderson RG (1990) Cholesterol controls the clustering of the glycophospholipid-anchored membrane receptor for 5-methyltetrahydrofolate. *The Journal of cell biology* **111:** 2931-2938

Salaita K, Nair PM, Petit RS, Neve RM, Das D, Gray JW, Groves JT (2010) Restriction of receptor movement alters cellular response: physical force sensing by EphA2. *Science* **327:** 1380-1385

Schaupp A, Sabet O, Dudanova I, Ponserre M, Bastiaens P, Klein R (2014) The composition of EphB2 clusters determines the strength in the cellular repulsion response. *The Journal of cell biology* **204:** 409-422

Schmidt HB, Gorlich D (2015) Nup98 FG domains from diverse species spontaneously phase-separate into particles with nuclear pore-like permselectivity. *eLife* **4**

Schneider CA, Rasband WS, Eliceiri KW (2012) NIH Image to ImageJ: 25 years of image analysis. *Nature methods* **9:** 671-675

Schultz J, Milpetz F, Bork P, Ponting CP (1998) SMART, a simple modular architecture research tool: identification of signaling domains. *Proceedings of the National Academy of Sciences of the United States of America* **95:** 5857-5864

Seet BT, Dikic I, Zhou MM, Pawson T (2006) Reading protein modifications with interaction domains. *Nature reviews Molecular cell biology* **7:** 473-483

Seiradake E, Schaupp A, del Toro Ruiz D, Kaufmann R, Mitakidis N, Harlos K, Aricescu AR, Klein R, Jones EY (2013) Structurally encoded intraclass differences in EphA clusters drive distinct cell responses. *Nature structural & molecular biology* **20:** 958-964

Shapiro L, Fannon AM, Kwong PD, Thompson A, Lehmann MS, Grubel G, Legrand JF, Als-Nielsen J, Colman DR, Hendrickson WA (1995) Structural basis of cell-cell adhesion by cadherins. *Nature* **374:** 327-337

Sheetz MP, Chasan R, Spudich JA (1984) ATP-dependent movement of myosin in vitro: characterization of a quantitative assay. *The Journal of cell biology* **99:** 1867-1871

Sieber JJ, Willig KI, Kutzner C, Gerding-Reimers C, Harke B, Donnert G, Rammner B, Eggeling C, Hell SW, Grubmuller H, Lang T (2007) Anatomy and dynamics of a supramolecular membrane protein cluster. *Science* **317:** 1072-1076

Simcha I, Kirkpatrick C, Sadot E, Shtutman M, Polevoy G, Geiger B, Peifer M, Ben-Ze'ev A (2001) Cadherin sequences that inhibit beta-catenin signaling: a study in yeast and mammalian cells. *Molecular biology of the cell* **12:** 1177-1188

Simons K, Ikonen E (1997) Functional rafts in cell membranes. *Nature* **387:** 569-572

Simons K, van Meer G (1988) Lipid sorting in epithelial cells. *Biochemistry* **27:** 6197-6202

Singer SJ, Nicolson GL (1972) The fluid mosaic model of the structure of cell membranes. *Science* **175:** 720-731

Smoligovets AA, Smith AW, Wu HJ, Petit RS, Groves JT (2012) Characterization of dynamic actin associations with T-cell receptor microclusters in primary T cells. *Journal of cell science* **125:** 735-742

Snapper SB, Rosen FS, Mizoguchi E, Cohen P, Khan W, Liu CH, Hagemann TL, Kwan SP, Ferrini R, Davidson L, Bhan AK, Alt FW (1998) Wiskott-Aldrich syndrome protein-deficient mice reveal a role for WASP in T but not B cell activation. *Immunity* **9:** 81-91

Snapper SB, Takeshima F, Anton I, Liu CH, Thomas SM, Nguyen D, Dudley D, Fraser H, Purich D, Lopez-Ilasaca M, Klein C, Davidson L, Bronson R, Mulligan RC, Southwick F, Geha R, Goldberg MB, Rosen FS, Hartwig JH, Alt FW (2001) N-WASP deficiency reveals distinct pathways for cell surface projections and microbial actin-based motility. *Nature cell biology* **3:** 897-904

Sourjik V, Berg HC (2004) Functional interactions between receptors in bacterial chemotaxis. *Nature* **428:** 437-441

Spector DL (2006) SnapShot: Cellular bodies. *Cell* **127:** 1071

Sykulev Y, Joo M, Vturina I, Tsomides TJ, Eisen HN (1996) Evidence that a single peptide-MHC complex on a target cell can elicit a cytolytic T cell response. *Immunity* **4:** 565-571

Takeuchi K, Sun ZY, Park S, Wagner G (2010) Autoinhibitory interaction in the multidomain adaptor protein Nck: possible roles in improving specificity and functional diversity. *Biochemistry* **49:** 5634-5641

Tanaka F (2011) Polymer Physics: Applications to Molecular Association and Thermoreversible Gelation.

Tanaka FD, Sun S.T., Nishio I., Swislow G. and Shah A. (1980) Phase Transitions in Ionic Gels. *Physical Review Letters* **45**

Tanaka M, Gupta R, Mayer BJ (1995) Differential inhibition of signaling pathways by dominant-negative SH2/SH3 adapter proteins. *Molecular and cellular biology* **15:** 6829-6837

Tanaka T (1978) Collapse of Gels and the Critical Endpoint. *Physical Review Letters* **40**

Tran D, Carpentier JL, Sawano F, Gorden P, Orci L (1987) Ligands internalized through coated or noncoated invaginations follow a common intracellular pathway. *Proceedings of the National Academy of Sciences of the United States of America* **84:** 7957-7961

van den Bogaart G, Lang T, Jahn R (2013) Microdomains of SNARE proteins in the plasma membrane. *Current topics in membranes* **72:** 193-230

van der Merwe PA, Dushek O (2011) Mechanisms for T cell receptor triggering. *Nature reviews Immunology* **11:** 47-55

Varma R, Campi G, Yokosuka T, Saito T, Dustin ML (2006) T cell receptor-proximal signals are sustained in peripheral microclusters and terminated in the central supramolecular activation cluster. *Immunity* **25:** 117-127

Varma R, Mayor S (1998) GPI-anchored proteins are organized in submicron domains at the cell surface. *Nature* **394:** 798-801

Veatch SL, Keller SL (2002) Organization in lipid membranes containing cholesterol. *Phys Rev Lett* **89:** 268101

Veatch SL, Keller SL (2003) Separation of liquid phases in giant vesicles of ternary mixtures of phospholipids and cholesterol. *Biophysical journal* **85:** 3074-3083

Vendome J, Felsovalyi K, Song H, Yang Z, Jin X, Brasch J, Harrison OJ, Ahlsen G, Bahna F, Kaczynska A, Katsamba PS, Edmond D, Hubbell WL, Shapiro L, Honig B (2014) Structural and energetic determinants of adhesive binding specificity in type I cadherins. *Proceedings of the National Academy of Sciences of the United States of America* **111:** E4175-4184

Verma R, Kovari I, Soofi A, Nihalani D, Patrie K, Holzman LB (2006) Nephrin ectodomain engagement results in Src kinase activation, nephrin phosphorylation, Nck recruitment, and actin polymerization. *The Journal of clinical investigation* **116:** 1346-1359

Voronina E, Seydoux G, Sassone-Corsi P, Nagamori I (2011) RNA granules in germ cells. *Cold Spring Harbor perspectives in biology* **3**

Wang JT, Smith J, Chen BC, Schmidt H, Rasoloson D, Paix A, Lambrus BG, Calidas D, Betzig E, Seydoux G (2014a) Regulation of RNA granule dynamics by phosphorylation of serine-rich, intrinsically disordered proteins in C. elegans. *eLife* **4**

Wang JT, Smith J, Chen BC, Schmidt H, Rasoloson D, Paix A, Lambrus BG, Calidas D, Betzig E, Seydoux G (2014b) Regulation of RNA granule dynamics by phosphorylation of serine-rich, intrinsically disordered proteins in C. elegans. *eLife* **3:** e04591

Weimbs T, Low SH, Chapin SJ, Mostov KE (1997) Apical targeting in polarized epithelial cells: There's more afloat than rafts. *Trends in cell biology* **7:** 393-399

Weisswange I, Newsome TP, Schleich S, Way M (2009) The rate of N-WASP exchange limits the extent of ARP2/3-complex-dependent actin-based motility. *Nature* **458:** 87-91

Welsh GI, Saleem MA (2010) Nephrin-signature molecule of the glomerular podocyte? *The Journal of pathology* **220:** 328-337

Wiesner S, Helfer E, Didry D, Ducouret G, Lafuma F, Carlier MF, Pantaloni D (2003) A biomimetic motility assay provides insight into the mechanism of actin-based motility. *The Journal of cell biology* **160:** 387-398

Wippich F, Bodenmiller B, Trajkovska MG, Wanka S, Aebersold R, Pelkmans L (2013) Dual specificity kinase DYRK3 couples stress granule condensation/dissolution to mTORC1 signaling. *Cell* **152:** 791-805

Wu H (2013) Higher-order assemblies in a new paradigm of signal transduction. *Cell* **153:** 287-292

Wu JQ, McCormick CD, Pollard TD (2008) Chapter 9: Counting proteins in living cells by quantitative fluorescence microscopy with internal standards. *Methods in cell biology* **89:** 253-273

Wu Y, Honig B, Ben-Shaul A (2013) Theory and simulations of adhesion receptor dimerization on membrane surfaces. *Biophysical journal* **104:** 1221-1229

Wu Y, Vendome J, Shapiro L, Ben-Shaul A, Honig B (2011) Transforming binding affinities from three dimensions to two with application to cadherin clustering. *Nature* **475:** 510-513

Xavier R, Brennan T, Li Q, McCormack C, Seed B (1998) Membrane compartmentation is required for efficient T cell activation. *Immunity* **8:** 723-732

Yamada S, Pokutta S, Drees F, Weis WI, Nelson WJ (2005) Deconstructing the cadherin-catenin-actin complex. *Cell* **123:** 889-901

Yap AS, Brieher WM, Gumbiner BM (1997) Molecular and functional analysis of cadherin-based adherens junctions. *Annual review of cell and developmental biology* **13:** 119-146

Yokosuka T, Sakata-Sogawa K, Kobayashi W, Hiroshima M, Hashimoto-Tane A, Tokunaga M, Dustin ML, Saito T (2005) Newly generated T cell receptor microclusters initiate and sustain T cell activation by recruitment of Zap70 and SLP-76. *Nature immunology* **6:** 1253-1262

Yonemura S (2011) Cadherin-actin interactions at adherens junctions. *Current opinion in cell biology* **23:** 515-522

Yu CC, Yen TS, Lowell CA, DeFranco AL (2001) Lupus-like kidney disease in mice deficient in the Src family tyrosine kinases Lyn and Fyn. *Current biology : CB* **11:** 34-38

Yu H, Chen JK, Feng S, Dalgarno DC, Brauer AW, Schreiber SL (1994) Structural basis for the binding of proline-rich peptides to SH3 domains. *Cell* **76:** 933-945

Yu Y, Smoligovets AA, Groves JT (2013) Modulation of T cell signaling by the actin cytoskeleton. *Journal of cell science* **126:** 1049-1058

Zwicker D, Decker M, Jaensch S, Hyman AA, Julicher F (2014) Centrosomes are autocatalytic droplets of pericentriolar material organized by centrioles. *Proceedings of the National Academy of Sciences of the United States of America* **111:** E2636-2645